1-2024

Assessment of Potential Impacts of Climate Change on Hydrology and Water Resource Availability in the Passaic River Basin, New Jersey

Felix Oteng Mensah

ASSESSMENT OF POTENTIAL IMPACTS OF CLIMATE CHANGE ON HYDROLOGY AND WATER RESOURCE AVAILABILITY IN THE PASSAIC RIVER BASIN, NEW JERSEY

A DISSERTATION

Submitted to the Faculty of

Montclair State University in partial fulfillment

of the requirements

for the degree of Doctor of Philosophy

by

Felix Oteng Mensah

Montclair State University

Montclair, New Jersey

January 2024

Dissertation Chair: Dr. Clement A. Alo

MONTCLAIR STATE UNIVERSITY

THE GRADUATE SCHOOL

DISSERTATION APPROVAL

We hereby approve the Dissertation

Assessment of Potential Impacts of Climate Change on Hydrology and Water Resource Availability in the Passaic River Basin, New Jersey

of

Felix Oteng Mensah

Candidate for the Degree:

Doctor of Philosophy

Graduate Program:

Environmental Science and Management

Certified by:

[redacted]

Dr. Kenneth Sumner
Associate Provost for Academic Affairs and
Acting Dean of the Graduate School

12/14/23

Date:

Dissertation Committee:

[redacted]

Dissertation Chair
Dr. Clement Alo

[redacted]

Dr. Duke Ophori

[redacted]

Dr. Huan Feng

[redacted]

Dr. Josh Galster

[redacted]

Dr. Menberu Meles

CLIMATE CHANGE IMPACTS ON WATER RESOURCE AVAILABILITY

ABSTRACT

Streamflow dynamics in a basin is known to be a major driver of available water resources. In the context of climate change, it is expected that global warming will accelerate the global hydrologic cycle, which will drive more intense floods and droughts leading to changes in streamflow and water resource availability. Most researchers agree that the amount and intensity of precipitation have a direct impact on runoff. Yet, there is no consensus as to how warming can affect streamflow. Evapotranspiration (ET) plays a crucial role here. However, there is a shortage of real-world observations on it. And yet, ET is considered as the primary determinant of available water resources. It is the water that would otherwise become streamflow if not released into the atmosphere. In the Passaic River Basin (PRB), this water loss constitutes on average 50 percent of the approximately 49-inches precipitation. Because of its substantial heterogeneity in land use, soils, geology, reservoirs, vegetation, slope, and topography, the PRB exhibit a highly complex river system. This complexity amidst the heterogeneous biophysical arrangement within the basin present a multifaceted mix of competing interests and water related issues. In a region where predicted temperature increases are anticipated to amplify evapotranspiration and reduce snowpack, the resulting impact on streamflow could be significant. It is with this consideration that this dissertation attempts to better understand the mechanism behind streamflow dynamics in the basin, noting that it is a major driver of available water resource. That way, the impacts of climate change can be properly assessed. In this work, three independent research studies using available hydrological and climate data for the Passaic River Basin were conducted to achieve this goal.

In the first study, I used Gridded datasets from Parameter-elevation Regressions on Independent Slopes Model (PRISM), TerraClimate, and Moderate Resolution Imaging Spectroradiometer

(MODIS) LAI product to develop spatially-varying monthly ET models. Beyond the widely used traditional type regression that has the effect of producing ‘global’ parameter estimates, assumed to be uniform throughout a study area, a more localized spatially non-stationary technique — the geographically weighted regression (GWR) — was utilized to estimate mean monthly ET in the Passaic River Basin (PRB). Key environmental controls of ET have been identified and new sets of spatially varying empirical ET models based on variable combinations that produced the best-fit model have been developed. The analysis showed that temporal and spatial variabilities in ET over the PRB are driven by climatic and biophysical factors. It was found that the key controlling factors were different from month to month, with wind speed being dominant throughout the year in the study basin. Monthly mean ET index map was further generated from the model to illustrate areas where ET exceeds precipitation.

In the second study, I bypassed the frequently used Mann-Kendal trend test in a novel application using the wavelet transform tool to identify the hidden monotonic trends in the inherently noisy hydro-climatic data. By this approach, the use of Mann Kendal trend test directly on the raw data whose results are almost always ambiguous and statistically insignificant in respect of precipitation data for instance, no longer pose a challenge to the reliability of trend results. The results showed that whereas trends in temperature and precipitation are increasing in the PRB, streamflow trends are decreasing. Based on results from the hydrological modelling, streamflow is more sensitive to actual ET than it is to precipitation. The general observation from climate elasticity results showed that in decades where water is available, energy limits actual evapotranspiration which makes streamflow more sensitive to precipitation increase. However, in meteorologically stressed or dry decades, water limits actual ET thereby making streamflow more sensitive to increases in actual evapotranspiration. It was found that the choice of baseline condition constitutes an important source of uncertainty in the sensitivities of streamflow to precipitation and evapotranspiration changes and should routinely be considered in any climate impact assessment.

In the third study, I forced a duly calibrated and verified hydrological model with advanced downscaled and bias-corrected climate scenarios in a rare application in the Rockaway sub-catchment of the Passaic River Basin to assess the impacts of climate change on water resource availability. A priori analysis however involved the selection of subset models from twenty (20) Multivariate Adaptive Constructed Analog (MACA) climate models that characterized the change in temperature and precipitation according to LEAST WARM, HOT, DRY, and WET at mid-21st century (2041—2070) as well as a mild future that typifies the MIDDLE of the temperature and precipitation range. In all, nine (9) different models, relative to two baseline periods, and under two different climate scenarios were selected. Results showed that against the 2041—2070 period, the margin of error owing to the use of different baseline conditions were +/- 0.3 — +/-0.23 ^{o}C for temperature and +/-8.15— +/-6.9% for precipitation, indicating the extent to which the time perspective used in climate change impacts assessment significantly affect outcomes. Across all five (5) climate projections, and the two scenarios, a consistent warming from +1.21 to + 4.70 ^{o}C is projected in the Rockaway catchment at mid-21st century relative to the 1981—2010 baseline period. While precipitation is generally projected to increase, streamflow prediction shows an overall decreasing signal, a trend likely induced by the projected increase in actual evapotranspiration. In terms of climate extremes, an increase in the number heavy rainy days of approximately 2 days is projected in the coldest future whiles an increase of about 4 days is expected in the wettest future. In similar vein, the number days with consecutive dry spells is expected to decrease by approximately 2 days in the driest future whereas an increase of about 3 days is projected in the wettest future. Overall, climate change is expected to fuel flooding and drought conditions in the study catchment, and to cause alterations in river flows which will in turn affect reservoir operations. With this advance knowledge in hand, swift mitigation and adaptation plans are therefore needed.

The results presented in this dissertation show that climate change will threatened available water resources through evapotranspiration. Because the availability of water resource is largely driven by river flows in channels, possible increase or decrease in flow as depicted in the study will fuel flooding and drought conditions. Given that streamflow is highly sensitive to precipitation increases in decades where water is sufficiently available, even higher risk of extreme floods can be expected. On the other hand, longer dry spells will lead to water scarcity and higher risk of drought potentials. Either way, alterations in river flows will affect routine reservoir operations under a changing climate. Particularly, a crucial basis for examining possible environmental impacts on dam failure, including physical sedimentation, erosion from floodwaters, and chemical contamination has been established in this study. With this advance knowledge in hand, swift mitigation and adaptation plans are therefore needed.

ACKNOWLEDGEMENTS

First of all, thanks be to God through our Lord Jesus Christ, by whom all things were created, in Heaven and on Earth, visible and invisible; Who is before all things and in Him all things consist.

My sincere gratitude and appreciation also goes to my academic advisor and mentor, Dr. Clement Alo, for his guidance, insights, and trust all these years while in his research group.

Thank you to my committee members Dr. Menberu Bitew Meles, Dr. Duke Ophori, Dr. Feng Huan, and Dr. Josh Galster for your valuable feedback and suggestions; not forgetting, Dr. Sandow Mark Yidana who played a significant role in my academic journey.

I have enjoyed sharing the graduate school experience with fellow students in the Earth and Environmental Studies Department at Montclair State University. It has been an honor to work and support one another. Special thanks to Archana Prasad, whose friendship I dearly cherish.

Finally, I am most grateful to my family: to my father Samuel Oteng Mensah, to my mother Augustina Owusu, and to my Auntie Felicia Oteng Mensah, for their endless love, support, prayers and encouragement throughout my academic pursuits. I want to also remember my son, Melchizedek Oteng Mensah, who I loved so much but left us too soon to be with his Maker. May you continue to rest well, Mel, until we meet again.

DEDICATION

To my son, Melchizedek Oteng Mensah, through whom I learnt three important virtues of the Spirit: Patience, Perseverance, and Long-suffering.

(2018—2023)

CLIMATE CHANGE IMPACTS ON WATER RESOURCE AVAILABILITY

TABLE OF CONTENTS

LIST OF TABLES

LIST OF FIGURES

CLIMATE CHANGE IMPACTS ON WATER RESOURCE AVAILABILITY

CHAPTER 1 : INTRODUCTION

1.1. **Background**

Having been accurately described as an era of ubiquitous climate change (Green et al., 2011), the 21st century has witnessed the most rapid changes in global temperatures (K. E. Trenberth et al., 2014), constituting a major environmental problem of global significance. On average, global surface temperature has shown a warming of 0.85ºC over the 1980—2012 period (IPCC, 2013), with the largest increases observed in several locations. Precipitation also showed mixed positive and negative trends across the globe, with increases observed over tropical oceans and decreases over some regions along mid latitude for the period 1979—2014(Adler et al., 2017).

This noticeable shift in global climate and the accompanying impacts to humankind motivated attempts to estimate the extent to which future climate would be affected by the anthropogenic modification of atmospheric composition. Consequently, emission scenarios were established by the Intergovernmental Panel on Climate Change, with the most recent based on four Representative Concentration Pathways (RCPs): RCP 8.5, RCP 6.0, RCP 4.5, and RCP 2.6. The RCP 8.5 is the most pessimistic (but highly probable), assuming a business as usual lifestyle where humans make no effort to reduce CO_2 emissions. The RCP 6.0 and RCP 4.5 scenarios assume that world governments make efforts to reduce emissions which will result in CO_2 concentrations stabilizing at 750ppm and 540ppm respectively in the next century. The most (hopelessly) optimistic is the RCP 2.6 scenario, peaking around 2020 and declines throughout the rest of the century (Dessler, 2015) (Fig 1.1).

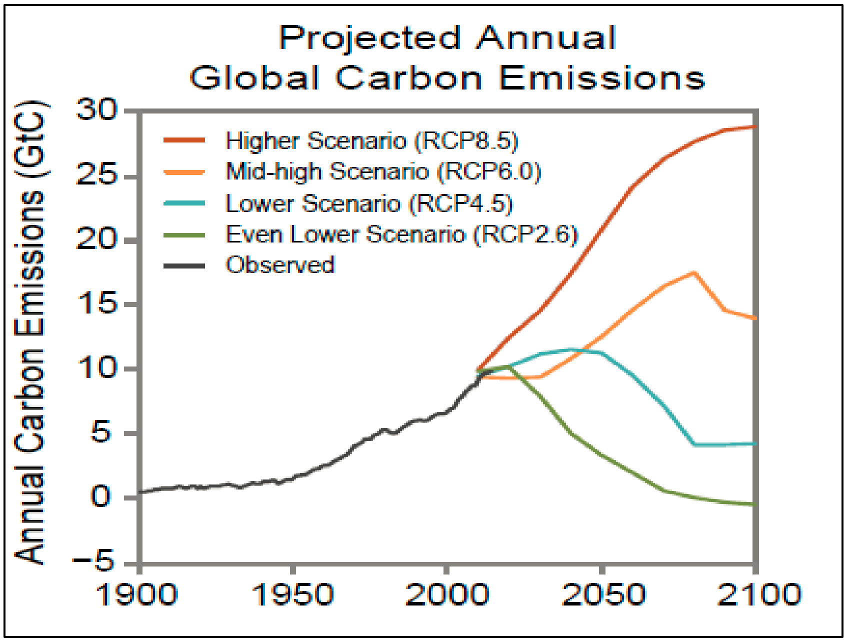

Figure 1.1: Representative concentration pathways (RCP) for atmospheric carbon dioxide by 2100 (U.S. Global Change Research Program et al., 2017)

Global Circulation Models (GCMs) used by IPCC provide outlooks of temperature, precipitation, and other climate variables for all the four RCPs by the end of the 21st century. In terms of temperature, an ensemble of models depicts a general agreement towards an increase, projected to exceed 2 ºC under RCP 4.5, 6.0, and 8.5, relative to 1986—2005 baseline (IPCC, 2013). However, precipitation changes are non-uniform, with increases projected along mid-latitude regions in the northern hemisphere and mix of increases and decreases along other latitudes (K. Trenberth, 2011). To derive local effects from global climate changes, regional climate models (RCMs) are used. RCMs are much closer to the scale of real-world observation, useful in the study of natural variations in climate as well as their impact, and necessary for informing strategic planning and adaptation of future climate change. Given that river systems are most sensitive to changes in climate (i.e., temperature and precipitation) (Stern, 2008; Ormerod, 2009; Kernan et al., 2011), the impacts are expected to reflect in the distribution of water resource through acceleration of the hydrologic cycle (IPCC, 2013; Bates et al., 2008;

Zhang and Wang, 2007). As a result, water resource availability will be affected primarily through evapotranspiration, and indirectly through vegetation water use (Cheng et al., 2014). Although the Northeast United State can generally be considered as a "water rich" region, the recent observed and projected reduction in snowfall as well as snowpack (Hodgkins and Dudley 2006; Burakowski et al., 2008; Campbell et al., 2010, NCA, 2018) threatens available water resource. This is because, while snowpack is not the dominant source of streamflow in the Northeast region, it plays a key role in recharging the groundwater system, which partly forms the base-flow component of streamflow. In a region whose economy and way of life depends largely on tourism, water supply, recreation, wastewater assimilation, power generation among others, changes in snow pack and streamflow owing to climate change will pose serious water-related issues, and thus require the application of new tools and techniques to inform adaptation and planning strategies. In lieu of this, the overall objective of the dissertation is to assess the potential impacts of climate change on the hydrology and water resource availability especially in a widely diverse and heterogeneous terrain, where future water stress and risks have been predicted in the context of climate change (NJDEP, 2017).

1.2. Research Motivation

More than 11000 scientists have, on November 5, 2019 sent a strong warning to the effect that the planet "clearly and unequivocally faces a climate emergency" (Ripple et al. 2019). Published in the Journal of BioScience and reported on by various news outlets (e.g. The Washington Post), these scientists note that, the current public posture to climate change and the measures taken are woefully inadequate to capture the breadth of human activities and the real dangers resulting from a warming planet (Briggs et al. 2015). Although climate change is a global phenomenon, the underlying impacts are very local. Therefore, it is necessary for societies to consider the options and responses to climate change by identifying the extent to which various sectors of the economy may be affected.

It has become evident that recent increase in the frequency of extreme weather events and associated intensification in hydrological extremes are manifestations that point to a warming climate (Kundzewicz, 2005). Serious devastating effects on the functioning of ecosystems have also been linked to climate change. For instance, crop and livestock yields have dwindled in productivity (Howden et al., 2007; Piao, et al., 2010), essential ecosystem service deliveries are in jeopardy (Mooney et al., 2009), energy systems are failing— threatening more frequent power outages and fuel shortages (DOE, 2015), and water security is in serious ruin due to recurrent flood events. Within these matrices, the impacts on water lie at the epicenter, tightly linked to the other systems. Water is known as the engine of growth to the agricultural, energy, tourism, and industrial sectors (NCA, 2018), and sustains the health and productivity of natural and human ecosystems. Although the threat due to climate change has already caught up with us, the character of the change at regional and local levels remains uncertain going into the future. Yet, it is at this level that water resource decisions and the varying environmental stresses that affect hydrologic systems converge.

Given that river systems are the major driver of available water resources, it is important to understand and quantify how future climate may influence streamflow. Climate variability and change may affect streamflow through one of two ways or both: 1) increases in temperature and 2) changes in hydro-meteorological cycle (Barnett et al. 2005, Trenberth 2011). Temperature increase can result in a shift in precipitation forms (i.e., from snow to rain), runoff timing, and changes in streamflow seasonality (Barnett et al. 2005). In terms of hydro-meteorological processes such as precipitation and evapotranspiration, warmer climates generally intensify the water cycle bringing about significant changes in precipitation extremes and consequently hydrologic alterations (e.g., increase in frequency and magnitude of floods) (Dai, 2013; Espinoza et al., 2018).

Through previous studies, it has become clear that the Northeast United States has witnessed the strongest increase in extreme precipitation and temperatures among all US regions in the past five decades (Trenberth, 1999; Groisman et al., 2005; Allan & Soden, 2008; Hoerling, 2016, Easterling, 2017). Whereas most regions have seen relative increases in precipitation extremes ranging from 5% to 37% (e.g., Groisman et al., 2005), the U.S. Northeast has experienced a whopping 71 percent increase (e.g., Melillo et al., 2014; Horton et al., 2014; NCA, 2014b)). In the Fourth National Climate Assessment report (NCA, 2018), it is projected that Northeast will continue to experience further increases in rainfall intensity, with total precipitation increase expected during the winter and spring seasons (Thibeault and Seth, 2014). On the other hand, temperatures are projected to increase beyond preindustrial average by 2ºC (3.6ºF) by 2035 under RCP4.5 and RCP8.5 scenarios. This is said to be the largest increase in the contiguous U.S. and is expected to occur as much as two decades before global average temperatures reach similar record (Karmalkar and Bradley, 2017). Under such climate conditions and given the largely varied physiographic characteristics of the Northeast, it is expected that the nature of climate vulnerabilities, impacts, and adaptation responses will be very unpredictable (Rosenzweig et al., 2011, Leichenko and Solecki, 2013), and spatially heterogeneous. More so, current water related infrastructure in the region while nearing the end of their planned life span (NCA, 2018), were not designed to cope with the projected wider variability in future climate conditions compared to climate records in the last hundred years. As a result, any climate related disruption would only worsen existing issues with the aging infrastructure, leading to disproportionate effects on at-risk communities in the region. Moreover, assumption of stationarity in conventional hydrologic considerations during the design of these water resource structures (e.g., dams, bridges, roads, culverts, etc.) may no longer hold under future climate conditions. A more locally relevant climate impact assessment is therefore needed. This will help build the needed resilience and adaptation to possible climate impacts through incorporation of climate related risks in future water resource decision and planning process.

The Passaic River Basin (PRB) of New Jersey, noted for its dense population with diverse land uses and many reservoirs, represent a suitable terrain to assess the impacts of climate variability and change on water resources. The major setbacks that have over the years challenged a research such as this to be conducted in the area have largely been surmounted because of the following:

1) The challenge of the numerous regulated streamflows that rendered such study impossible in the basin has, largely, been addressed by the now available time series records of reconstructed streamflows from 1920—2010 occasioned by Hickman and McHugh (2018).
2) Sufficiently high spatial resolution (4km x 4km) regional climate outputs based on the Multivariate Adaptive Constructed Analogs (MACA) downscaling technique are now available for the new sets of Coupled Model Inter-comparison Project Phase 5 (CMIP5) experiments. This dataset also complements the already available gridded (4km) meteorological observations from Parameter-elevation Regressions on Independent Slopes Model (PRISM) at a resolution relevant for basin level water resource planning.

3) A state-of-the-science physically-based hydrological model that integrates both surface and subsurface processes has been acquired and will for the first time, be applied to the PRB. Consequently, the duly calibrated and verified model will be forced with scenarios of future climate projections over the basin.

Thus under the overall objective of this dissertation, the specific goals are: (1) to establish a temporal and spatially-varying actual ET model from readily available data over the Passaic River basin; (2) to detect and analyze hydro-climatic trends and examine catchment hydrologic response to climate variability and change in historic time; and (3) to assess the hydrological impacts of climate variability/change based on selected climate models and projections that capture the range of future conditions in the PRB. In line with the objectives, this study will address the following research questions:

- How has the physiographic characteristics of the area influenced the spatial and temporal dynamics of actual evapotranspiration in the PRB?
- From a hydrological modeling perspective, what mechanism likely drives observed hydro-climatic patterns in the PRB?
- Will recent trends in precipitation and temperature change continue into the future, and if so, how will they alter water resource availability in the PRB?

1.3. Summary of the Research Tasks

The research questions raised in section 1.2. were addressed by carrying out the following research tasks: (1) identify key environmental controls on actual evapotranspiration and develop new sets of spatially varying empirical ET models over the twelve (12) months; (2) employ the advance wavelet transform tool to detect and analyze hydro-climatic trends and set up hydrological model to examine hydrologic response of recent climate changes using the Rockaway sub-catchment as case study; and (3) select appropriate regional climate models that represent the range of future climate conditions and assess future climate impacts on the hydrology of the modelled Rockaway sub-basin.

The above tasks have been carried out in the form of three independent research studies and presented in a research journal style format in three core chapters (Chapters 2, 3, and 4) in this dissertation. A brief summary of the three major research tasks and their main findings have been presented below:

To identify key environmental controls on actual evapotranspiration and develop new sets of spatially varying empirical ET models over the twelve (12) months.

Gridded datasets from Parameter-elevation Regressions on Independent Slopes Model (PRISM) (PRISM, Oregon State University, http://prism.oregonstate.edu), TerraClimate (Abatzoglou et al., 2018) (http://www.climatologylab.org/terraclimate.html), and Moderate Resolution Imaging Spectroradiometer (MODIS) LAI product (LAADS/DAAC, https://ladsweb.modaps.eosdis.nasa.gov/search/) provided environmental variables needed to develop the monthly ET models. Beyond the widely used traditional type regression that has the effect of producing 'global' parameter estimates, assumed to be uniform throughout a study area, we utilized a more localized spatially non-stationary technique — the geographically weighted regression (GWR) — to estimate mean monthly ET in the Passaic River Basin (PRB). Key environmental controls of ET have been identified and new sets of spatially varying empirical ET models based on variable combinations that produced the best-fit model have been developed. The analysis showed that temporal and spatial variabilities in ET over the PRB are driven by climatic and biophysical factors. It was found that the key controlling factors were different from month to month, with wind speed being dominant throughout the year in the study basin. Monthly mean ET index map was further generated from the model to illustrate areas where ET exceeds precipitation.

To detect and analyze hydro-climatic trends and set up hydrological model to examine hydrologic response of recent climate changes using the Rockaway sub-catchment as case study.

In a rather novel application using the wavelet transform tool, the frequently used Mann-Kendal trend test has been by-passed, and the hidden monotonic trends in the inherently noisy hydro-climatic data has been identified. By this approach, the use of Mann Kendal trend test directly on the raw data whose results are almost always ambiguous and statistically insignificant in respect of precipitation data for instance, no longer pose a challenge to the reliability of trend results. The results showed that whereas trends in temperature and precipitation are increasing in the PRB, streamflow trends are decreasing. Based on results from the hydrological modelling, streamflow is more sensitive to actual ET than it is to precipitation. The general observation from climate elasticity results showed that in decades where water is available, energy limits actual evapotranspiration which makes streamflow more sensitive to precipitation increase. However, in meteorologically stressed or dry decades, water limits actual ET thereby making streamflow more sensitive to increases in actual evapotranspiration. It was found that the choice of baseline condition constitutes an important source of uncertainty in the sensitivities of streamflow to precipitation and evapotranspiration changes and should routinely be considered in any climate impact assessment.

To select appropriate regional climate models that represent the range of future climate conditions for the basin and assess future climate impacts on the hydrology of the modelled Rockaway sub-basin.

Duly calibrated and verified hydrological modeling and advanced climate scenarios have been combined in a novel application in the Rockaway sub-catchment to assess impacts of climate change on water resource availability in the PRB. A priori analysis however involved the selection of subset models from the twenty (20) Multivariate Adaptive Construted Analog (MACA) models that characterized the change in temperature and precipitation according to LEAST WARM, HOT, DRY, and WET at mid-21st century (2041—2070) as well as a mild future that typifies the MIDDLE of the temperature and precipitation range. In all, nine (9) different models, relative to two baseline periods, and under two different climate scenarios were selected. Results showed that against the 2041—2070 period, the margin of error owing to the use of different baseline conditions were +/- 0.3 — +/-0.23 ^{o}C for temperature and +/-8.15— +/-6.9% for precipitation, indicating the extent to which the time perspective used in climate change impacts assessment significantly affect outcomes. Across all five (5) climate projections, and the two scenarios, a consistent warming from +1.21 to + 4.70 ^{o}C is projected in the Rockaway catchment at mid-21st century relative to the 1981—2010 baseline period. While precipitation is generally projected to increase, streamflow prediction shows an overall decreasing signal, a trend likely induced by the projected increase in actual evapotranspiration. In terms of climate extremes, an increase in the number heavy rainy days of approximately 2 days is projected in the coldest future whiles an increase of about 4 days is expected in the wettest future. In similar vein, the number of days with consecutive dry spells is expected to decrease by approximately 2 days in the driest future whereas an increase of about 3 days is projected in the wettest future. Overall, climate change is expected to fuel flooding and drought conditions in the study catchment, and to cause alterations in river flows which will in turn affect reservoir operations. With this advance knowledge at hand, swift mitigation and adaptation plans are therefore needed.

1.4 Innovation

Within the scope of this dissertation, key innovative work carried out is as follows:

- Selected high resolution (4 km) regional climate scenarios coupled with state of the art physically based, distributed hydrological model run for climate change impact assessment was seldom performed before and is relatively new within the Passaic River Basin and its environs.
- The modeling of environmental variables using conventional type regression technique has become one too many, clothe with an assumption of stationarity unbefitting of most environmental variable at the scale of the PRB. The use of a more localized approach—the geographically weighted regression—which overcomes the long-held “global” estimates of environmental variables over an area, represents an ideal alternative, and has until this study never been applied before in the study terrain. Being the first of its kind in the study basin, actual ET has been successfully mapped to key controlling environmental variables in such a complex terrain, and demonstrates the superiority of the geographically weighted regression over the ordinary least square approach in modeling spatially-varying environmental relationships.
- At long last, the frequently used Mann-Kendal (MK) trend test has been by-passed. The wavelet transform technique, commonly used in the field of signal processing but have found usefulness in hydrologic science, has been cleverly used in identifying the hidden monotonic trends in the almost always inherently noisy hydro-climatic data. By this approach, the use of MK test directly on raw data whose results are almost always

ambiguous and statistically insignificant in respect of precipitation data for instance, no longer pose a challenge to the reliability of trend results. This technique is also relatively new in the study basin and around, and has been successfully used in finding significant hydroclimatic trends in the PRB.

1.5. References

Adler, R. F., Gu, G., Sapiano, M., Wang, J. J., & Huffman, G. J. (2017). Global precipitation: Means, variations and trends during the satellite era (1979–2014). Surveys in Geophysics, 38, 679-699.

Allan, R. P., & Soden, B. J. (2008). Atmospheric warming and the amplification of precipitation extremes. *Science*, 321(5895), 1481-1484.

Barnett, T. P., Adam, J. C., & Lettenmaier, D. P. (2005). Potential impacts of a warming climate on water availability in snow-dominated regions. *Nature*, 438(7066), 303.

Bates, B. C., Kundzewicz, Z. W., Wu, S., & Palutikof, J. P. (2008). Climate Change and Water. Paper of the *Intergovernmental Panel on Climate Change*. IPCC Secretariat: Geneva.

Briggs, S., Kennel, C. F., & Victor, D. G. (2015). Planetary vital signs. *Nature Climate Change,* 5(11), 969.

Brydon, N. F. (1974). The Passaic River: past, present, future. Rutgers Univ Pr.

Carswell, L. D., & Rooney, J. G. (1976). Summary of geology and ground-water resources of Passaic County, New Jersey (No. 76-75). US Geological Survey.

Campbell, J. L., Ollinger, S. V., Flerchinger, G. N., Wicklein, H., Hayhoe, K., & Bailey, A. S. (2010). Past and projected future changes in snowpack and soil frost at the Hubbard

Brook Experimental Forest, New Hampshire, USA. Hydrological Processes, 24(17), 2465-2480.

Cheng, L., Zhang, L., Wang, Y. P., Yu, Q., Eamus, D., & O'Grady, A. (2014). Impacts of elevated CO2, climate change and their interactions on water budgets in four different catchments in Australia. *Journal of hydrology*, 519, 1350-1361.

Dai, A. (2013). The influence of the inter-decadal Pacific oscillation on US precipitation during 1923–2010. *Climate dynamics*, 41(3-4), 633-646.

Department of Energy (DOE), 2015: Climate Change and the U.S. Energy Sector: Regional Vulnerabilities and Resilience Solutions. DOE/EPSA-0005. U.S. Department of Energy (DOE), Washington, DC, 189 pp.

Dessler, A. (2015). Introduction to modern climate change. Cambridge University Press.

Drake, A.A., Volkert, R.A., Monteverde, D.H., Herman, G.C., Houghton, H.F., Parker, R.A. and Dalton, R.F. (1996) Bedrock geologic map of northern New Jersey. In: Miscellaneous Geological Investigation Map 1-2540-A. U.S. Geological Survey.

Easterling, D., Kunkel, K., Arnold, J., Knutson, T., LeGrande, A., Leung, L., ... & Wehner, M. (2017). Precipitation change in the United States. In climate science special report: fourth national climate assessment, volume I. [Wuebbles D, Fahey D, Hibbard K, Dokken D, Stewart B, Maycock T (eds.)]. US Global Change Research Program, Washington, DC, 207–230.

Espinoza, V., Waliser, D. E., Guan, B., Lavers, D. A., & Ralph, F. M. (2018). Global analysis of climate change projection effects on atmospheric rivers. *Geophysical Research Letters*, 45(9), 4299-4308.

FEMA, (2013) Flood Insurance Study Technical Report. United States Department of Homeland Security.

Green, T. R., Taniguchi, M., Kooi, H., Gurdak, J. J., Allen, D. M., Hiscock, K. M., ... & Aureli, A. (2011). Beneath the surface of global change: Impacts of climate change on groundwater. Journal of Hydrology, 405(3-4), 532-560.

Groisman, P. Y., Knight, R. W., Easterling, D. R., Karl, T. R., Hegerl, G. C., & Razuvaev, V. N. (2005). Trends in intense precipitation in the climate record. Journal of climate, 18(9), 1326-1350.

Hendricks, E. L. (1964). Compilation of Records of Surface Waters of the United States, October 1950 to September 1960: Cumberland and Tennessee River Basins. Part 3-B. US Government Printing Office.

Hoerling, M., Eischeid, J., Perlwitz, J., Quan, X. W., Wolter, K., & Cheng, L. (2016). Characterizing recent trends in US heavy precipitation. Journal of Climate, 29(7), 2313-2332.

Hoffman, J.L. (1989) Plan of Study for the Central Passaic River Basin Hydrogeologic Investigation, NJDEP New Jersey Geological Survey Open-File Report 88-4

Horton, R., Yohe, G., Easterling, W., Kates, R., Ruth, M., Sussman, E., Whelchel, A., Wolfe, D., Lipschultz, F., 2014. Chapter 16: Northeast, in: Climate Change Impacts in the United States: The Third National Climate Assessment. pp. 371–395. doi:10.7930/J0SF2T3P

Howden, S. M., Soussana, J. F., Tubiello, F. N., Chhetri, N., Dunlop, M., & Meinke, H. (2007). Adapting agriculture to climate change. Proceedings of the national academy of sciences, 104(50), 19691-19696.

IPCC, 2013a: Climate Change 2013: The Physical Science Basis. Contribution of Working Group I to the Fifth Assessment Report of the Intergovernmental Panel on Climate Change. Cambridge University Press, Cambridge, UK and New York, NY, 1535 pp. http://www.climatechange2013.org/report/

Karmalkar, A. V., & Bradley, R. S. (2017). Consequences of global warming of 1.5 C and 2 C for regional temperature and precipitation changes in the contiguous United States. PloS one, 12(1), e0168697.

Kernan, M., Battarbee, R. W., & Moss, B. R. (Eds.). (2011). Climate Change Impacts on Freshwater Ecosystems. John Wiley & Sons.

Kundzewicz, Z. W., Ulbrich, U., Graczyk, D., Krüger, A., Leckebusch, G. C., Menzel, L., ... & Szwed, M. (2005). Summer floods in Central Europe–climate change track?. Natural Hazards, 36(1-2), 165-189.

Leichenko, R. M., & Solecki, W. D. (2013). Climate change in suburbs: An exploration of key impacts and vulnerabilities. Urban Climate, 6, 82-97.

Masson-Delmotte, V., Zhai, P., Pirani, A., Connors, S. L., Péan, C., Berger, S., ... & Zhou, B. (2021). Climate change 2021: the physical science basis. Contribution of working group I to the sixth assessment report of the intergovernmental panel on climate change, 2.

Melillo, J. M., Richmond, T. T., & Yohe, G. (2014). Climate change impacts in the United States. Third national climate assessment, 52.

Mitchell, A. E. (1992). The New Jersey Highlands: Treasures at Risk. New Jersey Conservation Foundation.

Mooney, H., Larigauderie, A., Cesario, M., Elmquist, T., Hoegh-Guldberg, O., Lavorel, S., ... & Yahara, T. (2009). Biodiversity, climate change, and ecosystem services. Current opinion in environmental sustainability, 1(1), 46-54.

NCA (2018). Highlights of Climate Change Impacts in the United States: The Forth National Climate Assessment 2018 Global Change Research Program. U.S. Government Printing Office, Washington, D.C U.S. 10.7930/J0Z31WJ2

Neelin, J. D. (2010). Climate change and climate modeling. Cambridge University Press.

New Jersey Department of Environmental Protection (2017) New Jersey Water Supply Plan 2017-2022: 484p, http://www.nj.gov/dep/watersupply/wsp.html

Ormerod, S. J. (2009). Climate change, river conservation and the adaptation challenge. Aquatic Conservation: Marine and Freshwater Ecosystems, 19(6), 609-613.

Passaic County Hazard Mitigation Plan, 2015. Retrieved from: http://www.passaiccountynj.org/Departments/OEM/Passaic%20County%20HMP%20Vol%201.pdf. Access date: November 12, 2019.

Paulson, R.W., Chase, E.B., Roberts, R.S. and Moody, D.W. (1991) National Water Summary, 1988-89 -- Hydrologic Events and Floods and Droughts, U.S Geological Survey Paper 2375, United States Government Printing Office, Reston, V.A., https://pubs.er.usgs.gov/publication/wsp2375

Piao, S., Ciais, P., Huang, Y., Shen, Z., Peng, S., Li, J., ... & Friedlingstein, P. (2010). The impacts of climate change on water resources and agriculture in China. Nature, 467(7311), 43.

Ripple, W. J., Wolf, C., & Newsome, T. M. (2019) World Scientists' Warning of a Climate Emergency.

Rosenzweig, C., Solecki, W., & DeGaetano, A. (2011). ClimAID: Integrated assessment for effective climate change adaptation strategies in New York State. RESPONDING TO CLIMATE CHANGE IN NEW YORK STATE: THE CLIMAID INTEGRATED ASSESSMENT FOR EFFECTIVE CLIMATE CHANGE ADAPTATION IN NEW YORK STATE: FINAL REPORT, 1244, 1-14.

Rutgers University Climate Lab. n.d. "The Climate of New Jersey." Available at https://climate.rutgers.edu/stateclim_v1/njclimoverview.html.

Stanford, S. (2007b) Surficial Geology of the Pompton Plains Quadrangle Morris, Passaic, Essex,and Bergen Counties,, New Jersey. In: Open-File Map 68 edn. NJDEP, Land use management, NJGS.

Stern, N. (2008). The economics of climate change. American Economic Review, 98(2), 1-37.

Thibeault, J. M., and A. Seth, (2014). Changing climate extremes in the Northeast United States: Observations and projections from CMIP5. Climatic Change, 127 (2), 273–287. doi:10.1007/s10584-014-1257-2

Trenberth, K. E. (1999). Conceptual framework for changes of extremes of the hydrological cycle with climate change. In Weather and Climate Extremes (pp. 327-339). Springer, Dordrecht.

Trenberth, K. E. (2011). Changes in precipitation with climate change. Climate Research, 47(1-2), 123-138.

Trenberth, K. E., Dai, A., Van Der Schrier, G., Jones, P. D., Barichivich, J., Briffa, K. R., & Sheffield, J. (2014). Global warming and changes in drought. Nature Climate Change, 4(1), 17-22.

U.S. Global Change Research Program, Wuebbles, D. J., Fahey, D. W., Hibbard, K. A., Dokken, D. J., Stewart, B. C., & Maycock, T. K. (2017). Climate Science Special Report: Fourth National Climate Assessment, Volume I. U.S. Global Change Research Program. https://doi.org/10.7930/J0J964J6

United State Geological Survey, (1970). Surface water supply of the United States, 1961-65, Part 1, North Atlantic slope basins, v. 2, Basins from New York to Delaware. U.S. Govt. Print. Off.

US Army Corps of Engineers, N.Y.District (1987) Flood Protection Feasibility Mainstem Passaic River: Main Report Environmental Impact Statement U.S. Army Corp of Engineers, New York.

US Army Corps of Engineers, N.Y.District (2017) Fact Sheet-Passaic River Mainstem and Tributaries, New Jersey Flood Risk Management and Restoration Projects, http://www.nan.usace.army.mil/Media/Fact-Sheets/Fact-Sheet-Article-View/Article/487436/fact-sheet-passaic-river-mainstem-and-tributaries-new-jersey/

USGCRP (2017). Climate Science Special Report: Fourth National Climate Assessment, Volume I [Wuebbles, D.J., D.W. Fahey, K.A. Hibbard, D.J. Dokken, B.C. Stewart, and T.K. Maycock (eds.)]. U.S. Global Change Research Program, Washington, DC, USA, 470 pp., doi: 10.7930/J0J964J6.

Wang, G. Q., Zhang, J. Y., Jin, J. L., Pagano, T. C., Calow, R., Bao, Z. X., ... & Yan, X. L. (2012). Assessing water resources in China using PRECIS projections and a VIC model. Hydrology and Earth System Sciences, 16(1), 231-240.

Wells, J. V. B. (1960). Compilation of records of surface waters of the United States through September 1950. Part 1-B, North Atlantic slope basins New York to York River (No. 1302). US Govt. Print. Off.

Zhang, J. Y., & Wang, G. Q. (2007). Impacts of climate change on hydrology and water resources. Science and Technology Press, Beijing (in Chinese).

CHAPTER 2 : MODELING MONTHLY ACTUAL EVAPOTRANSPIRATION: AN APPLICATION OF GEOGRAPHICALLY WEIGHTED REGRESSION TECHNIQUE IN THE PASSAIC RIVER BASIN

Short title: Modeling of monthly actual evapotranspiration

Felix Oteng Mensah[*^], Clement Aga Alo[**]

Published in *Journal of Water and Climate Change* (https://doi.org/10.2166/wcc.2022.111)

[*,**]Department of Earth and Environmental Studies, Montclair State University, 1 Normal Avenue, Montclair, New Jersey, USA (Email: otengf1@montclair.edu; aloc@montclair.edu)

^ Corresponding Author

2.1. Abstract

Actual evapotranspiration (ET) is perhaps the most difficult quantity to directly measure among the major water balance components. Because of the high cost and labor constraints associated with the direct measurement of ET, empirical data-driven modeling has frequently been used to estimate ET. Beyond the widely used traditional type regression that has the effect of producing ‘global’ parameter estimates, assumed to be uniform throughout a study area, we utilized a more localized spatially non-stationary technique — the geographically weighted regression (GWR) — to estimate mean monthly ET in the Passaic River Basin (PRB). We identified the key environmental controls of ET and developed new sets of spatially varying empirical ET models based on variable combinations that produced the best-fit model. The analysis showed that temporal and spatial variabilities in ET over the PRB are driven by climatic and biophysical factors. We found that the key controlling factors were different from month to month, with wind speed being dominant throughout the year in the study basin. A monthly mean ET index map was further generated from the model to illustrate areas where ET exceeds precipitation. This

will among others enable water loss due to evapotranspiration to be accounted for in future water supply plans for the basin.

Keywords: Evapotranspiration, Climate Change, Geographically Weighted Regression, Passaic River Basin, Water resources

2.2. Introduction

Actual evapotranspiration (hereafter referred to as ET), involving soil-water evaporation (E) and vegetation transpiration (T), plays an integral role in the transfer of water and energy within the hydrologic cycle (Gowda et al., 2007). It accounts for more than 60% of precipitation input on a global scale (Ma and Szilagyi, 2019), and about 50 —70% in the United States (Sun et al., 2002; Brooks et al., 2012). Apart from being used as index for climate change, location specific data on ET has practical significance in water resources management planning and monitoring of hydrologic systems (e.g. storage changes) in river basins (Verstraeten et al., 2008; Senay et al., 2016). However, accurate quantification of this important variable at the watershed scale is often costly and time consuming (Gasca-Tucker et al., 2007), with underlying uncertainties due to the complex array of ET processes (Li et al., 2014), and data limitation. Because it occurs in the gaseous state, unlike precipitation and streamflow, ET is also the most difficult quantity to directly measure among the major water balance components.

The literature is replete with different techniques of quantifying ET at various spatial and temporal scales. Generally, direct measurement of ET includes the lysimeter method, water balance approach, sapflow, eddy covariance (EC), Bowen Ratio methods, and stable isotope techniques (Lu et al., 2003; Williams et al., 2004; Liu et al., 2013; Sanford & Selnick, 2013; Gebler et al., 2015). While it is acknowledged that each method exhibits some inherent limitations, the eddy covariance technique is by far the most accurate (Fang et al., 2016). It continuously measures site-level fluxes to generate data series at high temporal resolution. On the other hand, recent advances in optical remote sensing (RS) have also achieved sufficient accuracy in estimating ET and is widely used at large spatial scales (e.g. Zhang et al., 2016; Reitz et al., 2017; Chen and Liu, 2020; Ma and Zhang, 2022). In estimating ET, remote sensing models employ surface energy balance formulations to partition incident solar radiation into soil heat flux, sensible heat flux, and latent heat flux. At a relatively high spatial resolution (~4km) covering broader temporal record, ET has been estimated with the TerraClimate dataset (Abatzoglou et al., 2018). The water-balance based ET product from TerraClimate has received wide acceptance in the remote sensing community due to its demonstrated skill in capturing hydroclimatic variables across different regions (e.g. Hu and Hu, 2019; Salhi et al., 2019; Xu et al., 2019; Zhao and Gao, 2019;). It was developed by combining high-spatial resolution climatological normals of temperature and precipitation from the WorldClim dataset with time-varying datasets from the Climate Research Unit data (CRU Ts4.0) and Japanese 55-year Reanalysis (JRA-55) (Abatzoglou et al., 2018). The performance of resulting RS—Water-balance-based ET model products are often evaluated using EC flux observations (e.g. Ruhoff et al., 2013; Fang et al., 2016). However, Kalma et al. (2008), after reviewing 30 published validation studies underscored that more sophisticated physical and analytical methods do not necessarily perform better in estimating ET than empirical and statistical techniques.

Because of the high cost and labor constraints associated with the direct measurement of ET (e.g. eddy covariance method), coupled with its limited coverage, empirical data-driven modeling has largely been used to estimate ET (e.g. Lu et al., 2003; Sanford & Selnick, 2013; Valipor, 2015; Fang et al., 2016). These studies cover multiple scales, use different data types, and address various research questions. Data from such studies are typically drawn from specific geographical units where a single regression is estimated for ET based on a relationship between one or more controlling factors and a dependent variable. For example, Valipor (2015) used a linear regression technique to estimate evapotranspiration from eleven (11) temperature-based models in thirty-one (31) provinces of Iran and revealed that the best model for estimating evapotranspiration performed well (R^2 values > 0.99) in only 11 out of the 31 provinces. While this traditional type of regression has seen wide utility, it has the effect of producing "average" or "global" parameter estimates which are always assumed to be uniform over the study area — an implicit assumption that has frequently been overlooked. This assumption is inherently deficient particularly when applied to environmental variables such as ET which are spatially non-stationary over a large area coverage. Fotheringham et al. (2003) noted that relationships which are not stationary, when applied in a conventional regression model, create problems for the interpretation of estimated parameters. As such, more localized approach (i.e. geographically weighted regression (GWR)), may be an ideal alternative. Geographically weighted regression belongs to the family of local statistics, comprised of multi-valued estimates as opposed to global statistics. As location changes, local statistics can take on different values. The strength of GWR lies in its ability to explain spatially varying relationships by essentially allowing model parameters to vary over space. Within a highly heterogeneous space, this type of regression will provide opportunity to make significant progress towards understanding and predicting patterns in response variables on the basis of influential environmental factors.

One terrain inviting, and perhaps requiring a more localized regression (i.e. GWR) approach is the Passaic River Basin (PRB) (Figure 2.1). The PRB is a highly diverse and complex basin with substantial heterogeneity in land use, soils, geology, reservoirs, vegetation, slope, and topography. It has been distinctly separated into three sections: The Highlands Area, the Central Basin, and the Lower Valley. Trending northeast—southwest in the basin is the mountainous heavily-forested Highlands, which is by far the largest, and well noted for its pristine and environmental integrity. The Central Basin is described as the hydrologic centerpiece of the PRB (USACE NY District, 1987), with its many wetlands serving as buffer to flood waters generated from the Highlands region. The Lower Valley, as opposed to the Highlands, is a densely-populated, highly industrialized urban belt forming the eastern flank of the basin and features the tidal, saline lower reach of the Passaic River. In the New Jersey Water Supply Plan, 2017—2022 (NJDEP,2017), there is the recognition that the biophysical arrangement within New Jersey's five (5) water regions, including the PRB, represents a complex array of competing interests and issues in respect of water use and demand. Consequently, the amount of water loss due to evapotranspiration from reservoirs, vegetation, and soil, is unaccounted for in the water supply plan due to unavailability of reliable and complete data. Yet ET is considered as the primary determinant of available water resources. It is the water that would otherwise become streamflow if not released into the atmosphere; and this water loss constitutes on average 50 percent of the approximately 49-inches precipitation that occurs over the PRB (Newcomb, 2000).

It is therefore crucial that in order to accurately assess water resources availability in the PRB, the factors that control the amount and timing of ET in the basin be fully explored, based on which ET can be modelled and reliably quantified. This has become even relevant at this time in light of the pressing need to predict future water stress and risks in the context of climate change (e.g. NJDEP, 2017). Given the widely diverse and heterogeneous character of the basin, it will be necessary to identify and analyze the role that internal (e.g. biophysical) characteristics and external (e.g. climatic) conditions play in the spatial distribution of actual evapotranspiration within a spatiotemporal framework.

In that regard, the objectives of this study are to: 1) use the classical ordinary least square (OLS) method to identify and determine the major internal (i.e. leaf area index (LAI), elevation) and external (i.e. mean temperature, precipitation, dew point, mean vapor pressure deficit (VPD), solar radiation, wind speed) controls on ET at monthly time scale; and 2) employ GWR to develop spatially varying mathematical models from readily available datasets that can be used to estimate monthly ET within the PRB.

2.3. Materials and Methods

2.3.1. Study Area

The non-tidal Passaic River Basin is an oval-shaped area of about 2,135 square kilometers (824 square miles), of which about 84 percent is located in New Jersey and the rest in New York State (Figure 2.1). The surface elevation in the basin ranges from below sea level at 0.2m (0.66ft) to 454m (1490ft). As previously mentioned, physiographically, the basin is divided into three main regions: the series of parallel ridges that trend northeast/southwest forming the Highlands; the Central Basin, comprised of large areas of swamps and meadows; and the roughly flat Lower Valley.

According to Paulson et al. (1991), New Jersey is located in a modified continental climate zone (i.e. with hot summer and cold winter). Five different climate zones have been identified: North, Central, Southwest, Pine Barrens, and Coastal zones, with PRB located within the North and Central zones. Temperatures in the North are about 10 ºF colder than the coastal zone with above 90 ºF commonly observed within the Central zone during warm seasons. Annual precipitation typically ranges from 1016mm to 1321mm (40 to 52 inches), with peak values observed along the coast during summer and winter (Paulson et al., 1991). On average, approximately 1245mm

(49 inches) of precipitation occurs in the PRB annually (Newcomb, 2000). Of this, about 50 percent is lost to the atmosphere through evapotranspiration, another 5 percent becomes surface runoff, and the remaining 45 percent becomes available as recharge to groundwater aquifers (Mitchell 1992 as cited in NJ Watershed Basins, n.d).

Land use/ land cover patterns in the basin is dominated by forest type vegetation. According to the 2011 National Land Cover Dataset (NLCD) (https://www.mrlc.gov/viewer/), approximately 43% of the area is forested; 36% developed; 14% Woody Wetlands; 3% open water and the remaining 4% comprising of other land cover types. Land use decisions in the basin continue to

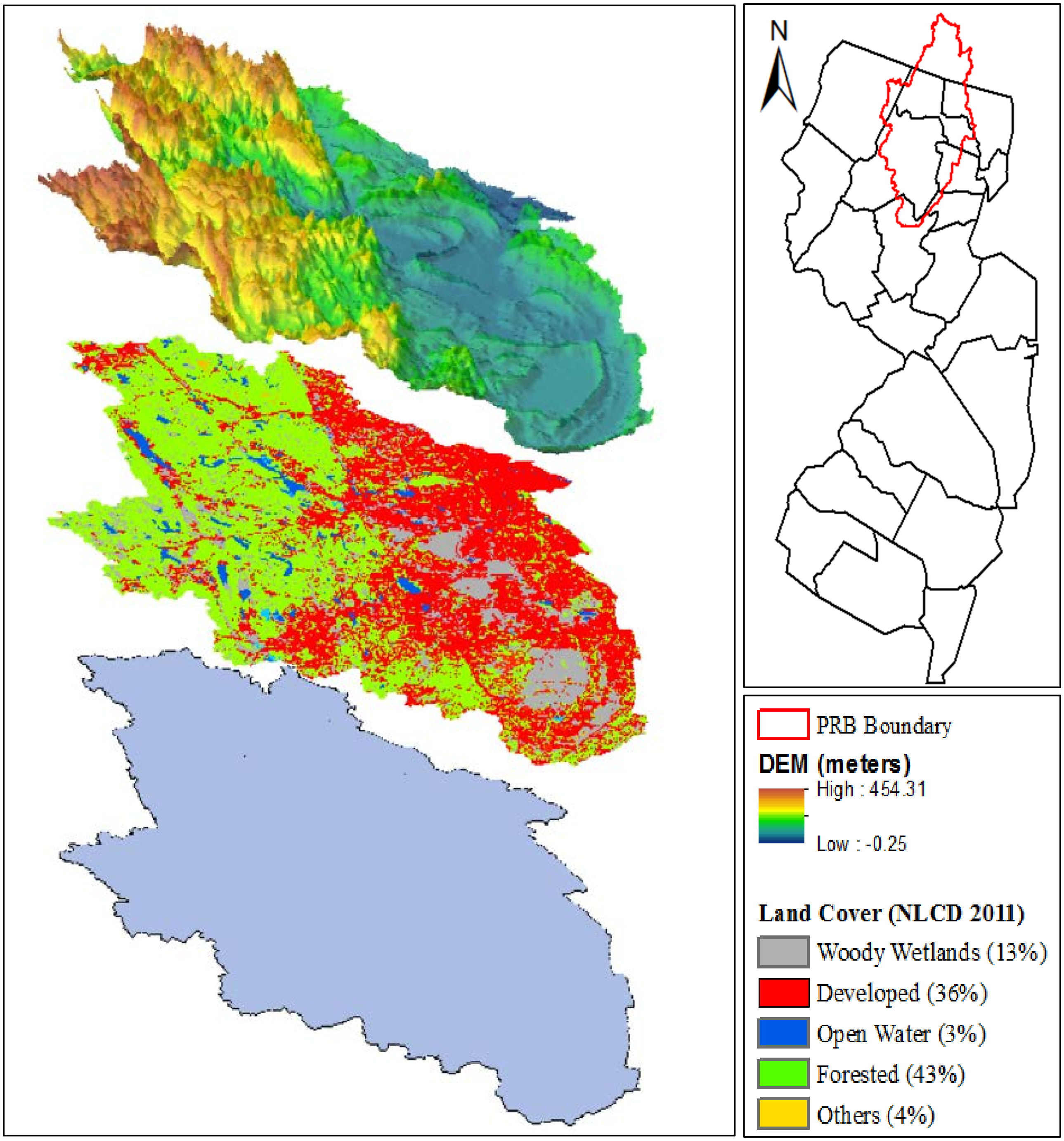

Figure 2.1: Physiographic map of the Passaic River Basin

encourage flood events, with direct and indirect consequence on water resources (i.e. in terms of flow, water quality, and water quantity). Driven by socioeconomic and biophysical factors, many communities in the lower urbanized section of the basin are close to being built out. Meanwhile, the Highlands region is currently undergoing suburban and rural development (NY Rapid Assessment Profile, 2011). Coupled with a historically unprecedented warming projected over New Jersey (State Climate Summaries, https://statesummaries.ncics.org/chapter/nj/), it is likely that climate and land use change will pose serious threat to the water supply systems in the basin. As climate change continues and is expected to accelerate the hydrological cycle, water resource availability and ecosystem services will be directly affected through alteration in evapotranspiration (ET) processes, and indirectly through vegetation water use.

2.3.2. Environmental factors and data sources

Gridded datasets from Parameter-elevation Regressions on Independent Slopes Model (PRISM, Oregon State University, http://prism.oregonstate.edu), TerraClimate (Abatzoglou et al., 2018) (http://www.climatologylab.org/terraclimate.html), and Moderate Resolution Imaging Spectroradiometer (MODIS) LAI product (LAADS/DAAC, https://ladsweb.modaps.eosdis.nasa.gov/search/) provided the environmental variables necessary to develop the ET models. PRISM has received wide acceptance because of its ability to reasonably reproduce weather patterns over areas with complex topography such as the study region, and serves as the official spatial climate data sets of the United States Department of Agriculture (USDA) (Daly et al., 2008). As actual observations of ET are not available for the basin, the water-balance based TerraClimate ET was used as a proxy. According to Abatzoglou et al. (2018), the accuracy of TerraClimate has been proven by its strong validation with station-based observations from meteorological networks including the Global Historical Climate Network (GHCN), Snow Telemetry (SNOTEL), and Remote Automatic Weather Stations (RAWS). TerraClimate fields of annual reference evapotranspiration also tracked well with reference evapotranspiration from FLUXNET stations (Abatzoglou et al., 2018). In the assessment of water balance through different sources of precipitation and actual ET datasets, Neto, et al. (2022) found that against other three sources, TerraClimate emerged as the most sensitive to variations in the spatial distribution of precipitation and actual ET variables. This demonstrated skill of the TerraClimate product in capturing both point and spatial observations is also corroborated by Soleimani-Motlagh et al. (2022), Wiwoho, & Astuti, (2022), and Lemenkova (2022), and therefore gives credence to its use as proxy in this study.

On the other hand, biophysical variables suggested to sufficiently explain variability in ET included precipitation (ppt, mm), air temperature (temp, ºC), dew point (dewpt, ºC), solar radiation (srad, MJm^{-2}), vapor pressure deficit (vpd, 100Pa), wind speed (ws, m/s), leaf area index (LAI), and surface elevation (elev, m) (Lu et al., 2003; Sanford and Selnick, 2013; Reitz et al., 2017). Table 2.1 provides details of data source, resolution, and time periods of each environmental variable. Further processing of the datasets was carried out using the raster calculator in ArcGIS 10.2.2 to compute mean monthly values. After converting each variable file from raster to feature class, a spatial join was performed to obtain attributes of all the environmental variables in a single layer. Rather than resampling which tends to compromise data values, a one-to-one join operation based on an intersect matching was used in the spatial join tool. This ensured that spatial relationship was still established between records of coarse versus finer resolution datasets. In the end, a single feature layer for each month containing attributes of all dependent and independent variables at 800m grid was prepared for further analysis in R (R, 2020).

2.3.3. Regression diagnostics and evaluation
Diagnosing a regression model involves using a class of techniques for detecting problems raised either by the model or the datasets that may compromise the predictive ability of the model. In arriving at an optimal model for predicting ET, environmental variables were assessed using: 1)

Pearson correlation metrics (r), 2) statistical significance, 3) Bayesian Information Criterion (BIC), 4) Mallow's Cp, and 5) adjusted R-square (R2). The presence of multi-collinearity that reveals near-redundancy among explanatory variables were also explored. Although multi-collinearity was detected, the exclusion or otherwise of explanatory variables from the model was guided by our understanding of the key processes that influenced the response variable (i.e. ET) as well as their statistical significance. Thus, because all variables were significant, and in order not to compromise the predictive ability of the model, we refrained from removing any variables just on the bases of multi-collinearity.

Table 2.1: Environmental variables used in the study

Data	**Abbrev.**	**Spatial resolution**	**Time frame**	**Source**
Dependent variable				
Actual evapotranspiration	ET	4km	1981 – 2010	TerraClimate
Independent variables				
Elevation	ELEV	800m	1981 – 2010	PRISM
Leaf Area Index	LAI	1km	2000 – 2010	MODIS
Precipitation	PPT	800m	1981 – 2010	PRISM
Minimum temperature	TEMPmin	800m	1981 – 2010	PRISM
Maximum temperature	TEMPmax	800m	1981 – 2010	PRISM
Dew point	DEWPT	800m	1981 – 2010	PRISM
Maximum vapor pressure deficit	VPDmax	800m	1981 – 2010	PRISM
Minimum vapor pressure deficit	VPDmin	800m	1981 – 2010	PRISM
Solar radiation	SRAD	4km	1981 – 2010	TerraClimate
Wind speed	WS	4km	1981 – 2010	TerraClimate

Further diagnostic analysis such as Best Subsets regression technique was performed to provide a reasonable subset of variables to include in the model. Unlike other selection techniques such as the Stepwise, the Best Subsets approach models every possible combination of variables that exist. For this study, the ten (10) independent variables underwent this technique and the best significant model selected according to a reasonable *adjusted r-square*, a lower *BIC*, and a minimum *Cp*. Note that underpinning our objectives was to identify the model with the minimum number of variables (i.e. not more than 5) that potentially provided an optimal model accuracy and whose variables are readily available from standard meteorological monitoring stations and regional remote sensing products.

2.3.4. Regression modeling approach

Classical regression modelling approaches such as OLS ride on the assumption that the statistical properties of variables (e.g. mean, standard deviation and covariance) are constant over space and time for a given area of interest. As such, parameter estimates of an OLS model is considered global. The downside to this is that important variations in the spatial pattern and relationship between independent and dependent variables are lost. The standard expression for spatially invariant OLS model is given as:

$$y_i = b_0 + \ b_h(x_{ih}) + \cdots + b_n(x_n) + \varepsilon_i \qquad \text{Equation 2.1}$$

where y_i represents a proxy ET variable, b_0, the intercept and $b_h — b_n$, the slope coefficients for the independent variables of interest $x_{ih} — x_n$ respectively that control ET, and ε_i is the error term.

In respect of environmental variables that are spatially dynamic, a better approach such as GWR was developed by Fortheringham et al. (2003). Their concept of GWR is based on Tobler's first law in Geography (Tobler, 1970) which states that "everything is related to everything else, but near things are more related than distant things". Unlike the traditional OLS regression framework, GWR allows local rather than global parameters to be estimated for each of the predictor variables. So that equation 2.1 is rewritten as:

$$y_i = b_0(u_i, v_i) + b_h(u_i, v_i)x_{ih} + \cdots + b_n(u_i, v_i)x_n + \varepsilon_i \qquad \text{Equation 2.2}$$

where (u_i, v_i) are coordinate locations of the $i-th$ point in space; $b_h(u_i, v_i)$ is the local regression coefficient for the $h-th$ independent variable of the $i-th$ point, x_{ih} is the $h-th$ independent variable of the $i-th$ point, and ε_i is the error term of the $i-th$ point.

Parameter estimates in a GWR model depend on a spatial weighting function and the selected bandwidth for model calibration. The weighting function determines the weight to assign to a local observation based on its closeness to a sample point. As formulated by Fortheringham et al. (2003), the local regression coefficients for the $i-th$ data point are estimated as:

$$\hat{b}(u_i, v_i) = [X^T W(u_i, v_i) X]^{-1} X^T W(u_i, v_i) Y \qquad \text{Equation 2.3}$$

where X is the matrices of independent variables, $\hat{b}$ represents an estimate of b in equation 2.2 and $W(u_i, v_i)$ is an $n \times n$ matrix (where n is the sample size) whose off-diagonal elements are zero and whose diagonal elements represent the geographic weighting for each n observed data around the $i-th$ data point, and Y is the vector of the dependent variable.

Here, the weighting scheme, as expressed in equation 2.4 below is applied to all observations in a certain sliding neighborhood around each data point. The size of this sliding neighborhood is the bandwidth and it determines which nearby observation is to be considered when calibrating coefficient for a data point. Bandwidths can either be constant (fixed kernel) or variable (adaptive kernel) depending on the density of data points at a location. Bandwidths are smaller where sample points are dense and larger at sparse locations (Fortheringham et al., 2003; Tu and Xia, 2008). A fixed bandwidth was chosen in this study because of the gridded structure of the datasets. Two schemes of weighting function can be used in calculation: Gaussian and the bi-square. In this study, the Gaussian scheme, suited for modelling numerical rather than binary response variables, was chosen. It is expressed as:

$$\omega_{ij} = \exp\left(\frac{-d_{ij}^2}{b^2}\right) \qquad \text{Equation 2.4}$$

where ω_{ij} is the weight observation j exerts at data point i, d_{ij} is the distance between observation i and j and b is the kernel bandwidth. Weight rapidly approaches zero when the distant observations is greater than the kernel bandwidth (Tu and Xia, 2008). The optimal bandwidth was selected automatically with the **spgwr** R package based on the corrected Akaike information criterion (AICc).

2.3.5. Evaluation of model performance

Performance of the modelled actual ET was evaluated based on two approaches: 1) an external basin-scale validation, and 2) an internal metric-based validation. For the external validation, precipitation, discharge, and storage data were utilized to estimate basin-level water balance ET for comparison with geographically weighted ET (GW ET). Total annual precipitation was based on the gridded 4km PRISM dataset (Daly et al., 1994). Discharge data at the outlet of the study basin (i.e. Passaic River at Little Falls NJ, site 01389500) was obtained from the USGS water data website (USGS, https://waterdata.usgs.gov/nwis/), and change in storage from Gravity Recovery and Climate Experiment (GRACE) data (Watkins et al., 2015; Wiese et al., 2019). Specifically, we used version 2 RL06 0.5° × 0.5° grids processed by the National Aeronautics and Space Administration (NASA) Jet Propulsion Laboratory (JPL) (https://grace.jpl.nasa.gov/data/get-data/jpl_global_mascons/). Constrained by the available time range of GRACE data as well as the end of our analysis period, we carried out our comparison for 2003—2010. The data were processed and aggregated into annual precipitation, annual discharge, and annual change in storage over the PRB to compute ET using the water balance equation (e.g. Ma and Szilagyi, 2019) below:

$$\mathrm{WBET} = \mathrm{P} - (\mathrm{Q} \pm \Delta \mathrm{S}) \qquad \text{Equation 2.5}$$

where P, Q, and ΔS are annual basin precipitation, basin discharge, and change in storage, respectively. Because of the tendency of water balance not closing at monthly scale, we chose to do the validation over the annual scale although our model was developed on a monthly basis (e.g. Ma et al., 2021). Indeed, water balance-based ET (WBET) validation is not new. It has been used extensively to verify remote sensing-based ET at regional and watershed scales (e.g. Zhang et al., 2010; Senay et al., 2011; Velpuri et al., 2013; Senay et al., 2016, Ma et al., 2021). In their study, Senay et al. (2016) used WBET to validate Landsat8-based ET estimates.

For the internal variable evaluation, three metrics were used to assess the performance of the geographically-weighted ET model. They are:

- The local coefficient of determination (local R^2), which denotes how much the model explained the variability in the independent variables.
- The prediction error (PE), which expresses the difference between Terraclimate ET and modelled geographically-weighted ET.
- The corrected Akaike Information Criterion (AICc), which estimates the quality of models relative to each other for a given set of data.

2.4. Results and Discussion

2.4.1. Model comparison analysis

Comparison of annual water balance-based ET (WBET) with aggregated annual geographically weighted modelled ET (GWET) is depicted in Figure 2.2, Table 2.2. GWET compared reasonably well with the WBET over the basin for the 2003—2010 validation period. The calculated water balance ET was, however slightly pronounced as against the modelled ET with

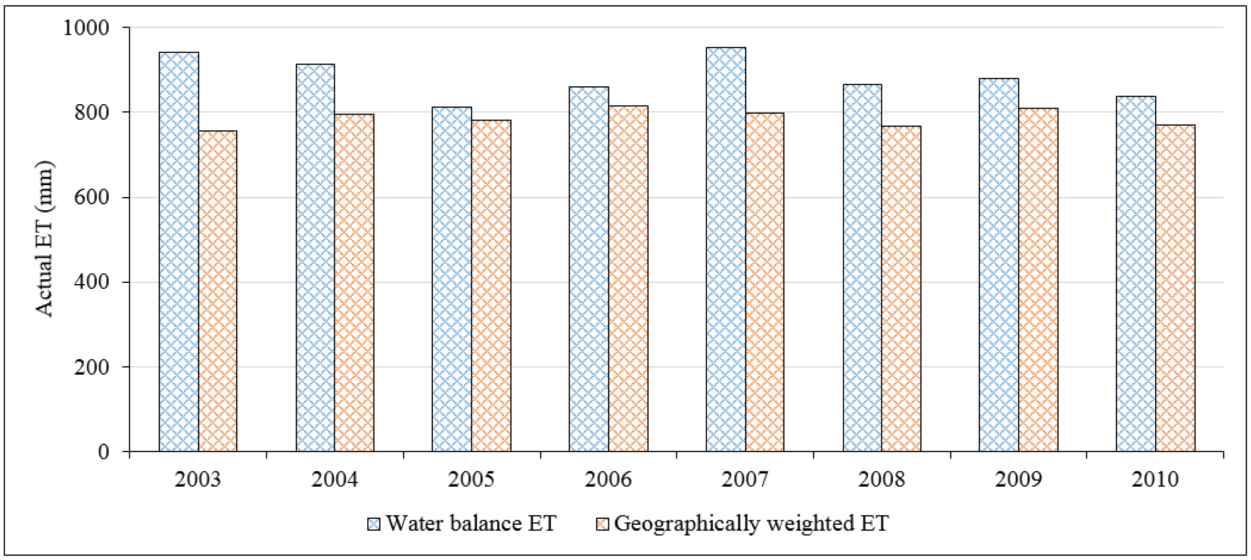

Figure 2.2: Comparison of the annual (2003—2010) geographically weighted modelled ET with ET water balance-based ET in the PRB

a mean bias of approximately 11 percent. This could be attributed to the numerous open water bodies within the basin. The runoff — rainfall coefficients (Q/P) of less than 0.55 in Table 2.2 are indicative of water balance closure. Velpuri et al. (2013) found that, coefficients more than 0.55 suggest dominant regional groundwater flows, and such conditions could introduce errors in the water balance computation thereby affecting closure. Similarly, computations should not result in negative water balance (where combined (Q+S)>P) (Table 2.2).

Table 2.2: Comparison of water balance-based ET with modelled Geographically weighted ET

Year	Precip	Discharge	Grace Storage	Q/P	(Q+S)>P	WB ET	GW ET
2003	1645.21	697.50	7.07	0.42	704.57	940.64	757.66
2004	1366.83	455.57	-1.73	0.33	453.84	913.00	796.89
2005	1343.87	531.78	0.79	0.40	532.58	811.30	780.92
2006	1392.75	531.44	0.91	0.38	532.36	860.39	815.67
2007	1383.73	432.44	-2.56	0.31	429.88	953.85	798.63
2008	1344.85	477.88	2.31	0.36	480.19	864.66	768.27
2009	1281.54	403.08	-0.28	0.31	402.80	878.74	809.98
2010	1327.27	491.78	-2.14	0.37	489.64	837.63	770.69

Over the entire PRB, the geographically weighted regression model successfully predicted the magnitude and seasonal ET patterns derived from the observed environmental variables (i.e. PPT, TEMP, DEWPT, SRAD. VPD, WS, LAI, ELEV). Figures 2.3 and 2.4 respectively illustrate ET from TerraClimate data and that predicted by the GW regression model over the PRB. Their close semblance demonstrates the clear spatial and seasonal patterns featured in the area. For approximately 95 percent of the basin’s area, the GWR model explained between 52—100 percent of the variations in monthly ET (Figure 2.5; Table 2.3). The local coefficient of determination (local R2) were all statistically significant at p-value < 0.001. These results showed the robustness and reliability of the geographically weighted ET model. There were, however, few locations in the area that showed somewhat large differences between the predicted and TerraClimate ET values. These were especially observed in the months of December, February, and March where predicted ET was either lower or higher than the

TerraClimate ET. Overall, the geographically weighted ET model was a good predictor when absolute PE values were less than 0.5 (Figure 2.6; Table 2.3).

Table 2.4 shows how the geographically weighted ET model compares with that of the traditional ordinary least square model in terms of their Akaike Information Criterion (AIC) (Akaike, 1974). The AIC determines which model performs best in associating explanatory variables to the dependent variable. A model with smaller AIC value is considered better as it is more likely to minimize information loss in contrast to the 'true' model that generates the observation data (Burnham and Anderson, 2002). The smaller AIC values obtained by the geographically weighted ET model in this study further corroborates the point that spatially non-stationary local models are an ideal alternative to the global ordinary least square models when explaining spatially varying relationships over large scale.

Table 2.3: Summary of monthly local coefficient and prediction error from the GWR ET model

	Jan	Feb	Mar	Apr	May	Jun	Jul	Aug	Sep	Oct	Nov	Dec
					Local coefficient of determination							
Minimum	0.374	-0.156	0.215	0.074	-0.122	-0.339	0.089	-0.169	0.275	-2.372	-1.590	-0.351
1st quantile	0.809	0.729	0.717	0.739	0.715	0.662	0.669	0.709	0.767	0.694	0.759	0.770
Median	0.883	0.858	0.815	0.815	0.846	0.824	0.791	0.864	0.822	0.879	0.911	0.880
Mean	0.867	0.820	0.793	0.801	0.808	0.778	0.776	0.813	0.810	0.805	0.851	0.846
Standard Deviation	0.098	0.148	0.124	0.113	0.157	0.180	0.141	0.171	0.100	0.225	0.162	0.143
3rd quantile	0.947	0.941	0.883	0.883	0.936	0.926	0.900	0.954	0.879	0.966	0.973	0.960
Maximum	1.000	1.000	0.996	0.998	0.999	1.000	0.999	1.000	0.983	1.000	1.000	1.000
					Prediction	error						
Minimum	-0.980	-1.443	-4.550	-1.021	-1.622	-1.087	-1.654	-0.651	-1.959	-1.069	-1.161	-1.444
1st quantile	-0.031	-0.050	-0.235	-0.090	-0.043	-0.028	-0.058	-0.023	-0.094	-0.024	-0.031	-0.042
Median	0.000	0.000	0.001	-0.001	-0.001	0.000	-0.001	0.000	-0.002	0.000	0.000	0.000
Mean	-0.001	0.000	0.008	0.004	0.000	0.000	0.002	0.000	0.000	-0.001	0.001	-0.002
Standard Deviation	0.112	0.148	0.803	0.220	0.205	0.121	0.203	0.087	0.238	0.124	0.154	0.224
3rd quantile	0.034	0.044	0.223	0.093	0.041	0.027	0.056	0.022	0.092	0.020	0.032	0.044
Maximum	0.903	1.715	6.410	1.376	2.329	1.134	2.117	0.614	1.646	1.367	1.495	1.768

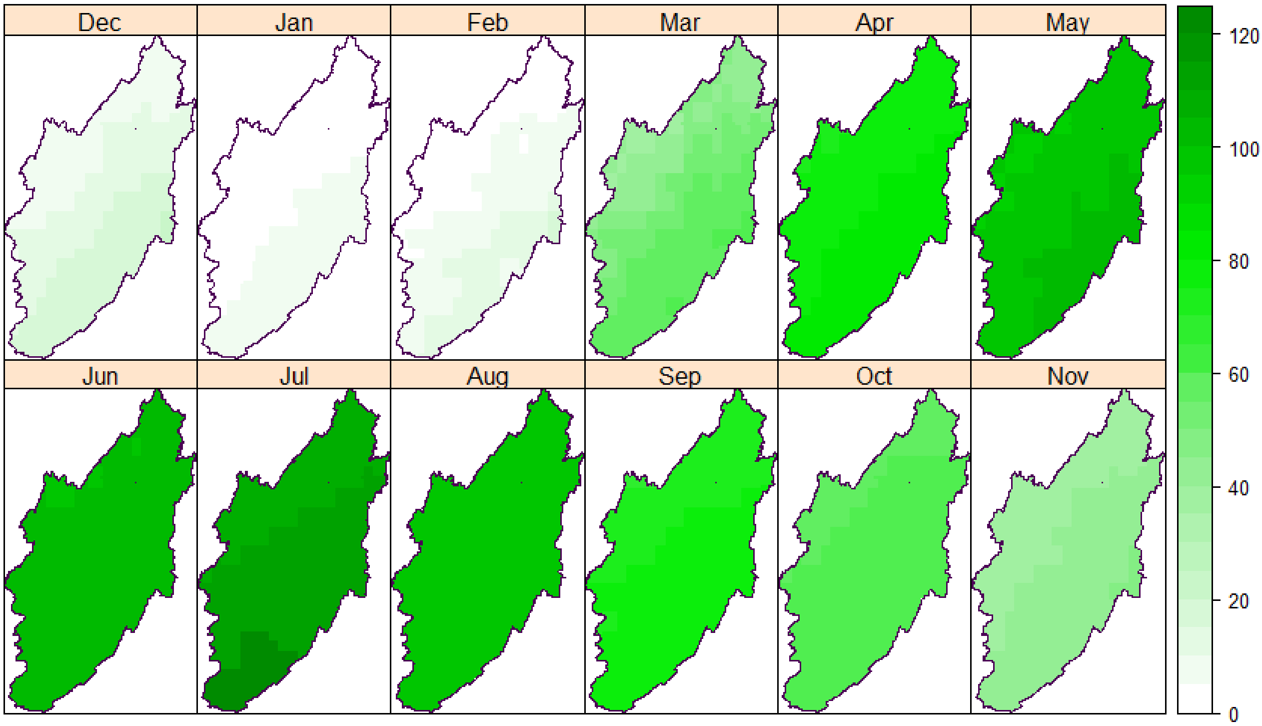

Figure 2.3: Monthly actual evapotranspiration (mm/month) maps of the Passaic River Basin from the TerraClimate dataset

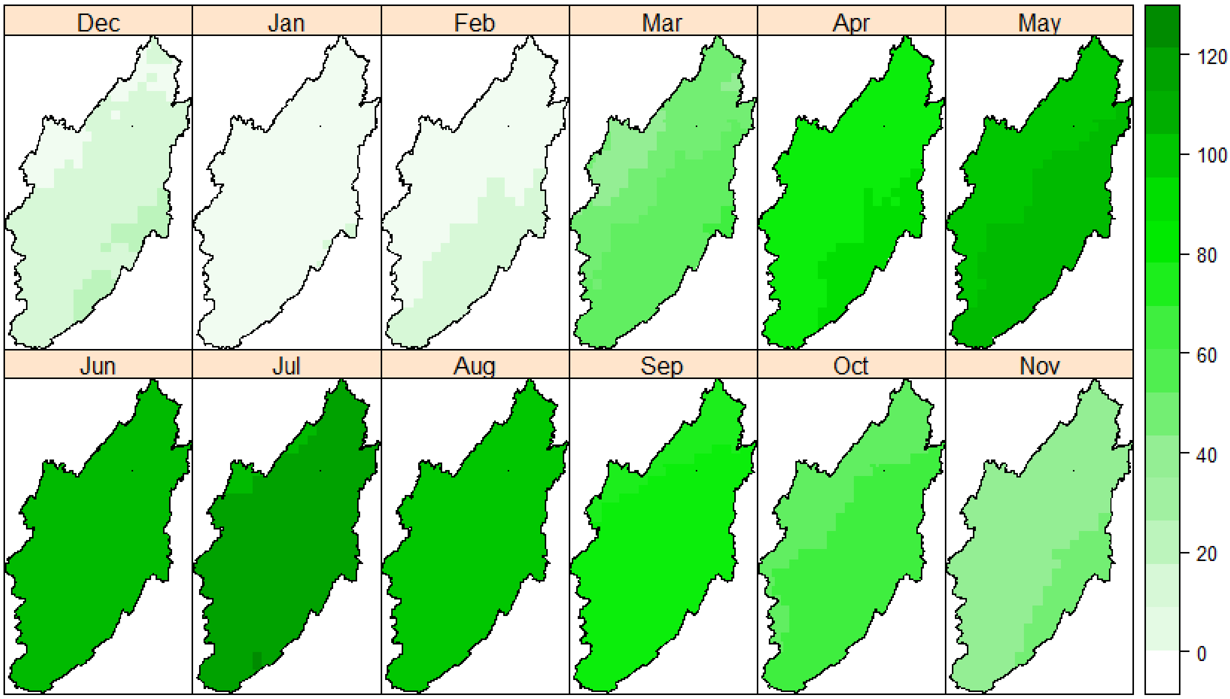

Figure 2.4: Modelled monthly actual evapotranspiration (mm/month) maps of the Passaic River Basin from Geographically Weighted Regression

Potential sources of uncertainty associated with the modeled ET can be linked to the corresponding uncertainties inherent in the TerraClimate data, remote sensing LAI data from MODIS, and other meteorological data from PRISM. For instance, any existing noise or errors in the MODIS LAI product will be propagated in the ET mathematical model. Additionally, relatively coarse grid cells from the MODIS LAI (1km) as well as TerraClimate data (4km) were applied to an 800m grid for the study basin to derive the ET model. At such smaller resolution, the MODIS LAI, for instance, may not sufficiently capture sub-grid scale vegetation signals in the basin, especially where the topography and land cover are highly complex and spatially heterogeneous, and thus introduce some errors in the model. Likewise, the coarse grid size of the radiative and aerodynamic variables obtained from the TerraClimate products may present some degree of errors to the derived ET model. In the course of our analysis, it was observed that the accuracy of ET estimates was largely dependent on the meteorological datasets. For the most part, these datasets, obtained from PRISM at a resolution of 800m, guaranteed a reasonably accurate ET model.

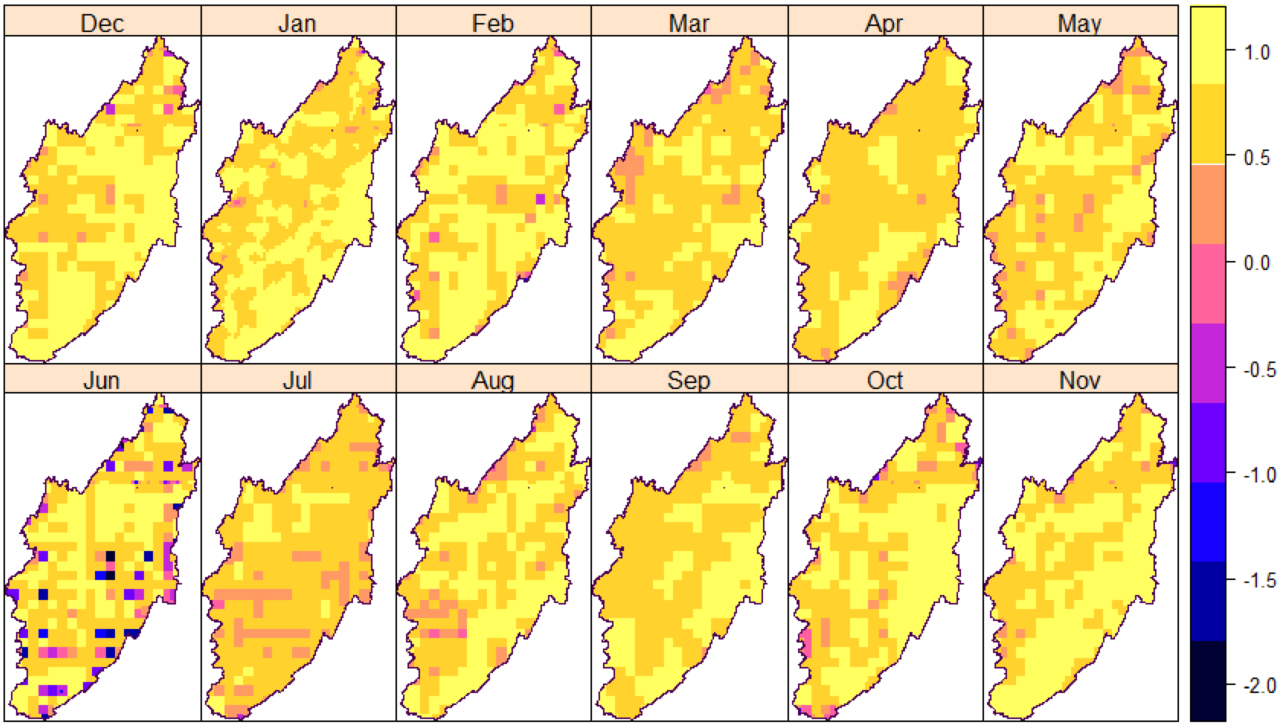

Figure 2.5: Map of local coefficient of determination for GWR over the PRB

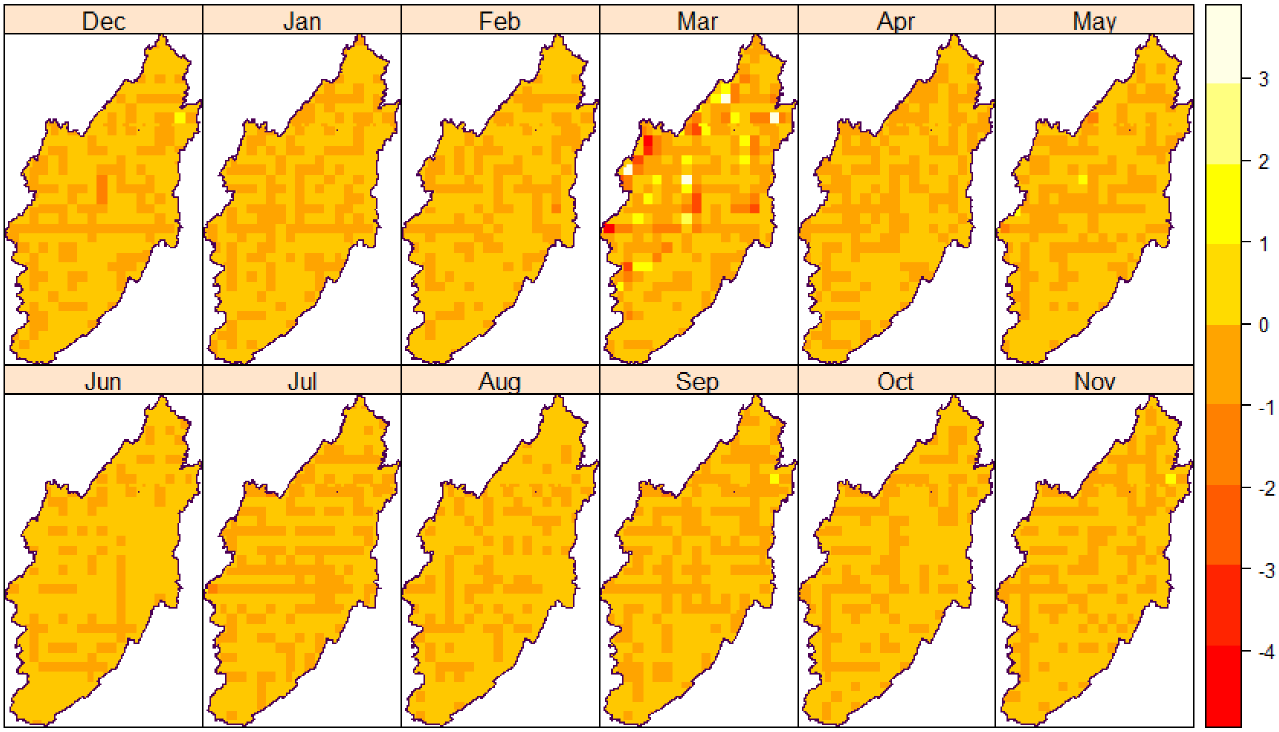

Figure 2.6: Map of residual error for GWR over the PRB

Table 2.4: Monthly comparison of Akaike Information Criterion of ordinary least square and geographically weighted regression models

	OLS AICc	**GW AICc**
Jan	4507	-898
Feb	8642	2490
Mar	14829	10490
Apr	6920	1545
May	7982	1495
Jun	5849	-1217
Jul	8172	1307
Aug	3504	-4059
Sep	7629	2082
Oct	6269	-1212
Nov	5991	-38
Dec	9088	2776

2.4.2. Spatiotemporal patterns of ET in the Passaic River Basin

The geographically-weighted ET model was carried out over the diverse physiographical and biophysical terrain of the PRB from 1981—2010 at $800 \times 800m$ grid resolution. Based on the ET maps (Figures 2.2 and 2.3), there is evidence of sharp basin-wide variation and longitudinal gradients of ET, with lower values trending from northwest to higher values in the southeast. Generally, the ET patterns reflect the climatic conditions at the time and varies depending upon land use/land cover type, topography, and availability of water. Lower values are typically observed in the north climate zone where the temperatures are relatively low, with high topographic relief and largely forested vegetation cover. Mean annual ET value of about 748mm/year is estimated in the upper mountainous region. In contrast, the high ET values are seen in the central climate zone where temperatures are intermediate to high, and in highly developed urban communities. Estimated mean annual ET is approximately 793mm/year. Although some uncertainties are present and methodologies may differ, the magnitude and spatial patterns of the estimated ET rates over the PRB are consistent with other investigations in the vicinity (e.g. Sumner et al., 2012).

Mean monthly ET rates over the basin from 1981—2010, based on the TerraClimate as well as the GW-modelled ET show distinct seasonal fluctuations (Figures 2.2 and 2.3). The temporal patterns of ET and their spatial variability reflect the controlling effects of prevailing climatic conditions as well as the vegetation distribution. In order of magnitude, ET rates in the PRB are generally greater in the summer months (Jun-Jul-Aug), followed by spring (Mar-Apr-May), fall

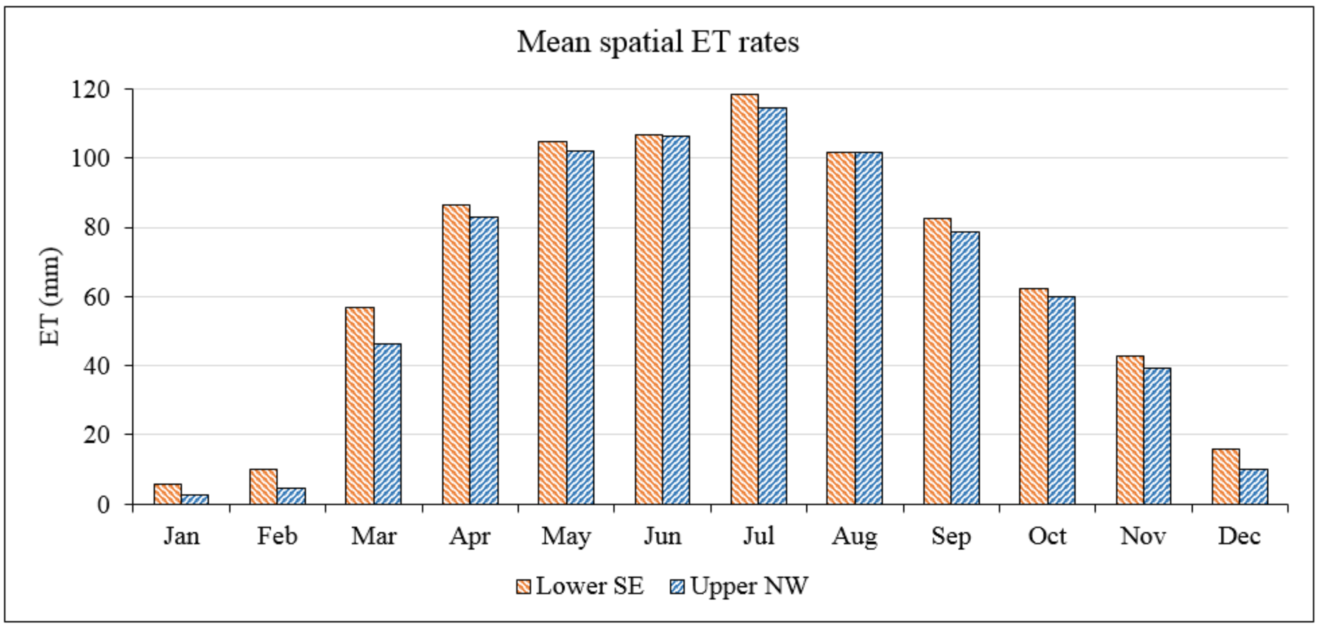

Figure 2.7: Mean monthly spatial ET rates in the lower and upper halves of the PRB

(Sep-Oct-Nov), and winter months (Dec-Jan-Feb). In the summer months, particularly July, the lower southeast half of the basin shows significantly high ET values because of relatively warm temperature and high radiation (Figure 2.7).

In contrast, low ET rates are observed in the largely forested upper northwest half because of precipitation deficit. Although vegetation and water bodies typically dominate the upper half, the winter months show significantly low ET values as a result of relatively low mountainous temperatures and sparse deciduous vegetation. Following the trajectory of ET rates in Figure 2.7 [monthly time series], it can be seen that ET values in all the months are higher in the lower SE half than the upper NW portion of the basin. The lowest mean ET values are observed in January (Lower SE: 5.65mm; Upper NW: 2.53mm) and the highest values in July (Lower SE: 118mm; Upper NW: 115mm).

2.4.3 Dominant controls on monthly ET

Pearson correlation coefficient values show that elevation correlates strongly with ET across all seasons (Table 2.5). This is followed by energy inputs (DEWPT>TMAX>TMIN>SRAD), aerodynamic input (i.e. WS), atmospheric demand (VPD_MAX>VPD_MIN), vegetation biomass (i.e. LAI), and water input (i.e. PPT) in that order. After elevation, the two most important drivers on monthly ET were DEWPT and TMIN in the winter and spring, DEWPT and TMAX in the summer, and SRAD and TMAX in the fall. Interestingly, the strength of the correlation of explanatory variables with ET is relatively weak in the summer (i.e. <0.5) across the study basin, although these variables are, to a large extent, strongly correlated among themselves. It was also noted that PPT correlated negatively with ET in all seasons except in the summer, suggesting that water was not available to meet evaporative demand.

The Best Subset regression technique afforded the opportunity to select at most five (5) out of the ten (10) variable combinations that produced the best-fit ET model for each month. As represented in Table 2.6, the estimated coefficients from OLS regression revealed the most influential variables that control monthly ET. For example, four (4) variables (WS, TMAX, LAI, and ELEV) explained 93% of the variability in ET in November. Wind speed (WS) shows a strong positive influence on ET followed by TMAX, LAI and ELEV in that order. Indeed, WS appears to be the most dominant ET controlling factor throughout the year, appearing in 10 out of the 12 months. Quite notably, details of the relatively weak correlation observed between environmental variables and ET in the summer is revealed clearly in the month of June. While it may appear that only 39% of the variability in ET has been explained by the 5 variables, it is worth pointing out that all the 10 variables included in the model could only explain approximately 41% of variability in ET for June. This counters what may be construed as the model's inability to predict ET in the summer. It clearly indicates that the model is quite robust and largely represents the key processes that strongly influence monthly ET in the study basin. More so, corresponding Mallow's Cp and BIC were relatively low compared to other model sets. Lower Cp and BIC are indicative of relatively precise and best model respectively. Thus, the surprisingly large unexplained variance in the relationship for June may be attributed to some inherent data error propagated from the source data.

Table 2.5: Pearson correlation coefficient between ET and independent environmental variables

	AET	ELEV	DEWPT	LAI	PPT	SRAD	TMAX	TMIN	VPD_MIN	VPD_MAX	WS	AET	ELEV	DEWPT	LAI	PPT	SRAD	TMAX	TMIN	VPD_MIN	VPD_MAX	WS
AET	1						Winter					1						Spring				
ELEV	-0.89	1										-0.88	1									
DEWPT	0.89	-0.93	1									0.8	-0.87	1								
LAI	-0.49	0.43	-0.42	1								-0.5	0.45	-0.41	1							
PPT	-0.37	0.47	-0.4	0.26	1							-0.24	0.33	-0.37	0.1	1						
SRAD	0.86	-0.77	0.8	-0.39	-0.17	1						0.44	-0.48	0.55	-0.13	-0.15	1					
TMAX	0.86	-0.91	0.88	-0.38	-0.3	0.84	1					0.77	-0.86	0.84	-0.37	-0.17	0.64	1				
TMIN	0.88	-0.91	0.96	-0.45	-0.48	0.7	0.79	1				0.82	-0.82	0.88	-0.45	-0.37	0.28	0.7	1			
VPD_MIN	0.62	-0.56	0.6	-0.37	-0.48	0.3	0.38	0.79	1			0.39	-0.31	0.27	-0.32	-0.18	-0.15	0.13	0.66	1		
VPD_MAX	0.77	-0.81	0.73	-0.33	-0.23	0.78	0.97	0.64	0.23	1		0.63	-0.7	0.61	-0.29	-0.01	0.65	0.93	0.45	0.03	1	
WS	0.7	-0.51	0.51	-0.4	-0.35	0.43	0.41	0.65	0.76	0.32	1	0.69	-0.54	0.44	-0.42	-0.07	0.16	0.42	0.63	0.58	0.32	1
AET	1						Summer					1						Fall				
ELEV	-0.42	1										-0.83	1									
DEWPT	0.4	-0.85	1									0.74	-0.86	1								
LAI	-0.32	0.5	-0.46	1								-0.55	0.5	-0.5	1							
PPT	0.34	0.22	-0.2	0.11	1							-0.28	0.42	-0.51	0.28	1						
SRAD	0.03	-0.27	0.31	0.02	-0.22	1						0.75	-0.74	0.69	-0.39	-0.36	1					
TMAX	0.39	-0.91	0.85	-0.44	-0.24	0.32	1					0.8	-0.86	0.75	-0.42	-0.31	0.83	1				
TMIN	0.36	-0.8	0.86	-0.49	-0.12	0.01	0.78	1				0.66	-0.74	0.88	-0.46	-0.38	0.4	0.53	1			
VPD_MIN	0.13	-0.36	0.29	-0.33	0.02	-0.4	0.33	0.73	1			0.18	-0.13	0.24	-0.18	0	-0.24	-0.09	0.66	1		
VPD_MAX	0.34	-0.8	0.62	-0.37	-0.23	0.33	0.94	0.57	0.23	1		0.59	-0.58	0.33	-0.22	-0.07	0.69	0.87	0.1	-0.33	1	
WS	0.37	-0.66	0.54	-0.49	-0.05	-0.05	0.64	0.75	0.66	0.56	1	0.78	-0.59	0.57	-0.46	-0.08	0.43	0.48	0.71	0.54	0.24	1

Table 2.6: Best fit ET models according to key monthly environmental variables controlling ET

Variable	Jan	Feb	Mar	Apr	May	Jun	Jul	Aug	Sep	Oct	Nov	Dec
					Estimated Coefficient							
(Intercept)	-6.0217 ***	-14.1613 ***	20.7849 ***	59.2585 ***	85.7725 ***	92.6907 ***	291.3125 ***	49.7324 ***	25.6541 ***	43.5208 ***	9.0569 ***	-10.7300 ***
TMIN	0.3401 ***	-	-	-	0.8166 ***	-	7.4594 ***	-	-	-	-	-1.6440 ***
TMAX	-7.6322 ***	-9.9541 ***	-	0.5113 ***	-	-	-15.0457 ***	4.4419 ***	1.9057 ***	-	1.0366 ***	-
WS	3.4407 ***	5.7222 ***	8.9909 ***	5.5493 ***	4.3073 ***	-	-	3.9956 ***	7.8044 ***	5.7030 ***	6.7321 ***	8.0780 ***
LAI	-	-0.9655 ***	-	-	-	-0.0591 ***	-	-0.0297 ***	-0.1012 ***	-0.0996 ***	-0.2760 ***	-
ELEV	-	-	-	-0.0120 ***	-0.0079 ***	-0.0058 ***	-	-	-	-0.0057 ***	-0.0054 ***	-0.0096 ***
VPD_MAX	16.4220 ***	20.4178 ***	6.2951 ***	-	-	0.0872 ***	6.3268 ***	-2.1246 ***	-	0.3785 ***	-	2.6220 ***
VPD_MIN	-	-	-	-	-1.1314 ***	-0.6552 ***	-9.3819 ***	-	-2.2326 ***	-1.8201 ***	-	-
DEWPT	5.0595 ***	6.5406 ***	4.0319 ***	-	-	-	-	-2.5923 ***	-	-	-	4.1380 ***
PPT	-	-	-	-	-	0.1202 ***	0.1485 ***	-	-0.0816 ***	-	-	-
Cp	78	157	365	204	258	206	650	71	382	325	248	255
BIC	-8885	-8254	-6747	-7315	-5465	-1598	-7343	-3581	-7153	-5966	-8687	-8464
R-squared	0.93	0.92	0.87	0.89	0.81	0.39	0.89	0.67	0.89	0.84	0.93	0.93

Significant codes (p-values): 0 '***' 0.001 '**' 0.01 '*' 0.05 '.' 0.1 ' ' 1

2.4.4. Geographically weighted monthly ET models

Based on the intercept and coefficient values, a mathematical expression of the different sets of key independent variables controlling monthly ET could be formulated from Table 2.6. However, such an expression will only result in a basin-wide average value of ET, concealing the complex nuances of the spatially varying environmental factors that influence monthly ET in the basin.

A new set of mathematical models derived for monthly ET according to the GW regression analysis is presented in Table 2.7. Rather than the single, fixed value applied uniformly over space by the OLS technique, the GW regression model provides a range of values of intercepts and coefficients that reflects the local variations in environmental variables as they relate with ET in space (Table 2.7). By this, ET has been spatially mapped to key environmental variables across the PRB for each month, depicting the range of values in both intercept and coefficient. This will provide a reasonable first approximation of evapotranspiration rates and its spatial distribution to aid in the quantification of ET for water resource planning and decision making to serve communities in the largely diverse PRB.

To avoid being redundant, we only show, in Figure 2.8, the spatial map of results relating to April as revealed in the geographically weighted ET model. Tabular data for each month that includes coordinates locations can be provided upon request. A visual distribution of the coefficients of respective variables for selected months are also presented in Figure 2.9. Unlike the OLS model, the results of the GWR technique indicates a major degree of spatial and temporal variation in the relationship between ET and predictor variables in the study basin. As shown in Figure 2.8, the influence of wind speed on ET is both positive and negative. For the most part, the lower section of the basin showed a more dominant positive effect on ET whereas portions of the upper part showed a negative effect. Positive coefficient at the lower section is intuitive, given its location near the Atlantic Ocean where wind speed is high. The rate of evapotranspiration would typically be greater in very windy areas. The mostly negative coefficient observed in the upper Highlands region is a reflection of the largely forested vegetation in the area, and suggests that at a reduced wind speed, ET decreases. Although elevation and maximum temperature feature as key variables in the area, their relatively low coefficients suggest that, unlike wind speed, they are less influential in driving mean long-term ET in the month of April. Thus, unlike the OLS approach, the changing pattern in coefficients for each controlling factor is clearly depicted by the GWR analysis (Figures 2.8 and 2.9).

Table 2.7: Monthly GWR ET models for the PRB using best-fit environmental variables

Month	Geographically Weighted Model
January	$ET = (-103.36\ to\ 86.93) + (-5.22\ to\ 13.20)t_{min} + (-31.22\ to\ 45.37)t_{max} + (-12.94\ to\ 17.99)ws + (-86.16\ to\ 67.44)vpd_{max} + (-27.13\ to\ 16.51)dewpt$
February	$ET = (-397.34\ to\ 239.09) + (-154.65\ to\ 156.57)t_{max} + (-6.17\ to\ 6.74)lai + (-34.21\ to\ 64.23)ws + (-73.04\ to\ 76.19)dewpt + (-252.24\ to\ 229.25)vpd_{max}$
March	$ET = (-410.94\ to\ 395.42) + (-13.80\ to\ 18.82)dewpt + (-4.08\ to\ 1.81)ppt + (-16.30\ to\ 48.95)vpd_{max} + (-72.02\ to\ 113.97)ws$
April	$ET = (-19.82\ to\ 134.65) + (-0.018\ to\ 0.007)elev + (-17.31\ to\ 27.15)ws + (-1.29\ to\ 4.09)t_{max}$
May	$ET = (19.41\ to\ 243.40) + (-7.76\ to\ 4.91)t_{min} + (-32.82\ to\ 24.94)ws + (-0.025\ to\ 0.012)elev + (-35.43\ to\ 28.40)vpd_{min}$
June	$ET = (-796.63\ to\ 770.43) + (-1.05\ to\ 0.59)lai + (-0.13\ to\ 0.035)elev + (-27.82\ to\ 7.49)ppt + (-12.48\ to\ 20.06)vpd_{max} + (-52.21\ to\ 28.46)vpd_{min}$
July	$ET = (-508.31\ to\ 904.23) + (-4.29\ to\ 2.05)ppt + (-53.64\ to\ 44.52)t_{max} + (-26.68\ to\ 23.79)t_{min} + (-16.59\ to\ 21.88)vpd_{max} + (-32.92\ to\ 46.85)vpd_{min}$
August	$ET = (-689.15\ to\ 641.54) + (-7.15\ to\ 12.25)ws + (-30.08\ to\ 23.61)vpd_{max} + (-0.304\ to\ 0.123)lai + (-52.08\ to\ 70.33)t_{max} + (-37.84\ to\ 33.08)dewpt$
September	$ET = (-87.56\ to\ 191.84) + (-2.07\ to\ 5.57)t_{max} + (-0.163\ to\ 0.122)lai + (-8.06\ to\ 0.61)ppt + (-38.71\ to\ 22.25)ws + (-22.99\ to\ 11.82)vpd_{min}$
October	$ET = (-18.73\ to\ 104.77) + (-7.31\ to\ 22.19)ws + (-0.022\ to\ 0.015)elev + (-0.307\ to\ 0.311)lai + (-4.66\ to\ 5.73)vpd_{max} + (-24.01\ to\ 30.52)vpd_{min}$
November	$ET = (-49.14\ to\ 77.67) + (-1.21\ to\ 4.24)t_{max} + (-0.965\ to\ 1.265)lai + (-0.024\ to\ 0.009)elev + (-13.97\ to\ 27.05)ws$
December	$ET = (-347.89\ to\ 504.96) + (-28.83\ to\ 25.01)t_{min} + (-30.49\ to\ 79.77)ws + (-32.40\ to\ 46.75)dewpt + (-101.82\ to\ 85.27)vpd_{max} + (-0.041\ to\ 0.057)elev$

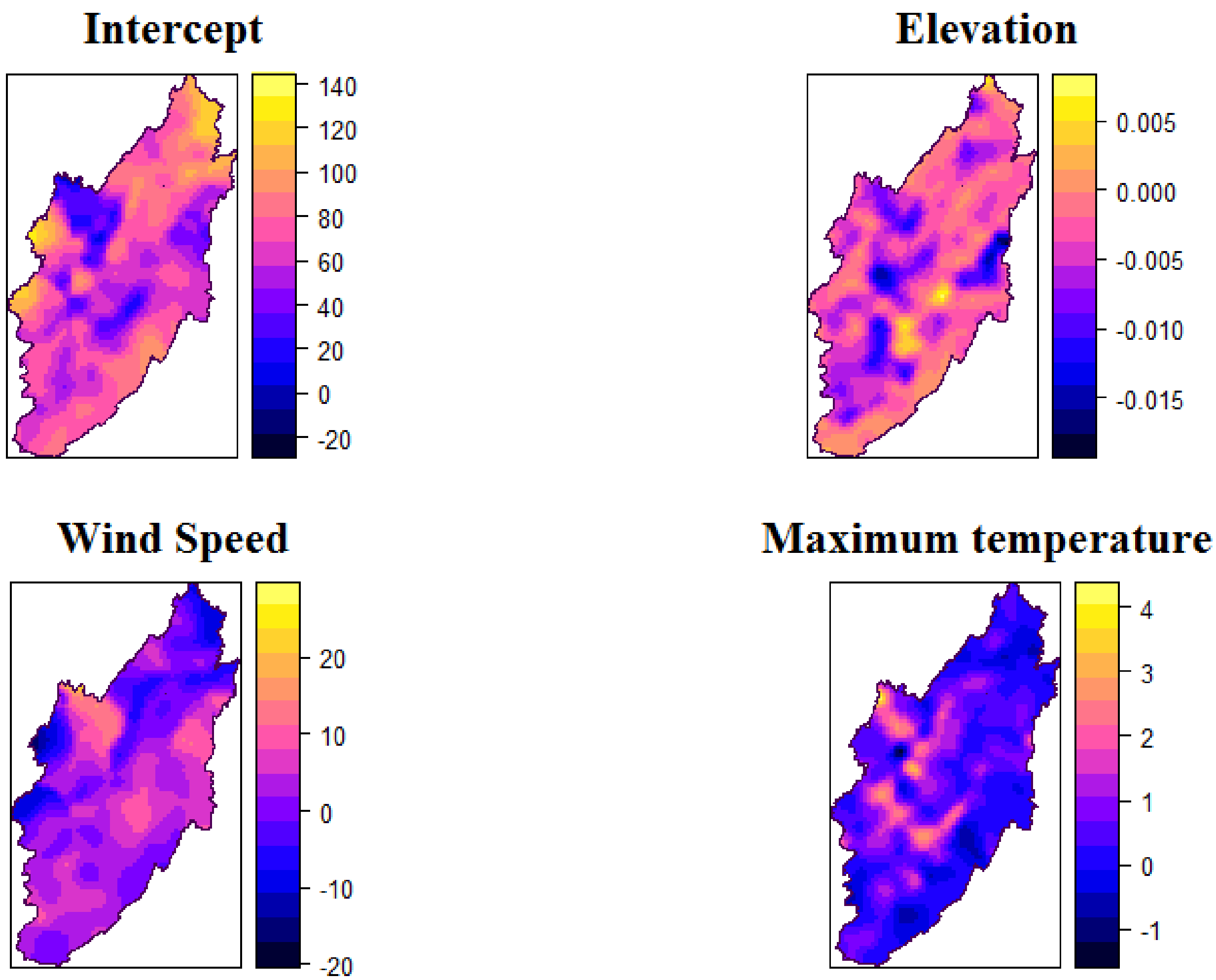

Figure 2.8: Spatial distribution of intercept and coefficients [ws (m/s), tmax (ºC), elev (m)] of key environmental variables predicting ET in April over the PRB

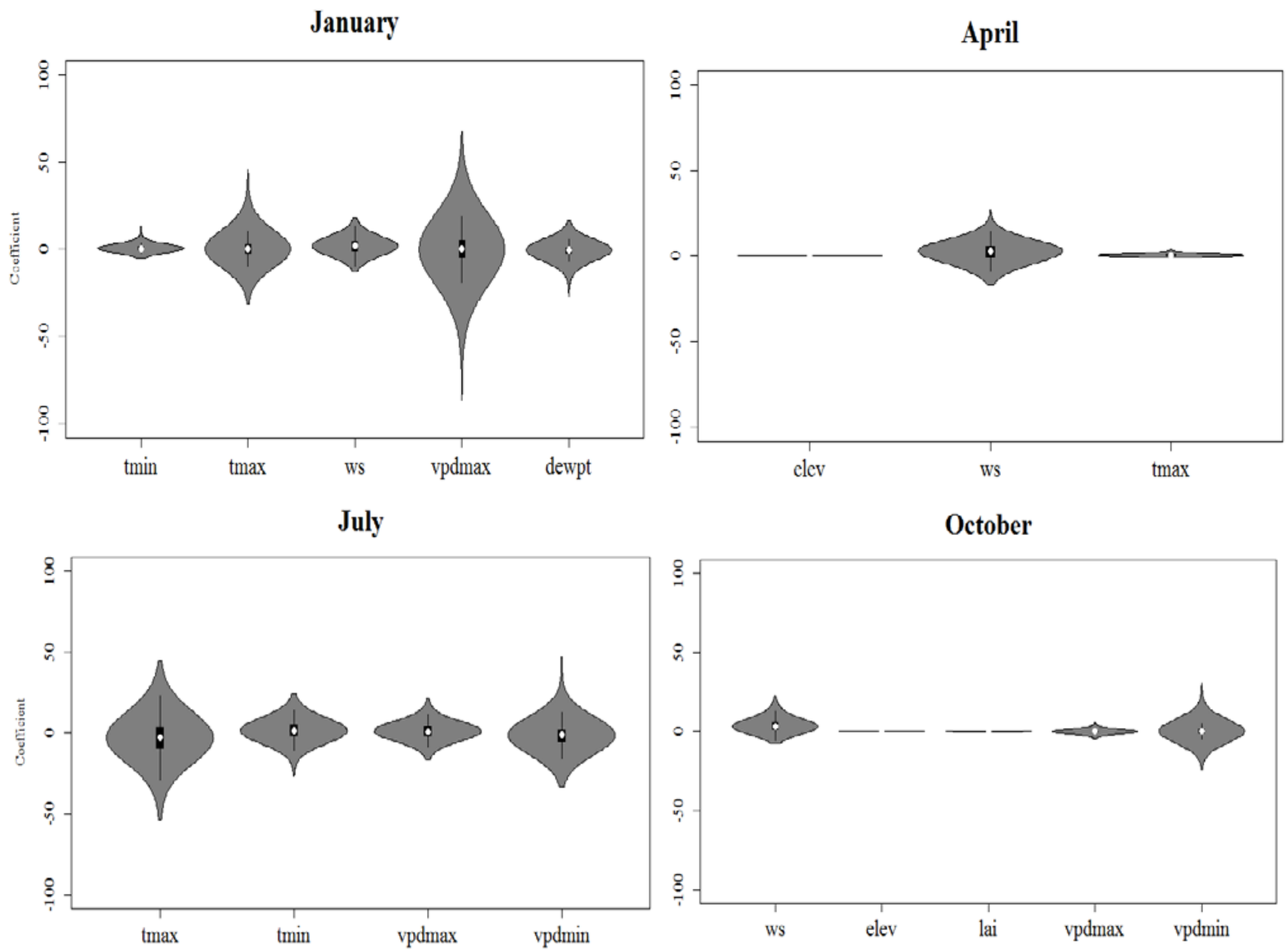

Figure 2.9: Violin plot distribution of the coefficients of key environments variables predicting ET for selected months in the PRB

Our results generally support the well-known notion that long term mean ET for a region is controlled by precipitation and potential evapotranspiration (Budyko, 1947). However, it appears that ET is insensitive to precipitation for the most part of the year in the study basin. While this could indicate that the PRB is rarely under water stress, the summer months may be an exception (see Table 2.6). Although our analyses reveal that wind speed is the main driving force behind long term mean monthly ET, precipitation, appears to be the limiting factor in the summer, particularly the month of June. Overall, a combination biophysical and climatic factors contributes to long term ET on a monthly scale. More importantly, the spatial heterogeneity that characterize the PRB brings to bare the complex challenge in appropriately quantifying ET. However, this has been made possible because of the geographically weighted regression technique adopted in this study. Flowing from our results, a monthly ET index (i.e. ET/PPT) was reproduced to show how much of precipitation is lost to evapotranspiration across the PRB (Figure 2.10).

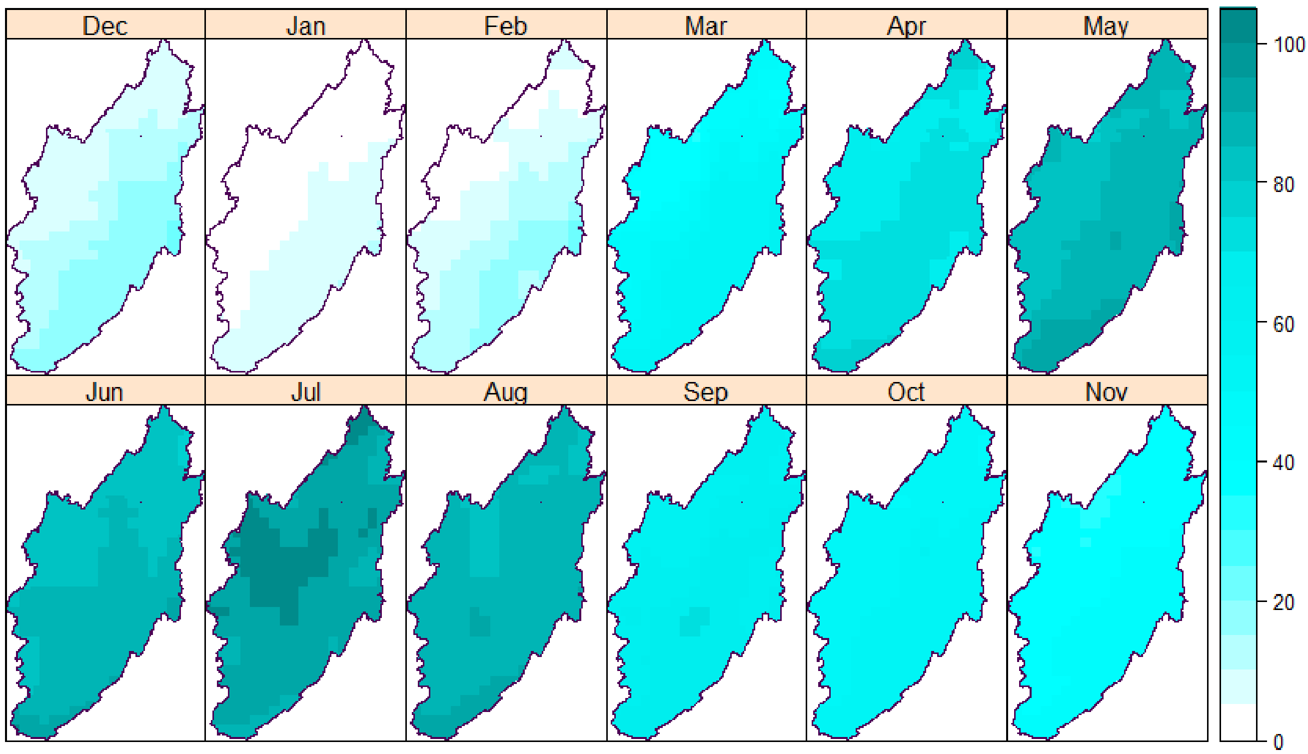

Figure 2.10: Monthly ET index (%) map over the Passaic River Basin based on GWR

While the GWR technique can be more appropriate than the global regression approaches, it is not without concerns. There are concerns raised over issues such as kernel and bandwidth selection including those shared with conventional regression techniques. However, the key issue here is that the local variation in the relationship between significant predictor variables and ET would have gone unnoticed in the commonly used global, OLS method. The monthly ET model outputs generated by the GW regression analysis offer new insights into the key external and internal controls on ET. Within the Passaic River Basin, these models can assist in effectively quantifying ET under typical climatic conditions and to a large extent, accurately estimate mean monthly ET at similar locations. Practical models such as this have been widely used to estimate ET given the huge cost involved in measuring ET on large temporal and spatial scales (Sun et al., 2011 a,b). Here, we have established a reasonably accurate non-stationary monthly ET model that uses readily available input data over the PRB.

2.5. Conclusions

The 30-year continuous ET and other gridded hydroclimatic and biophysical observations from PRISM/TerraClimate/MODIS provided the means to carefully examine and identify the key environmental variables controlling ET at a fine temporal (i.e. monthly) and spatial (i.e. 800m grid resolution) scale. From this, the best subset variables for each month were used to develop twelve (12) empirical geographically weighted ET models that will potentially estimate monthly ET over the Passaic River Basin with reasonable accuracy under mean climate conditions. These variables are readily available from any standard meteorological monitoring stations and regional remote sensing products. Key conclusions from our analyses may be summarized as follows:

1) Temporal and spatial variabilities in mean monthly ET over the PRB are significantly controlled by climatic (i.e. TEMP, WS, DEWPT, VPD, PPT) and biophysical (i.e. LAI, ELEV) drivers. The analysis revealed that key controlling factors may be different from month to month, with wind speed taking dominance throughout the year in the study basin. Precipitation, while appearing insignificant in the course of the year, appears to be a limiting factor in the summer months.

2) The ability to successfully map ET to key environmental variables in such a complex terrain in this study demonstrates the superiority of the geographically weighted regression over the ordinary least square approach in modeling spatially varying environmental relationships. Given the usually unquestioned limitation of the OLS technique, one further refinement that could be included in studies concerned with spatial analyses should be the use of a more appropriate localized (i.e. geographically weighted) method when attempting to explain spatial relationships.
3) Modeled spatially varying monthly ET developed from this study offer convenient and cost effective means to empirically estimate monthly water loss from similar ecosystems. The ET index map generated for the PRB illustrates areas where ET exceeds precipitation especially in the summer months, and hence useful for water resource planning and decision making by water managers in the basin. Moreover, reliable quantification of ET has been made possible in the study basin. As such, the amount of water loss due to evapotranspiration can be accounted for in future water supply plans for the basin.

It is hoped that this work, being the first of its kind in the study basin to the best of our knowledge, will form the foundation for future climate impact studies in the basin and in the region at large.

2.6. References

Abatzoglou, J. T., Dobrowski, S. Z., Parks, S. A., & Hegewisch, K. C. (2018). TerraClimate, a high-resolution global dataset of monthly climate and climatic water balance from 1958–2015. Scientific data, 5, 170191.

Akaike, H. (1974). A new look at the statistical model identification. IEEE transactions on automatic control, 19(6), 716-723.

Bouwer, L. M., Biggs, T. W., & Aerts, J. C. (2008). Estimates of spatial variation in evaporation using satellite-derived surface temperature and a water balance model. Hydrological Processes: An International Journal, 22(5), 670-682.

Brooks, K. N., Ffolliott, P. F., & Magner, J. A. (2012). Hydrology and the Management of Watersheds. John Wiley & Sons.

Burnham, K. P., & Anderson, D. R. (2003). Model selection and multimodel inference: a practical information-theoretic approach. Springer Science & Business Media.

Chen, J. M., & Liu, J. (2020). Evolution of evapotranspiration models using thermal and shortwave remote sensing data. Remote Sensing of Environment, 237, 111594.

Daly, C., Halbleib, M., Smith, J. I., Gibson, W. P., Doggett, M. K., Taylor, G. H., ... & Pasteris, P. P. (2008). Physiographically sensitive mapping of climatological temperature and precipitation across the conterminous United States. International Journal of Climatology: a Journal of the Royal Meteorological Society, 28(15), 2031-2064.

Daly, C., Neilson, R. P., & Phillips, D. L. (1994). A statistical-topographic model for mapping climatological precipitation over mountainous terrain. Journal of Applied Meteorology and Climatology, 33(2), 140-158.

Fang, Y., Sun, G., Caldwell, P., McNulty, S. G., Noormets, A., Domec, J. C., ... & Zhou, G. (2016). Monthly land cover-specific evapotranspiration models derived from global eddy flux measurements and remote sensing data. Ecohydrology, 9(2), 248-266.

Fotheringham, A. S., Brunsdon, C., & Charlton, M. (2003). Geographically weighted regression: the analysis of spatially varying relationships. John Wiley & Sons.

Gasca-Tucker, D. L., Acreman, M. C., Agnew, C. T., & Thompson, J. R. (2007). Estimating evaporation from a wet grassland.

Gebler, S., Franssen, H. H., Pütz, T., Post, H., Schmidt, M., & Vereecken, H. (2015). Actual evapotranspiration and precipitation measured by lysimeters: a comparison with eddy covariance and tipping bucket. Hydrology and Earth System Sciences, 19(5), 2145.

Gowda, P. H., Chavez, J. L., Colaizzi, P. D., Evett, S. R., Howell, T. A., & Tolk, J. A. (2007). Remote sensing based energy balance algorithms for mapping ET: Current status and future challenges. Transactions of the ASABE, 50(5), 1639-1644.

Hu, Y., & Hu, Y. (2019). Land Cover Changes and Their Driving Mechanisms in Central Asia from 2001 to 2017 Supported by Google Earth Engine. Remote Sensing, 11(5), 554. index in northern Morocco: a need for an adaptive environmental policy. SN Applied Sciences, 1(3), 277.

Kalma, J. D., McVicar, T. R., & McCabe, M. F. (2008). Estimating land surface evaporation: A review of methods using remotely sensed surface temperature data. Surveys in Geophysics, 29(4-5), 421-469.

Lemenkova, P. (2022). Mapping Climate Parameters over the Territory of Botswana Using GMT and Gridded Surface Data from TerraClimate. ISPRS International Journal of Geo-Information, 11(9), 473.

Li, X., Liang, S., Yuan, W., Yu, G., Cheng, X., Chen, Y., ... & Liu, S. (2014). Estimation of evapotranspiration over the terrestrial ecosystems in China. Ecohydrology, 7(1), 139-149.

Liu, S. M., Xu, Z. W., Zhu, Z. L., Jia, Z. Z., & Zhu, M. J. (2013). Measurements of evapotranspiration from eddy-covariance systems and large aperture scintillometers in the Hai River Basin, China. Journal of Hydrology, 487, 24-38.

Lu, B., Charlton, M., Harris, P., & Fotheringham, A. S. (2014). Geographically weighted regression with a non-Euclidean distance metric: a case study using hedonic house price data. International Journal of Geographical Information Science, 28(4), 660-681.

Lu, J., Sun, G., McNulty, S. G., & Amatya, D. M. (2003). Modeling actual evapotranspiration from forested watersheds across the southeastern united states 1. Jawra Journal of the American Water Resources Association, 39(4), 886-896.

Ma, N., & Szilagyi, J. (2019). The CR of evaporation: A calibration-free diagnostic and benchmarking tool for large-scale terrestrial evapotranspiration modeling. Water Resources Research, 55(8), 7246-7274.

Ma, N., & Zhang, Y. (2022). Increasing Tibetan Plateau terrestrial evapotranspiration primarily driven by precipitation. Agricultural and Forest Meteorology, 317, 108887.

Ma, N., Szilagyi, J., & Zhang, Y. (2021). Calibration-free complementary relationship estimates terrestrial evapotranspiration globally. Water Resources Research, 57(9), e2021WR029691.

mascons. Journal of Geophysical Research: Solid Earth, 120(4), 2648-2671.

Neto, A. K., Ribeiro, R. B., & Pruski, F. F. (2022). Assessment water balance through different sources of precipitation and actual evapotranspiration.

New Jersey Department of Environmental Protection (2017). New Jersey Water Supply Plan 2017-2022: 484p, access [May 7, 2020], at URL [http://www.nj.gov/dep/watersupply/wsp.html]

Newcomb, D. J., Stanuikynas, T. J., & Van Abs, D. J. (2000). Setting of the Raritan River Basin: A technical report for the Raritan Basin Watershed Management Project.

PRISM Climate Group, Oregon State University, http://prism.oregonstate.edu, data created 4 Feb 2014, accessed 15 Nov 2020.

R Core Team (2020). R: A language and environment for statistical computing. R Foundation for Statistical Computing, Vienna, Austria. URL https://www.R-project.org/.

Reitz, M., Sanford, W. E., Senay, G. B., & Cazenas, J. (2017). Annual estimates of recharge, quick-flow runoff, and evapotranspiration for the contiguous US using empirical regression equations. JAWRA Journal of the American Water Resources Association, 53(4), 961-983.

Ruhoff, A. L., Paz, A. R., Aragao, L. E. O. C., Mu, Q., Malhi, Y., Collischonn, W., ... & Running, S. W. (2013). Assessment of the MODIS global evapotranspiration algorithm using eddy covariance measurements and hydrological modelling in the Rio Grande basin. Hydrological Sciences Journal, 58(8), 1658-1676.

Salhi, A., Martin-Vide, J., Benhamrouche, A., Benabdelouahab, S., Himi, M., Benabdelouahab, T., & Ponsati, A. C. (2019). Rainfall distribution and trends of the daily precipitation concentration

Sanford, W. E., & Selnick, D. L. (2013). Estimation of evapotranspiration across the conterminous United States using a regression with climate and land-cover data 1. JAWRA Journal of the American Water Resources Association, 49(1), 217-230.

Senay, G. B., Friedrichs, M., Singh, R. K., & Velpuri, N. M. (2016). Evaluating Landsat 8 evapotranspiration for water use mapping in the Colorado River Basin. Remote Sensing of Environment, 185, 171-185.

Soleimani-Motlagh, M., Soleimani-Sardo, M., & Mossivand, A. M. (2022). The efficiency of the Standardized Evapotranspiration Deficit Index (SEDI) in assessing the impact of drought on vegetation cover. Environmental Monitoring and Assessment, 194(4), 1-12.

Sumner, D. M., Nicholson, R. S., & Clark, K. L. (2012). Measurement and simulation of evapotranspiration at a wetland site in the New Jersey Pinelands. US Geological Survey Scientific Investigations Report 2012–5118, 30 p., 5118.

Sun, G., Alstad, K., Chen, J., Chen, S., Ford, C. R., Lin, G., ... & Zhang, Z. (2011). A general predictive model for estimating monthly ecosystem evapotranspiration. Ecohydrology, 4(2), 245-255.

Sun, G., Caldwell, P., Noormets, A., McNulty, S. G., Cohen, E., Moore Myers, J., ... & Chen, J. (2011). Upscaling key ecosystem functions across the conterminous United States by a water‐centric ecosystem model. Journal of Geophysical Research: Biogeosciences, 116(G3).

Sun, G., McNulty, S. G., Amatya, D. M., Skaggs, R. W., Swift Jr, L. W., Shepard, J. P., & Riekerk, H. (2002). A comparison of the watershed hydrology of coastal forested wetlands and the mountainous uplands in the Southern US. Journal of Hydrology, 263(1-4), 92-104. the Earth, Parts A/B/C, 30(1-3), 69-79.

Tobler, W. R. (1970). A computer movie simulating urban growth in the Detroit region. Economic geography, 46(sup1), 234-240.

Tu, J., & Xia, Z. G. (2008). Examining spatially varying relationships between land use and water quality using geographically weighted regression I: Model design and evaluation. Science of the total environment, 407(1), 358-378.

U.S. Geological Survey (2016). National Water Information System data available on the World Wide Web (USGS Water Data for the Nation), accessed [October 5, 2022], at URL [https://waterdata.usgs.gov/nwis/]

US Army Corps of Engineers, New York District. (1987). Flood Protection Feasibility Report for the Main Stem of the Passaic River, Volume I, Main Report and Environmental Impact Statement; Volume IV, Appendix C, Plan Formulation. N.Y.: N.Y.

USDA Natural Resources Conservation Service (NRCS) (2011). NEW YORK Rapid Watershed Assessment Profile, Hackensack - Passaic Watershed. United States Department of Agriculture: Syracuse State Office

Valipour, M. (2015). Temperature analysis of reference evapotranspiration models. Meteorological Applications, 22(3), 385-394.

Verstraeten, W. W., Veroustraete, F., & Feyen, J. (2008). Assessment of evapotranspiration and soil moisture content across different scales of observation. Sensors, 8(1), 70-117.

Watkins, M. M., Wiese, D. N., Yuan, D. N., Boening, C., & Landerer, F. W. (2015). Improved methods for observing Earth's time variable mass distribution with GRACE using spherical cap

Wiese, D. N., Yuan, D. N., Boening, C., Landerer, F. W., & Watkins, M. M. (2019). JPL GRACE Mascon Ocean, Ice, and Hydrology Equivalent Water Height RL06 CRI Filtered Version 02, version 2. PO. DAAC.

Wiwoho, B. S., & Astuti, I. S. (2022). Runoff observation in a tropical Brantas watershed as observed from long-term globally available TerraClimate data 2001–2020. Geoenvironmental Disasters, 9(1), 1-18.

Xu, B., Hicke, J. A., & Abatzoglou, J. T. (2019). Drought and moisture availability and recent Western spruce budworm outbreaks in the Western United States. Forests, 10(4), 354.

Zhang, K., Kimball, J. S., & Running, S. W. (2016). A review of remote sensing based actual evapotranspiration estimation. Wiley Interdisciplinary Reviews: Water, 3(6), 834-853.

Zhao, G., & Gao, H. (2019). Estimating reservoir evaporation losses for the United States: Fusing remote sensing and modeling approaches. Remote sensing of environment, 226, 109-124.

CHAPTER 3 : HYDRO-CLIMATIC TRENDS AND STREAMFLOW RESPONSE TO RECENT CLIMATE CHANGE: AN APPLICATION OF DISCRETE WAVELET TRANSFORM AND HYDROLOGICAL MODELING IN THE PASSAIC RIVER BASIN

3.1. Abstract
The exigency of the current climate crisis demands a more comprehensive approach to addressing location-specific climate impacts. In the Passaic River Basin (PRB), two bodies of research—hydroclimatic trend detection and hydrological modeling—have been conducted with the aim of revealing the basin's hydro-climate patterns as well as the hydrologic response to recent climate change. In a rather novel application of the wavelet transform tool, we sidelined the frequently used Mann-Kendal (MK) trend test, to identify the hidden monotonic trends in the inherently noisy hydro-climatic data. By this approach, the use of MK trend test directly on the raw data whose results are almost always ambiguous and statistically insignificant in respect of precipitation data for instance, no longer pose a challenge to the reliability of trend results. Our results showed that, whereas trends in temperature and precipitation are increasing in the PRB, streamflow trends are decreasing. Based on results from the hydrological modeling, streamflow is more sensitive to actual evapotranspiration (ET) than it is to precipitation. Generally, for decades where water is available, energy limits actual evapotranspiration which makes streamflow more sensitive to precipitation increase. However, in meteorologically stressed or dry decades, water limits actual ET thereby making streamflow more sensitive to increases in actual evapotranspiration. We found that the choice of baseline condition constitutes an important source of uncertainty in the sensitivities of streamflow to precipitation and evapotranspiration changes and should routinely be considered in any climate impact assessment.

3.2. Introduction
Global climate change is expected to accelerate the global hydrologic cycle, which will drive more intense floods and droughts leading to changes in streamflow and water resource

availability. An alteration of the discharge regime of rivers (Huntington, 2006) is usually the ultimate consequence. In the past decades, empirical evidence of warming-driven intensification of the hydrologic cycle has led to an increasing interest in the linkage of climatic variability or change to hydrological processes across space and time (Fan and He, 2015). More often than not, the literature is either rich on the detection and analysis of hydro-climatic trends (e.g. Hu et al., 2011; Tekleab et al., 2013; Chen and Georgakakos, 2014; Ahmad et al., 2015; Chattopadhyay and Edwards, 2016; Mahmood et al., 2019; Qian et al., 2020) or hydrological modeling studies (e.g. Chattopadhyay et al., 2017; Marvel et al., 2021, Ziervogel et al., 2014, Roudier et al., 2014, Ding et al., 2021; Leng et al., 2015, Saintilan et al., 2019; Lansbury & Crosby, 2022, Schnorbus et al., 2014; Shrestha et al., 2017 [Canada], Nolan et al., 2017 , Pastén-Zapata et al., 2020) without considering both. At a time when the global warming problem has evolved into a crisis (Sanson et al., 2019; Ojala et al., 2021), it is important that hydrological impact assessments be carried out from a holistic standpoint. Although the analysis and detection of trends can provide useful insights in terms of a general estimate of the direction and changes in magnitudes of hydro-meteorological series, they lack the ability to predict unprecedented future conditions. Process-based models, although are only capable of representing processes to the scope that they are quantitatively understood, can provide a robust framework for assessing hydrological response to climate change (Campbell et al., 2011). More so, because the direction and extent of changes in river flows are dependent on the relative balance between precipitation and the processes that govern evapotranspiration (Campbell et al., 2011), the causes of discharge changes—which oftentimes seem controversial (Do et al., 2017; Sharma et al., 2018), can effectively be examined from a hydrological modeling standpoint.

In studies that emphasize on the detection and analysis of hydro-climatic trends (e.g. Sharma et al. 2016; Meng et al. 2016; Suhaila, and Yusop, 2018; Citakoglu, and Minarecioglu, 2021), one statistical tool that is commonly used is the non-parametric Mann-Kendall (MK) test and its modified forms. The MK trend test identifies changes in hydroclimatic series by simply fitting a monotonic (e.g. linear) trend at a certain time period where a significant level is assigned by a statistical test. While the robustness of this test is not in doubt, its application to hydroclimatic time series can be particularly challenging due to the non-monotonic and non-uniform character of hydroclimatic variables. Fitichi et al. (2009) noted that, because the stochastic structure of time series data has the tendency to assume trend-like features, analyzing trends in non-stationary time series can cause a purely stochastic behavior to appear deterministic, leading to a likely erroneous interpretation of results. Furthermore, because climatic phenomena and events (e.g. precipitation, hurricanes) are products of various complex atmospheric processes (Lutgens & Tarbuck, 2010), the presence of noise is inevitable and this can affect the variability and trend in the data series. In hydro-climatic times series where non-monotonicity is more the rule rather than the exception (Dixon et al., 2006; Gong et al., 2010), identifying the hidden monotonic trend and assessing their statistical significance subsequently provide more reliable results than those derived from the direct trend analysis of the raw data (Araghi et al., 2015).

Because the structure of hydro-climatic data is often hidden behind the noise, a precise mathematical operation that looks at the data through the noise and quantifies the structure present in the signal is needed. One such tool is the wavelet transform (WT). WT is a relatively recent development in the field of signal processing (Hernández and Weiss, 1996; Kirchgässner et al., 2012), and has, in recent times, emerged as an effective tool to analyze trends in hydro-climatic series especially in the atmospheric and hydrological science space [Shiri and Kisi, 2010; Adamowski and Chan, 2011; Wang and Li, 2011; Nalley et al., 2012). It can be thought of as a 'mathematical microscope' with the ability to zoom in and out of the signal (or time series) to pull out the patterns. In its application, a signal or time series data is decomposed into their low-frequency components and high-frequency components. The different decomposition levels, representing different periodic time scales are subsequently analyzed for trends. The last decomposition level, which contains the lowest frequency component usually represents the trend component of the time series. Thus among the methods presently used in analyzing time series data, the wavelet approach has the superior ability to handle the non-stationary characteristics of hydro-climatic time series on multiple temporal resolutions (Labat, 2005), making it well suited for identifying trends over a long period of time.

In light of understanding and quantifying the hydrological impacts of climate variability/change, different approaches (i.e. conceptual methods, analytical, experimental, and hydrological modeling) have been used. Among these, process-based hydrological models provide a means to examine the physical mechanisms and processes that drive hydrological changes and variations. Their primary purpose is to partition precipitation into evapotranspiration and streamflow. They must however be thoroughly evaluated against field observations that sufficiently represent the region and timeframe of interest (Gardner and Urban, 2003; Kucharik et al., 2006). By applying a rigorously calibrated and validated physically-based hydrological model, MIKE SHE, to the Rockaway catchment — a sub-basin of the Passaic River Basin (PRB) in New Jersey, USA, we explored the mechanisms underpinning streamflow changes through the examination of MIKE SHE simulated water balance terms under various climate scenarios.

Thus the novelty of this study lies in the application of advanced trend analysis tool with a physically-based hydrological model that simulates both surface and subsurface flows in the land phase of the hydrological cycle. This combination will provide important clues on the key underlying variables behind the trend as well as insights into how hydroclimatic patterns may change into the future.

In the PRB (Passaic River Basin) and its surrounding areas, the lingering effects of a troubled history of improper environmental practices from the industrial boom continue to be experienced. According to Brydon (1974), the Passaic River played a central role in the early development of New Jersey. In the late 18th century, the river served as navigable routes connected by a system of canals to the Delaware River. It was also an early source of hydroelectric power at the Great Falls in Paterson, making the region a focal point for industrial mills. Consequently, the lower Passaic suffered the significant burden of environmental pollution from years of industrialization in the area. By 1970, issues with flooding were already noticeable due to the dams, and they still plague the inhabitants of the basin to this day. The complex river systems amidst the heterogeneous biophysical arrangement within the basin further present a multifaceted mix of competing interests and water related issues. In a region where projected temperature increases (Karmalkar and Bradley 2017, NCA 2018) — amidst the already existing issues — are expected to enhance evapotranspiration and snowpack loss (Campbell et al., 2010, 2011), the concomitant effect on streamflow can be far reaching. It is in this light that we carry out two bodies of research — hydro-climatic trend detection and hydrological modelling studies—, with the aim to provide important foundations for the predictive understanding of impacts of climate change on water resources in the PRB and its vicinity.

To this end, the present study employs a two-fold objective: 1) To detect changes in hydro-meteorological trends in the PRB for the period 1979 — 2021; and 2) To examine the response and sensitivities of hydrologic systems to climate phenomenon in the Rockaway River basin, a sub-catchment of the PRB. The discrete wavelet transform and Mann-Kendal test are applied in the hydro-climatic trend analysis whereas hydrological modeling approach coupled with sensitivity analysis are used in assessing the implications of recent climate change in the PRB. Specifically, the Ringwood, Rockaway, and Upper Passaic catchments of the PRB were selected for the hydro-meteorological trend analysis because of their physio-graphically distinct locations. The hydrological modeling was, however, conducted for only the Rockaway sub-basin given its relatively large size and available groundwater data.

The remaining part of the paper is organized as follows. Section 3.3 describes the study area and data source. Section 3.4 details the methodology used which includes the discrete wavelet transform, hydrological model evaluation, and hydrologic impacts assessment. Results of the trend analysis and hydrological model performance, and model assessment are presented under results and discussion in section 3.5 followed by the conclusion in section 3.6.

3.3. Study Area and Data Source

3.3.1. Study area

The non-tidal portion of the Passaic River basin (PRB) is elliptical in shape, draining approximately 2135 square kilometers of Northern New Jersey (NJ) and Southern New York State (NY). It is bounded by longitude 74º1′1″ and 74º39′16″W and latitude 40º35′23″ and 41º23′37″ N, intersecting six (6) counties in NJ, two (2) in NY. The entire basin stretches across three (3) Watershed Management Areas (WMA-03-04-06) with seven major tributaries: Whippany River, Rockaway River, Pompton River, Pequannock River, Wanaque River, Ramapo River, and Saddle River. Physio-graphically, the basin can be divided into three main regions: the series of parallel ridges that trend northeast/southwest forming the Highlands; the Central Basin, comprised of large areas of swamps and meadows; and the roughly flat Lower Valley. Winding through seven counties and 45 municipalities, the Passaic river originates from near the

Borough of Mendham (Morris County), and finally empties into the Newark Bay. The non-tidal part of the river is regulated by 10 major reservoirs (Canister, Greenwood lake, Clinton, Oak Ridge, Charlotte-burg, Echo lake, Split Rock, Monksville, Wanaque, and Boonton) to provide flood control, water supply among others to surrounding municipalities. Aggregated reservoir storage in the basin is about 68533 million gallons (MG). Of this, Wanaque reservoir is the largest, with storage capacity of 29630 MG (43%) of the basin total (Wells, 1960; Hendricks, 1964; USGS, 1970; NJWDR, www.usgs.gov/centers/nj-water). Summary of the hydro-meteorological conditions in the basin are described in Table 3.1. Mean annual flow at the outlet of the basin is estimated at 402088 m^3/s for the 1983 – 2021 period. On average, the Rockaway river (RA) contributes about 0.62 percent of flow to the Passaic river. The study basin lies within the modified continental climate zone, characterized by hot summer and cold winter (Paulson et al., 1991). Moving from north to south in New Jersey the modified climate zone is comprised of five (5) main divisions: North, Central, Southwest, Pine Barrens, and Coastal zones with PRB located in the North and Central climate zones. For the period 1981-2010, mean annual precipitation of 1281mm (50.4 in) occurred over the PRB with higher values (1298mm or 51.1 in) in the Ringwood catchment and the lower values (1269mm or 49.96 in) in the Upper Passaic (UP) catchment. Mean temperature for same period in the study basin is calculated as 10.59 °C. Colder temperatures are observed over the RW and RA catchments whereas hotter temperatures occur in the UP area. Throughout the PRB, mean annual actual evapotranspiration is estimated to be approximately 793mm or 31.2in (Oteng Mensah and Alo, 2023).

Table 3.1: Basic hydro-climatic information in the Passaic River Basin

	Drainage area (sqkm)	Area (% of PRB)	Annual flow (m^3s) mean(min-max)	Temperature (°C)	Precipitation (mm)
PRB	2135	–	402088 (30968-958992)	10.59	1281
RA	300.4	14.07	2513 (611-4037)	9.52	1296
RW	46.4	2.17	337 (122-721)	9.74	1298
UP	356.3	16.67	1916 (344-2977)	11.11	1269

PRB (1983-2021 WY); RA (1971-2010 WY); RW (1986-2021 WY); UP (1971-2010 WY)

3.3.2. Hydro-meteorological data

For this study, the widely used gridded observations from Parameter-elevation Regression on Independent Slopes Model (PRISM, Oregon State University, http://prism.oregonstate.edu) provided meteorological data. Flow data for the Rockaway and Upper Passaic sub-catchments were obtained from records of reconstructed streamflow by Hickman and McHugh (2018) whereas data for the Ringwood catchment were sourced from the United States Geological Survey (USGS) water data website (USGS, https://waterdata.usgs.gov/nwis/).

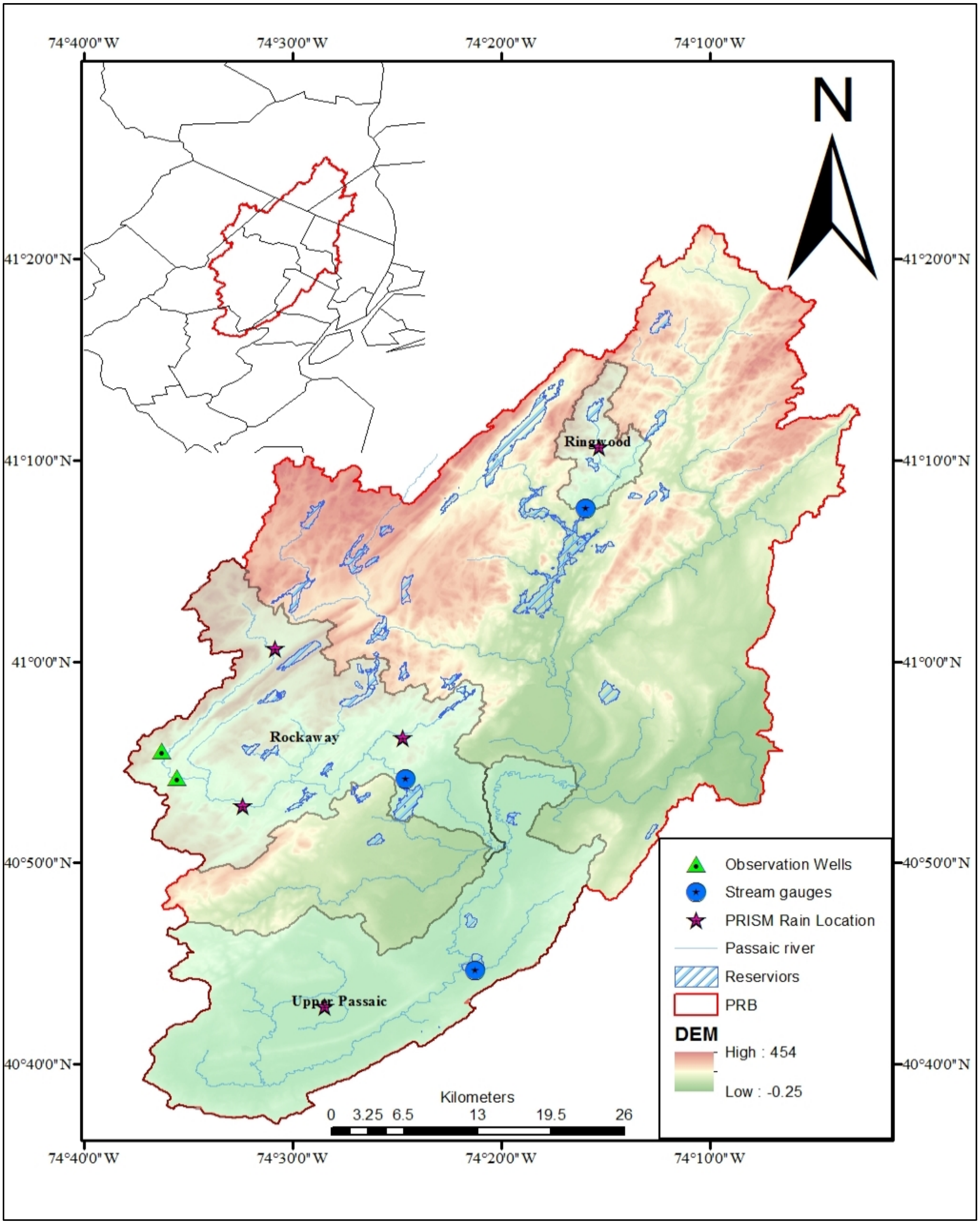

Figure 3.1: Location map of the study area showing available hydro-meteorological stations

The data used in this study spanned the periods 1979—2021 and 1981—2021 water years for the trend analysis and hydrological modelling respectively. Missing flow data, when present, were handled based on streamflow outputs from a duly calibrated and validated hydrological model of the sub-catchment [Ringwood, correlation coefficient: 0.85 and Nash-Sutcliffe: 0.71]. In all, seven (7) hydro-meteorological variables (i.e. flow, precipitation [precip], minimum temperature [Tmin], mean temperature [Tmean], maximum temperature [Tmax], number of days with precipitation greater that 10mm [R10], and consecutive dry days [CDD]) for the three (3) studied sub-catchments were processed and aggregated into annual time scales for the trend analysis.

3.3.3. Land use, soil, and elevation data

In hydrological processes, the combined effect of land cover, soil, elevation and other catchment characteristics are reflected in the flow dynamics of river systems in a basin. The 2011 Land cover data were available from the National Land Cover Dataset (NLCD) [https://www.mrlc.gov/viewer/], and simplified into six (6) dominant land cover/ vegetation classes (i.e. developed, forest, agricultural, wetlands, bare land, and water). Soil information were accessed using the United States Department of Agriculture (USDA) soil data viewer software [version 6.2] (NRCS, 2009). The topography of the PRB was defined by a digital elevation model (DEM) extracted from the USGS database at 10m spatial resolution (https://apps.nationalmap.gov/downloader/).

3.4. Methods

In line with the objectives of the study, two major tasks were carried out: 1) the analysis of hydro-climatic trends via the discrete wavelet transform (DWT) approach; and 2) the development of a hydrological model to assess the impacts of recent climate changes on water balance terms (i.e. precipitation, evapotranspiration, and streamflow). As alluded to earlier, the hydro-climatic trend detection was conducted for seven (7) indicator variables in three (3) sub-catchments whereas the hydrological study was conducted for the Rockaway catchment. Summary of the steps involved in our analysis are outlined below and described in more detail in the forthcoming sub-sections:

1. Seven (7) different hydro-climatic indicator variables used in the trend analysis were derived from temperature, precipitation, and streamflow data series obtained for each sub-catchment. They were mean annual Tmin, Tmean, Tmax, Precip, Flow, R10, and CDD spanning the period 1979-2021;
2. Each time series was decomposed via the DWT, having selected the Daubechies (db) wavelet, deemed an appropriate mother wavelet in our study context, to split the series into their high frequency detailed (D) and low frequency approximate (A) components;
3. Compute the MK Z-values of the original signal and the approximation of each Daubechies (db) wavelet form starting from db4-db10 (e.g. Adarsh and Janga Reddy, 2015) to determine the wavelet form that gives MK Z-value closer to that of the original signal. This will be the optimal trend from the approximation components of each analyzed time series.
4. Having selected the optimal monotonic trend, a MK test was subsequently applied to determine the statistical significance of the DWT-based trend.
5. Develop, calibrate, and validate a hydrological model for the Rockaway sub-basin and evaluate the performance of the model against observed streamflow and groundwater data using standard statistical criterion. The water balance module is run to obtain outputs of water balance components for impact assessment.
6. Carry out change point analysis to divide data into the naturalized or baseline periods, where minimum effects of human activity on streamflow is expected and impacted

periods. Subsequently, a climate elasticity exercise was undertaken to explore sensitivities of climate variables to streamflow and corresponding contributions in the Rockaway sub-basin.

3.4.1. Discrete wavelet transform

Wavelet transform (WT) is a mathematical tool that uses wave functions known as wavelets—akin to the sine and cosine functions in Fourier transforms (FT), to convert signals or time series data into different frequency components. WT rides on the fundamental concept of Fourier transform, which operates on the idea that any function can be decomposed into a sum of pure waves with different frequencies. Such that, the frequency domain represents the relative contributions of each frequency that comprises the function. The major limitation with FT is that, knowledge about frequency is accessed at the expense of the temporal dynamics (i.e. there is no clue as to when certain frequencies begin or end). As a result, wavelets come into play to resolve this inherent trade-off of information between frequency and time in the FT (Li et al., 2013). Through the application of wavelet transform, an optimal frequency-time balance is attained. The key feature about wavelets is that the wave-like oscillations are short-lived and localized in time. It is worth noting that, a wavelet is not just a function, but a whole family of functions which all satisfy certain requirements. The popular family of functions include Daubechies, Coiflet, Symlet, Haar, Morlet, Gaussian, Shannon, Meyer, and Mexican Hat; and each one of these is tuned for specific applications. In general, to be considered a proper wavelet, a function must satisfy two main constraints; 1) the admissibility condition of having a zero mean, and 2) the finite energy condition of having a limited duration, from which a function attains its localized nature in time. In short, wavelet analysis is a completely flexible windowing technique that allows a function to change over time based on the shape and compactness of the time series signal (Daubechies, 1990). By this very nature, different modes of variability that varies in time can be extracted in the WT process, allowing the time-frequency characteristics of any kind of signal to be analyzed (Wei et al., 2012). The recent years has seen a wide range of studies using WT, especially to analyze hydro-meteorological time series. (e.g. Partal and Kahya, 2006; Adamowski, 2008; Chellali et al., 2010; Adamowski and Chan, 2011; Nalley et al., 2013; Araghi et al., 2015; Sang et al., 2018). While the vast majority of these studies focused on trends, others emphasized on the dominant periodic time scale responsible for the trends.

In the WT process, as a mother wavelet moves across the signal, several coefficients are generated according to the similarity between the signal and the mother wavelet at any specific scale. Generally, WT is divided into two main types, the continuous wavelet transform (CWT) and the discrete wavelet transform (DWT). The continuous type can generate quite numerous and often redundant coefficients at every resolution level, making its application and interpretation more complex and uncertain. The DWT is however, considered a more effective approach, having the ability to overcome the data redundancy issue by simplifying the transformation process based on the dyadic (power of 2) scale (Partal and Küçük, 2006). Given a suitable wavelet family and decomposition level, the DWT decomposes a series into several sub-series during the transformation process (Whitcher et al., 2002). Following equation 3.1 below (reader is referred to Partal and Küçük, 2006 for details), the coefficients of DWT can be calculated:

$$W_{\varphi}(a,b) = \frac{1}{(2)^{a/2}} \sum_{t=0}^{N-1} X(t)\varphi\left(\frac{t}{2^a} - b\right) \qquad \text{Equation 3.1}$$

where 2^a denotes the dyadic scale of the DWT.

Note that the resulting detail and approximation coefficients from the decomposition are merely intermediate coefficients, and has to be reconstructed, first to their approximation and detail components and then to the original signal. This readjustment to the original one-dimensional signal ensures that each component has the same length as the original signal, thereby enabling proper investigations of their contribution to the signal (Dong et al., 2008). In a simplified form, the reconstruction of the detail and approximation components can be computed as:

$$S(t) = A_n(t) + \sum_{l=1}^{n} D_l(t) \qquad \text{Equation 3.2}$$

where $S(t)$ is the original signal, and $A_n(t)$ is the approximation component at level n, and $D_l(t)$ is the details component at different levels (where l = 1, 2, 3, …, n denotes index for the levels). In MATLAB, computation of a perfect signal reconstruction is achieved using the Inverse Discrete Wavelet Transform (IDWT).

Although nearly all hydro-climatic processes are continuous in nature, their available time series outputs are delivered in discrete formats (Wilks, 2011), making its use with DWT more appropriate than that of CWT. In the application of DWT, original time series signal is passed through low-pass and high-pass filters and emerge as Approximation (A) and Detail (D) components respectively. While component D represents the small scale, high-frequency series, component A comprises the high scale, low-frequency series. The decomposition process can continue iteratively, where component A from the first decomposition is further divided into new A and D components (Partal, 2010; Li et al., 2013; Nalley et al., 2012, 2013). In this studies, the Daubechies mother wavelet was chosen because of its characteristic orthogonality, and compact support—which are very important properties for localizing events in signal analysis, and deemed appropriate for hydro-meteorological time series (Nalley et al., 2012; Venkata Ramana et al, 2013).

3.4.2. Time series decomposition via DWT

In our wavelet analysis, the one dimensional flow signal (data series) and each of the temperature and precipitation indicator variables served as inputs to the multi-level 1-D wavelet decomposition function in the MATLAB Wavelet Toolbox (MATLAB version R2021a). With the db wavelet family as the mother wavelet, the operation produced a wavelet transform of each input time series signal at all dyadic scales. Three main parameters were taken into account during the DWT process (Nalley et al., 2012): 1) the appropriate type of db wavelet; 2) a suitable signal border extension method; and 3) the most appropriate number of decomposition levels. First, several forms of db wavelet (e.g. db1—db10) exist, and the appropriate type must be selected for the decomposition process (Vonesch et al., 2007). As suggested by Nalley et al. (2012), a useful method in selecting the appropriate db wavelet type is to calculate the relative error (R_E) between the MK Z-values of the original signal and that of the approximation (A) of the last decomposition level. R_E is computed as follows:

$$R_E = \frac{|Z_a - Z_o|}{|Z_0|} \qquad \text{Equation 3.3}$$

where Z_a and Z_o are the MK Z-values of the approximation of the last decomposition level and the original dataset respectively. For each indicator variable and study catchment, the appropriate db wavelet was selected to minimize R_E. Because trends are supposed to be gradual and slowly changing process, smoother db wavelets (i.e. db4—db10), considered as better in detecting time varying behavior over the long term (Adamowski et al., 2009; Nalley et al., 2012), was used in the selection of the appropriate db wavelet in the study (Table 3.2). Second, border extension is an important consideration due to the issue of border distortions in the DWT process, arising because of the finite length of the signal. Thus, the decomposition process cannot occur outside the two limits (i.e. the start and end points) of a signal as there is no available information beyond the ends (Su et al., 2011). As suggested by Su et. al. (2011), three different border extension methods are employed to address the issue: zero-padding, symmetrization, and periodic padding. In our analysis, symmetrization—which is the default mode in MATLAB, was used. It assumes that signals beyond the original support can be retrieved by symmetric boundary replication (Nalley et al., 2013). Finally, the relevant number of decomposition level must be determined in order to avoid unnecessary levels of data decomposition especially, for larger datasets (see Nalley et al., 2012, 2013). This will however depend on the length of data points as well as the type of mother wavelet used. According to de Artigas et al. (2006), the maximum number of decomposition level, L, can be calculated from equation 3.4 below.

$$L = \frac{Log(\frac{n}{2v-1})}{Log(2)} \qquad \text{Equation 3.4}$$

where n is the number or length of data points in the time series and v is the number of vanishing moment of a db wavelet. In MATLAB, the number of vanishing moments (v) is equal to the db wavelet type number (i.e. 1—10). Note that the number of data points (n) in a time series is not exactly in a dyadic format (as in the case of this study, 43 data points). Thus the DWT computation in MATLAB is carried out using the nearest upper dyadic arrangement. Therefore, the maximum decomposition level based on our data points was calculated to be 6 in the study. Additionally, because data decomposition via DWT assume a dyadic format, each of the decomposed component represents a different period of integer powers of two from the lowest scale. Therefore, D1, D2, and D3 respectively represents 2, 4, and 8-unit periodic component in that order according to the time scale (e.g. seasonal, monthly, annual) used in the analysis. For example, D2 will represents a 4-year or 4-month intervals in an annual or monthly data series respectively, but a 12-month intervals for a seasonal data series since its time step is 3 months.

3.4.3. Trend and change-point detection tests

In this study, the Mann-Kendal (MK) test (Mann, 1945; Kendal, 1975) was used to determine the statistical significance of the DWT-based trend (Adarsh and Janga Reddy, 2015). It is probably the most widely used nonparametric statistical test for monotonic trend evaluation (McBean and Motiee, 2006); and well noted for its simplicity, robustness, and resilience to missing values in a data series (Adamowski et al., 2009). One key issue that may arise when using MK test is the presence of serial correlation or autocorrelation, very common in precipitation and streamflow data (Partal and Küçük, 2006). It occurs when a variable and a lagged version of itself is observed to be correlated between two successive time intervals. If the lag-1 autocorrelation in a time series is found to be significant, the modified MK test must be used (Hamed and Rao, 1998). Although autocorrelation issues are not common in annual data series, we applied the modified version of the MK test in this study where significant lag-1 autocorrelation was detected in our data series.

Furthermore, a change-point analysis was performed to identify the most likely year(s) in our streamflow data where significant changes could occur (Gao et al., 2010; Guo et al. 2018). This was key in our hydrological impacts analysis where we needed to explore a naturalized period or baseline period when stream flow experienced little or no disturbance. Various change-point methods exist, including the sequential Mann-Kendal test (Sneyers, 1990), Pettit's test (Pettitt, 1979), the cumulative sum (CUSUM) test (Inclan and Tiao, 1994), and the Worsley Likelihood Ratio Test (Worsley, 1979). Using the R packages *changepoin*t and *ecp (R Core Team, 2023)*, the distribution free CUSUM test (Csörgö et al., 1997), complemented by the Permutation test (Matteson and James, 2014) was used because they revealed similar break-point years in our streamflow time series. These methods detect significant changes in the mean or distribution of a time series when the exact times of the changes are not known. For a detailed description of these methods, we refer the reader to the relevant literature cited.

3.4.4. Hydrological model development for the Rockaway river basin

In the present study, the numerical code used for our hydrological assessment studies is MIKE SHE (Abbott et al., 1986a, b). MIKE SHE is an integrated, fully distributed, physically-based hydrological modeling system (DHI, 2017; Refsgaard, 1997), that simulates all the major hydrologic process in the land phase of the hydrological cycle including evapotranspiration, overland flow, unsaturated flow, saturated flow, and streamflow (Figure 3.2). It uses the hydrodynamic model MIKE 11 to simulate channel flow and lakes (using flood code) in one dimension. For a detailed description on the development and modelling structure of the MIKE SHE hydrologic model the reader is referred to the MIKE Zero user manual by DHI (2017).

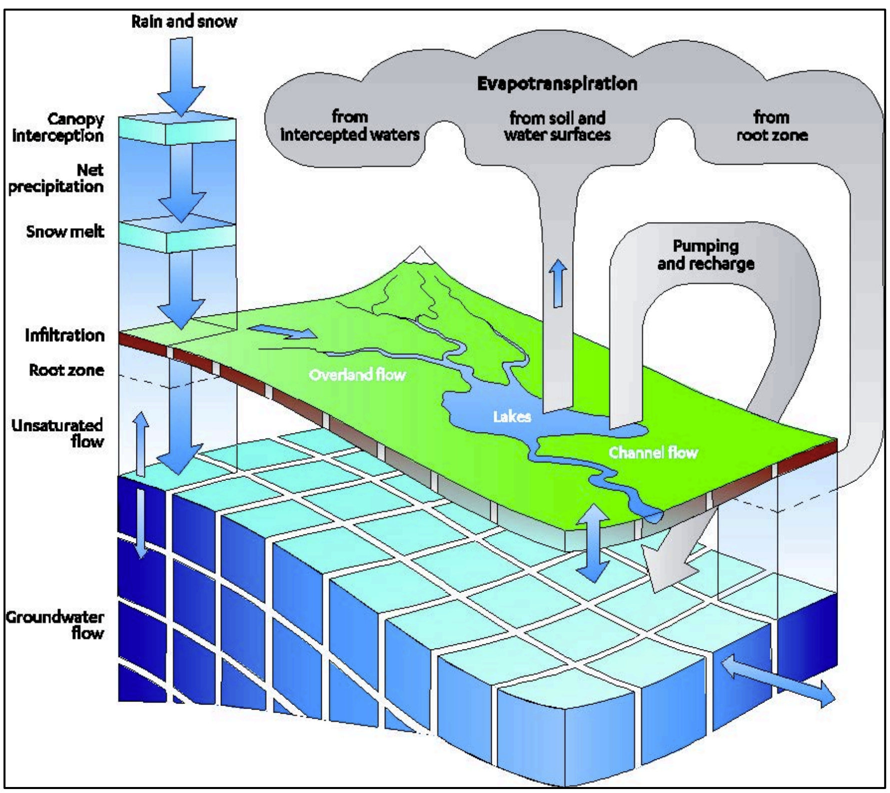

Figure 3.2: Hydrologic processes simulated by MIKE SHE (Butts et al. 2015)

3.4.5. Model calibration and validation

A distributed hydrologic model such as MIKE SHE typically requires large number of model parameters to be assigned. Although, these parameters have a clear physical meaning and can be defined explicitly from field measurements, Singh (1995) suggested that the number of parameters subject to calibration should be as small as possible. For this study, initial values as well as ranges of primary parameters from field data, published literature, and prior modelling experience guided the calibration process. The manual “trial and error” procedure was first applied, which involves perturbing one parameter while keeping all other parameters unchanged. This was done repeatedly within a reasonable range of values for a series of model runs until a favorable agreement between measured and simulated flow and groundwater level was achieved. Following the manual approach, an automatic calibration was conducted. Finally, validation was done to ensure that model parameters derived from calibration were generally valid.

Prior to the model calibration, change point analysis was performed on the streamflow data for the time span of 1981—2022 to find likely break-point year(s). Accordingly, the data was divided into baseline periods (1982—1991, 1992—2001, and 1982—2001) and impacted periods (2002—2011 and 2012—2021) as mentioned earlier. The calibration and validation of the model was carried out within the baseline period for 1982—1986 and 1986—1991 respectively. Typically, the simulation period includes the first few months of warm-up period to stabilize the model; as well as the calibration and validation periods. The adequacy of the model was evaluated based on four standard statistical criteria used in MIKE SHE: mean error (ME), root mean square error (RMSE), correlation coefficient (R), and the widely used Nash-Sutcliffe coefficient (R2). These indicators detect system errors and the goodness of fit between simulated and observed monitoring observations in the form:

$$ME_i = \frac{\sum_t (Obs_{i,t} - Calc_{i,t})}{n} \qquad \text{Equation 3.5}$$

$$RMSE = \frac{\sqrt{\sum_t (Obs_{i,t} - Calc_{i,t})^2}}{n} \qquad \text{Equation 3.6}$$

$$R = \sqrt{\frac{\sum_t (Calc_{i,t} - \overline{Obs_i})^2}{\sum_t (Obs_{i,t} - \overline{Obs_i})^2}} \qquad \text{Equation 3.7}$$

$$R2 = 1 - \frac{\sum_t (Obs_{i,t} - Calc_{i,t})^2}{\sum_t (Obs_{i,t} - \overline{Obs_i})^2} \qquad \text{Equation 3.8}$$

where t is the simulation time in day; n is the total simulation days; i is the calibration point i; $Obs_{i,t}$ is the observed daily discharge at location i at day t; $\overline{Obs_i}$ is the mean of the observed discharge at location i for the simulation period, and $Calc_{i,t}$ is the simulated discharge at location i at day t.

3.4.6. Hydrological Impacts Assessment

After successfully calibrating and validating the hydrologic model for the period (1982-1991) considered to be within the naturalized undisturbed periods, the model was run with climatic inputs to simulate discharge for both the naturalized periods and the impacted periods identified by the change point analysis. In all, discharge for five (5) different periods were simulated, and a water balance output obtained for precipitation (P), streamflow (Q), actual evapotranspiration (ET). Further, we assessed the hydrological impacts by computing changes between the control or baseline periods and impacted periods for the water balance components. Finally, the concept of elasticity as proposed by Schaake (1990) was employed to evaluate the sensitivities of streamflow to changes in climate. According to this concept, climate elasticity of streamflow is the proportional change in streamflow divided by the proportional change in a climate variable. For instance, the precipitation elasticity of streamflow is defined as:

$$\varepsilon_p = \frac{dQ/Q}{dP/P} = \frac{dQ}{dP} \cdot \frac{P}{Q} \qquad \text{Equation 3.9}$$

Likewise, the actual evapotranspiration elasticity of streamflow is:

$$\varepsilon_{ET} = \frac{dQ/Q}{dET/ET} = \frac{dQ}{dET} \cdot \frac{ET}{Q} \qquad \text{Equation 3.10}$$

In applying equations (3.9) and (3.10) to the water balance outputs obtained for the Rockaway catchment model, the relative contributions of precipitation and actual ET changes to streamflow changes can be quantified. Over the long term, the water balance model can be expressed as:

$$\bar{Q} = \bar{P} - \overline{ET} \qquad \text{Equation 3.11}$$

where $\bar{Q}$, $\bar{P}$, and $\overline{ET}$ denote long term mean values. In Equation (3.11), there is an implicit assumption that groundwater flow into and out of the Rockaway sub-catchment cancels out and storage change over the long term is negligible.

For a largely undisturbed catchment, the changes in streamflow between two periods (dQ) based on equation (3.11) can be estimated as:

$$dQ = dQ_P + dQ_{ET} \qquad \text{Equation 3.12}$$

with dQ_P and dQ_{ET} denoting the contribution to streamflow from precipitation and actual ET respectively. Combining equations (3.9), (3.10), and (3.12), dQ can be rewritten as:

$$dQ = dQ_P + dQ_{ET} = (\varepsilon_{P \cdot dP/P} + \varepsilon_{ET \cdot dET/ET})Q \qquad \text{Equation 3.13}$$

where dP and dET are changes in precipitation and actual evapotranspiration between two periods. ε_p and ε_{ET} are precipitation elasticity and actual evapotranspiration elasticity of streamflow respectively. According to Tang et al. (2013), a 1% change in P or ET triggers an ε_p or ε_{ET} percent change in Q.

Note that flow data used in this analysis form part of the reconstructed streamflow records by Hickman and McHugh (2018) for selected watersheds in the PRB, and therefore the Rockaway sub-catchment is assumed to be largely undisturbed for the purpose of this study. Being mindful of the fact that climate elasticity to streamflow varies depending on the location and reference period (Vano et al., 2012), we explored the sensitivities of flow relative to different baseline periods. Thus, equation (3.13) was set up for the two impacted periods (2002—2011, and 2012—2021) relative to three baseline periods (i.e. 1982—1991, 1992—2001, and 1982—2001). The values of ε_p and ε_{ET} were then computed simultaneously from two equations to obtained the contributions of P and ET changes to streamflow change in the Rockaway sub-basin.

3.5. Results and Discussion

3.5.1. Decomposition of time series data via DWT

According to equation 3.3, the type of db mother wavelet that produced the optimal parameters for the decomposition process for each dataset are presented in Table 3.2. Figure 3.3 illustrates an example of the decomposition results for the flow data in the Rockaway sub-catchment. The original time series or signal (S) can be reconstructed by summation of all the Detailed components (D1—D6) and the Approximation component of the last decomposition level (A6). It can be seen that at higher decomposition levels, the frequency of the D components decrease. The last decomposition level of the A component (A6) shows the trend of streamflow in the Rockaway catchment. On a dyadic scale, D1 depicts time series of a 2-year mode, D2 shows a 4-year mode, D3 is in an 8-year mode, D4, a 16-year mode, D5 corresponds to a 32-year mode, and 64-year mode for D6. These modes are the time scales at which those cycles are revealed, implying that for a dataset spanning a period of 42 years, the trend as revealed by the DWT for stream flow in the Rockaway catchment could only emerge over a 64-year cycle. It was thus impossible to see this trend just by applying the MK trend test on the raw dataset. The same process was replicated in all three sub-catchments for each hydro-climatic indicator variable as depicted by figures 3.4, 3.5, and 3.6. At a confidence level of 95% (i.e. p-value= 0.05), MK statistics were subsequently applied to the decomposed times series.

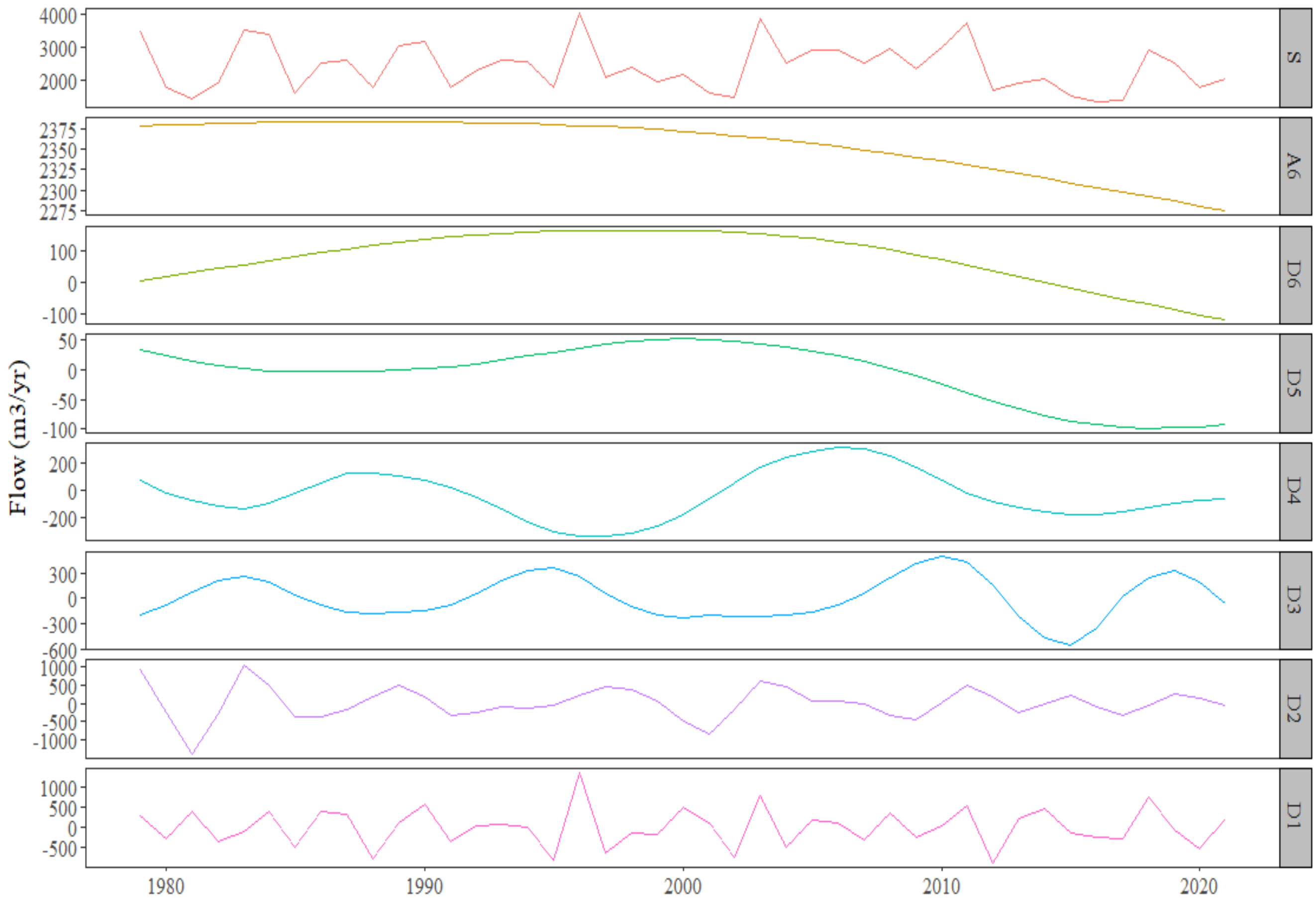

Figure 3.3: Annual streamflow time series of the original dataset and its decomposed components via DWT (level 6) for the Rockaway sub-catchment

3.5.2. DWT Trend analysis of hydro-climatic indicators

Results from the trend analysis using the discrete wavelet transform for Precip, Flow, R10, CDD, Tmin, Tmean, and Tmax from the Ringwood, Rockaway, and Upper Passaic catchments are shown in Figures 3.4, 3.5, and 3.6. Mann-Kendall statistics (i.e. significant level (SL) and Sen's slope (SS)) applied on the DWT trend results are also summarized in Table 3.2. The positive and negative MK values indicate significantly increasing and decreasing trends respectively, the magnitude of the trends are described by the SS values. All the analyzed hydro-climatic signals were significant at p=0.05, identified by the asterisk.

Table 3.2: Daubechies (db) wavelet type, minimum relative error (RE), Mann-Kendal test, and Sen’s slope (SS) for each metric in each sub-catchment

Sub-catchment	Parameter	Metrics						
		Precip	Flow	R10	CDD	Tmin	Tmean	Tmax
Ringwood	Wavelets	db7	db6	db8	db5	db4	db4	db4
	R_E	3.75	0.03	4.86	5.72	3.93	4.48	13.46
	MK^{SL}	871*	-457*	-457*	-877*	903*	903*	903*
	SS	0.723	-0.165	-0.024	-0.051	0.047	0.033	0.018
Rockaway	Wavelets	db5	db6	db8	db4	db4	db4	db10
	R_E	7.29	4.18	2.91	3.02	4.43	4.29	10.33
	MK^{SL}	635*	-745*	577*	293*	903*	903*	831*
	SS	0.129	-2.406	0.083	0.0042	0.059	0.035	0.0034
Upper Passaic	Wavelets	db4	db4	db7	db4	db4	db4	db4
	R_E	7.49	6.32	67.10	7.79	3.21	3.79	6.86
	MK^{SL}	903*	903*	433*	213*	903*	903*	903*
	SS	2.401	7.712	0.0134	0.0062	0.0375	0.0253	0.013

3.5.3 Hydro-climatic trends in the Ringwood, Rockaway, and Upper Passaic sub-catchments

DWT trend results for all hydro-climatic variables in the Ringwood sub-catchment are shown in Figure 3.4. Precipitation shows a significant increasing signal at a rate of 0.723mm/year. However, this increase does not reflect in the streamflow trend in the Ringwood sub-catchment. Flow is rather showing a significant downward trend beginning from 1996 through to 2021 at a rate of 0.165m^3yr^{-1}. It does appear that the downward trend observed for streamflow largely tracks with heavy precipitation (R10) rather than mean precipitation, and corroborated by the decreasing trend in consecutive dry days (CDD). The observed significantly increasing trend in minimum, mean, and maximum temperatures suggest that temperature drives the flow dynamics in the Ringwood sub-catchment with minimum temperature having the highest magnitude at $0.047^{o}Cyr^{-1}$and maximum temperature having the least at $0.018^{o}Cyr^{-1}$.

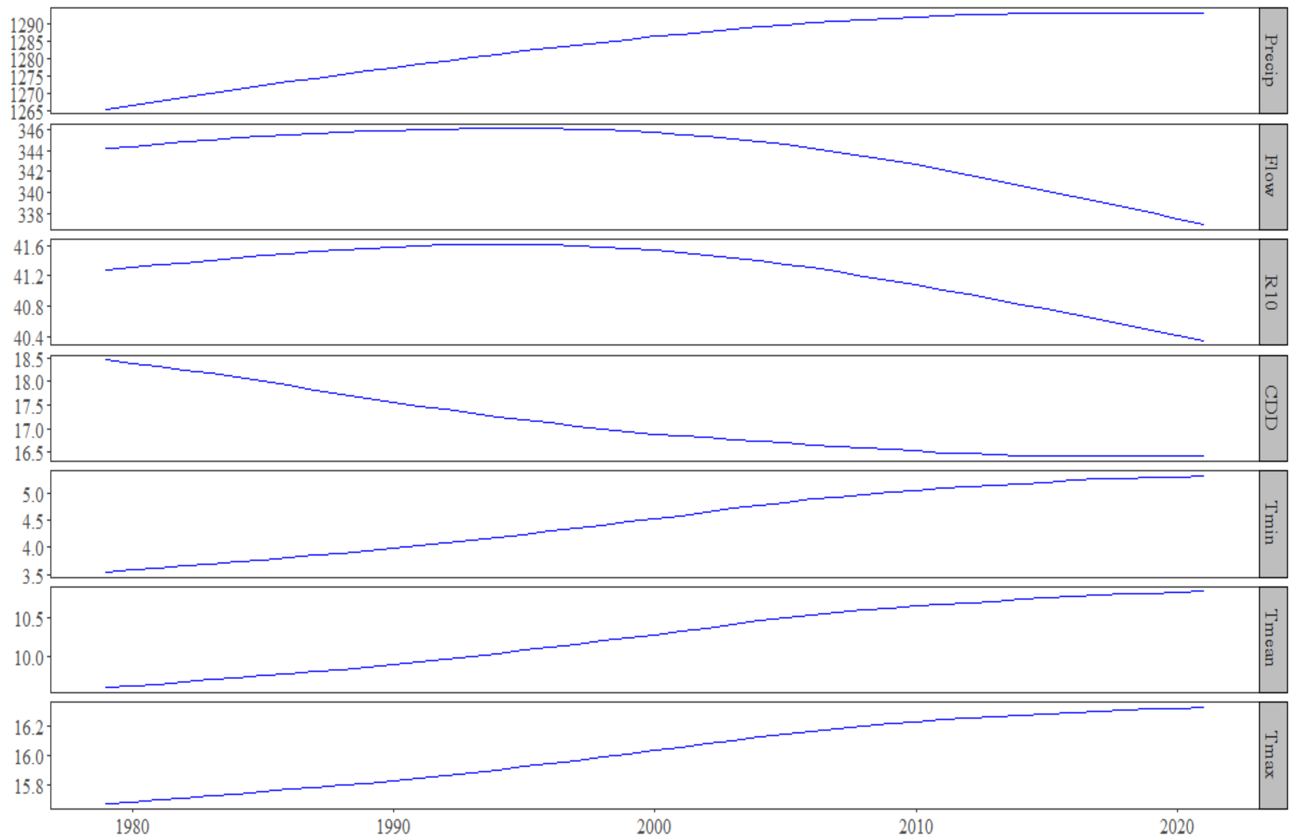

Figure 3.4: Trends in precipitation, flow, and temperature variables for the Ringwood sub-catchment from 1979—2021

Long term trends in hydro-climatic indicator variables in the Rockaway catchment are illustrated in Figure 3.5. Similar to the Ringwood sub-catchment, precipitation and streamflow are trending in opposite directions. As precipitation trends upward, flow is trending downward at rates of $0.129mmyr^{-1}$ and $2.406cmyr^{-1}$ respectively. Quite interestingly, a significantly upward trend is observed for heavy precipitation, in line with mean precipitation yet these increases do not reflect in the observed flow trend. Given that consecutive dry days show significantly increasing trend in tandem with minimum, mean and maximum temperatures, there is a likelihood that precipitation is overwhelmed by relatively high temperatures in the Rockaway sub-catchment, thereby translating in the observed downward trend in streamflow.

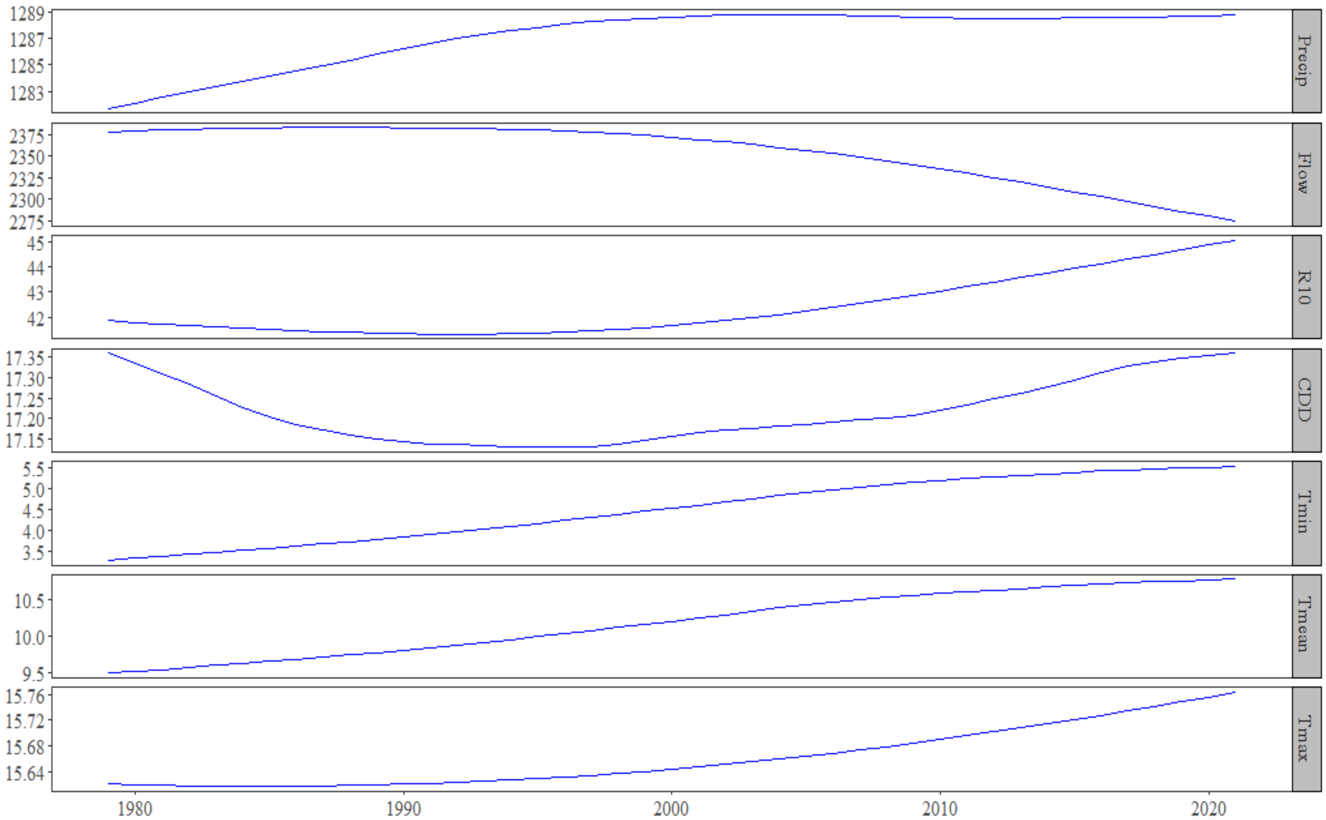

Figure 3.5: Observed trends in precipitation, flow, and temperature indicator variables for the Rockaway sub-catchment from 1979—2021

Figure 3.6 shows the hydro-climatic trends in indicator variables for the Upper Passaic sub-catchment. All the metrics showed significantly increasing trends over the period. The observed upward trend in mean and heavy precipitation in the same direction as flow and temperatures indicate that, the hydrology of the Upper Passaic sub-catchment is largely driven by precipitation than temperature. Precipitation and flow are increasing at a rate of 2.401mmyr^{-1} and 7.712cmyr^{-1} respectively. In the case of temperature, the rate is higher in minimum temperature (0.038 ^{o}Cyr^{-1}) followed by mean temperature (0.025 ^{o}Cyr^{-1}), and maximum temperature (0.013 ^{o}Cyr^{-1}) (Table 3.2).

3.5.4. Comparison of hydro-climatic trends by catchment

Spatially, trending from North to South of the PRB, the results suggest that hydro-climatic indicator variables are spatially non-uniform in terms of magnitude and direction. Over the analyzed period (1979—2021), precipitation is observed to show increasing signals in all sub-catchments. Relatively, the rate of change is observed to be rapid in the Upper Passaic sub-catchment at 2.401mmyr^{-1} and smooth in the Rockaway sub-catchment at 0.129mmyr^{-1}. Likewise, temperatures also show significantly upward trends in all sub-catchments with mean temperature displaying the highest rate of change in the Rockaway sub-catchment, followed by Ringwood, and Upper Passaic sub-catchments. The observed long-term increasing trend in precipitation and temperature in the PRB is indicative of a changing climate in the basin, consistent with the dominant trends in the broader Northeast United States region (Hayhoe et al., 2007; Lynch et al., 2016). In terms of extremes, precipitation intensity (R10) and consecutive dry days (CDD) point towards an upward trend from North to South in the PRB, beginning from Ringwood sub-catchment with a decreasing signal to increases in the Rockaway and Upper Passaic sub-catchments. This observed increasing trend is also consistent with patterns in rainfall intensity in the Northeast (Thibeault and Seth, 2014; Hoerling et al., 2016), and provides further evidence to the linkage between extreme weather events and climate change.

In the case of streamflow, the results suggest that flow patterns appear to be influenced both by surface characteristics and climate in the PRB. Although trends in precipitation and temperature are observed to increase throughout the basin, the dynamics on streamflow is different, with downward trends observed in the Ringwood and Rockaway sub-catchments and an upward trend seen in the Upper Passaic sub-catchment. Given that Ringwood and Rockaway sub-catchments lie in the mountainous heavily forested Highlands region as against Upper Passaic in the densely populated highly industrialized urban belt, the observed trends are not surprising. With regards to attributing causes of streamflow changes in the PRB, the sections that follow, involving the hydrological modeling study using the Rockaway sub-basin as a case study, provide sufficient clues on the driving mechanism behind the flow dynamics in the study basin.

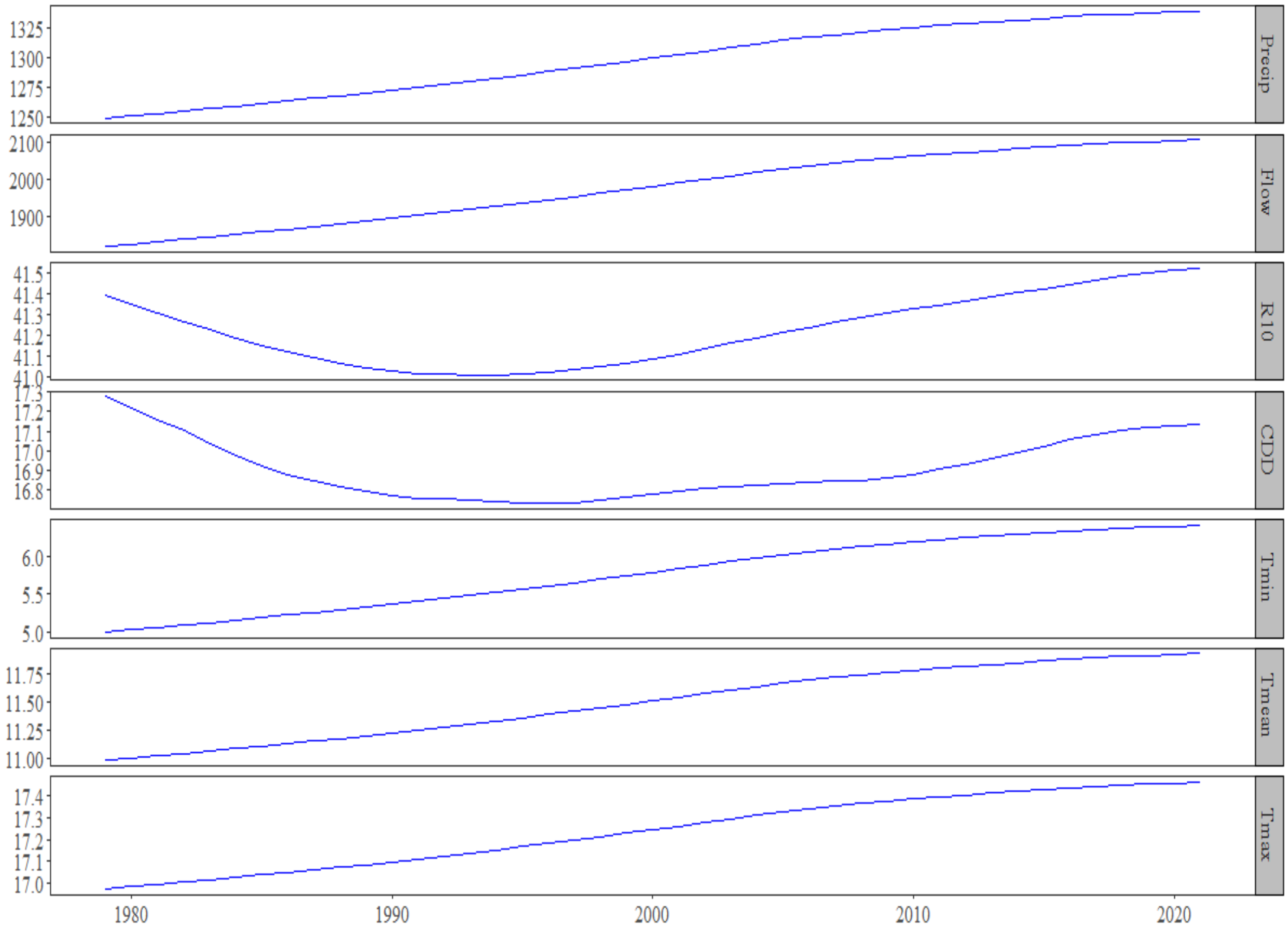

Figure 3.6: Observed trends in precipitation, flow, and temperature indicator variables in the Upper Passaic sub-catchment from 1979—2021

3.6.1. Change point analysis and calibration and validation of MIKE SHE model

3.6.1.1. Change point detection.

For the purpose of the hydrological impact assessment, change point detection was carried out to determine approximate years of abrupt changes in hydro-climatic time series. As presented in Table 3.3, precipitation and streamflow time series were explored in the Rockaway sub-catchment using the CUSUM test as well as the permutation test, and were significant at α=0.05. Given that river flow in the PRB is largely regulated, the similarities as revealed by the break point years for both precipitation and streamflow seem to corroborate the findings by Ficklin et al. (2016) that climate change signals are apparent in both regulated and natural river systems. Following from this, the causes of streamflow were explored by examining outputs of water balance terms from the hydrological model developed for the Rockaway sub-catchment. Accordingly, we performed decadal changes in water balance terms in line with the break point years given in Table 3.3. Over the study period (1979—2021), decades 1 and 2 spanned the periods 1982—1991 and 1992—2001 respective, representing baseline periods 1(BLP I) and 2 (BLP II). The overall period from 1982—2001 was also considered, denoting baseline period 3 (BLP III). For the impacted periods, 2002—2011, and 2012—2021 respectively represents decades 3 (D III) and 4 (D IV).

Table 3.3: Estimated break point years in precipitation and streamflow in the Rockaway sub-catchment (α=0.05)

	Cumulative sum test	Permutation test
Variables	Break point	Break point
Precipitation	1980	1979
	1990	1991
	2002	2003
	2011	2012
Streamflow	1980	1979
	1990	1991
	2002	2003
	2011	2012

3.6.1.2. Calibration and validation of Rockaway model.

The Rockaway model was calibrated using both streamflow and groundwater level data. The full model simulation spanned the period 1981-1991 for streamflow and 2005-2016 for groundwater flow. Observed streamflow was calibrated and validated at the outlet of the Rockaway catchment along with two (2) groundwater well observations located in the catchment. As shown in Table 3.4 and figure 3.7, the performance of the model was assessed using a combination of statistical indicators and graphical representation respectively. Generally, the model can be said to have captured the evolution of the observed flow sufficiently well, with few mismatches in peak flows likely due to the gridded structure of the forcing data. Rising limbs of hydrographs and baseflow were also reasonably simulated. The resulting correlation coefficient (R), Nash-sutcliffe (R2), mean error (ME), and RMSE values for both calibration and validation periods are shown in Table 3.4.

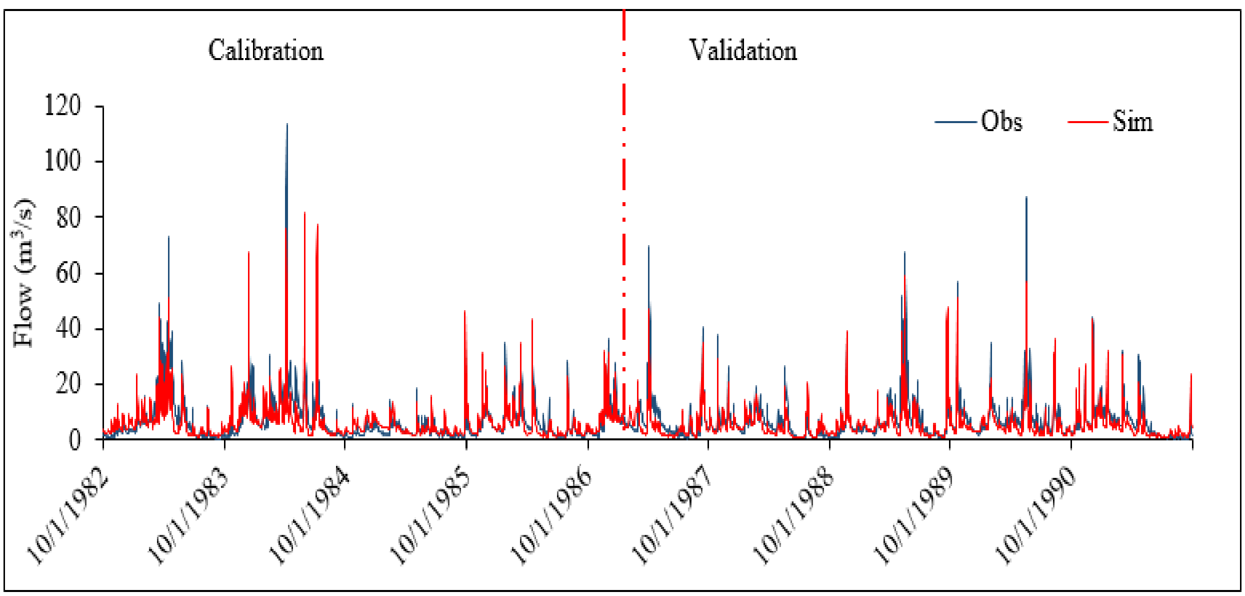

Figure 3.7: Simulated and observed daily streamflow at the Rockaway sub-catchment for the calibration (1982—1986), validation (1986—1991), and the full simulation (1981—1991)

In the groundwater level simulation, the transient dynamics of water level were satisfactorily simulated for the Berkshire Valley well, but poor in the Morris Maint well. Aside possible errors from the DEM, the observed bias could be linked to boundary conditions at the border, that favored the Berkshire Valley well more than the Morris Maint well. Although individual biases such as this is inevitable, the multiple mode of calibration (i.e. using both streamflow and groundwater data) in this study allows for simultaneous optimization of model parameters to ensure proper balance between the two solutions (i.e. simulated hydrograph and groundwater level dynamics). Thus in general, the MIKE SHE performed reasonably well in capturing the observed streamflow and groundwater levels in the Rockaway sub-catchment. On the basis of this results, we explore and quantify the possible mechanisms behind the observed streamflow changes in the sub-basin.

Table 3.4: Performance criterion of calibrated and validated MIKE SHE model at the Rockaway sub-catchment

	Streamflow			Groundwater	
Statistics	Calibration	Validation	Full simulation	Berkshire Obs well	Morris Obs well
	1982-1986	1987-1991	1982-1991	2011-2016	2007-2012
Correlation coefficient (R)	0.85	0.87	0.85	0.83	0.28
Nash efficiency (R2)	0.72	0.71	0.72	-	-
ME	0.57	1.34	0.96	6.01	-1.86
RMSE	4.78	3.89	0.85	6.07	1.91

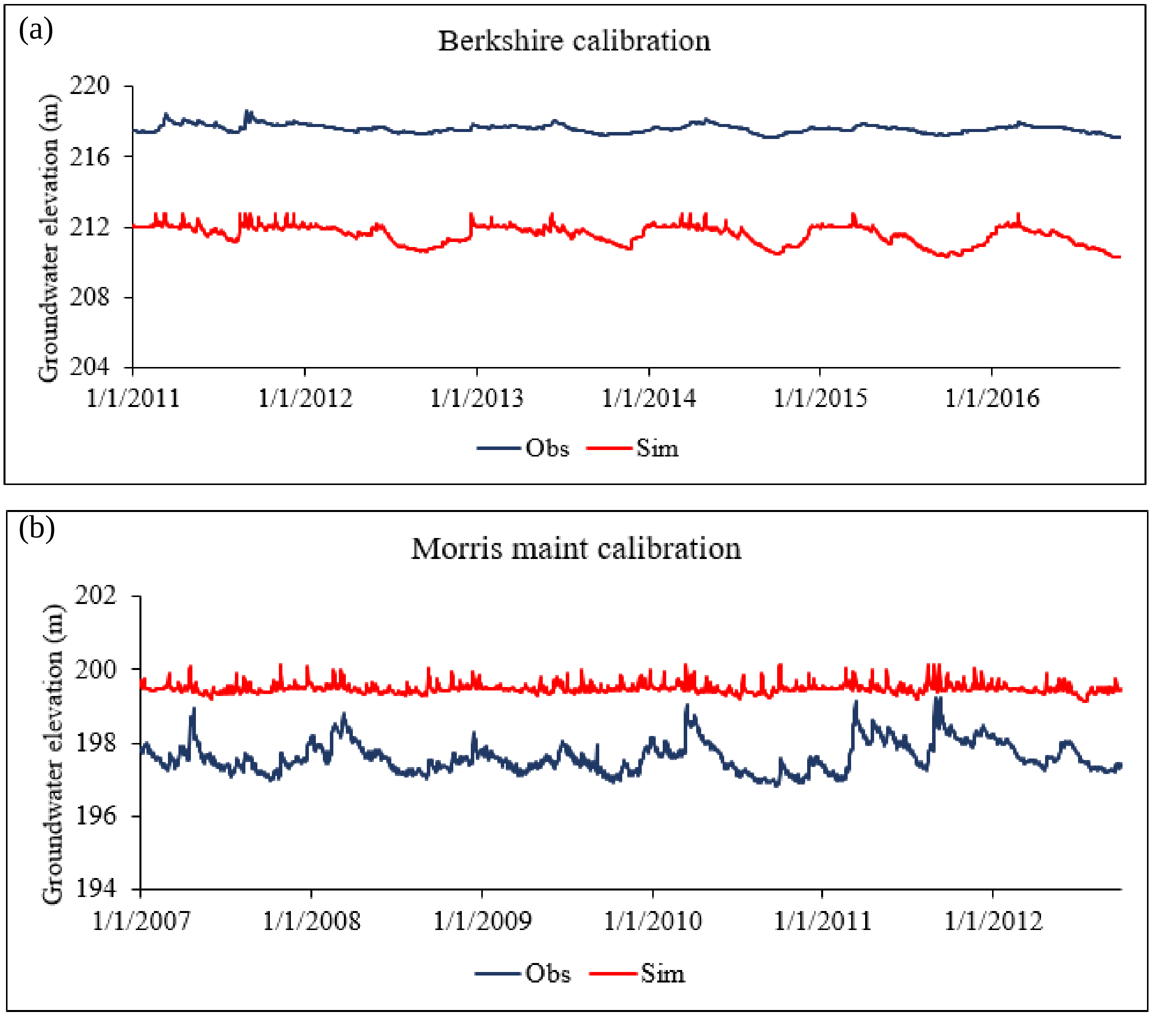

Figure 3.8: Simulated groundwater level dynamics at a) Berkshire valley and b) Morris Maint well locations in the Rockaway sub-catchment

3.6.2. Decadal changes in hydro-meteorological variables

Relative to the three different naturalized and baseline periods (i.e. 1982—1991, 1992—2001, and 1982—2001), decadal changes in hydro-meteorological variables were computed from the impacted periods (i.e. 2002—2011 and 2012—2021) (Table 3.5).

Table 3.5: Mean annual changes in climatic and streamflow variables of the Rockaway sub-basin for the baseline (BLP) and impacted periods (D)

Period	Tmin (°C)	Tmean (°C)	Tmax (°C)	Precip (mm)	Evapo (mm)	Flow (m^3)
BLP I: 1982~1991	2.76	9.27	15.78	1306	805	2244
BLP II: 1992~2001	2.99	9.40	15.82	1208	777	1898
BLP III: 1982~2001	2.87	9.34	15.80	1257	791	2071
D III: 2002~2011	4.31	10.09	15.89	1427	826	2277
D IV: 2012~2021	5.24	10.56	15.88	1282	837	1947
D III minus BLP I	1.55	0.82	0.11	9.29%	2.58%	1.46%
D IV minus BLP I	2.49	1.29	0.11	-1.83%	3.98%	-13.22%
D III minus BLP II	1.32	0.69	0.07	18.13%	6.25%	19.94%
D IV minus BLP II	2.25	1.16	0.07	6.11%	7.71%	2.59%
D III minus BLP III	1.44	0.75	0.09	13.54%	4.38%	9.93%
D IV minus BLP III	2.37	1.23	0.09	1.99%	5.81%	-5.97%

3.6.2.1. Hydro-climatic response to changes relative to 1982—1991 baseline, BLP I. Decadal changes (i.e. 2002—2011 and 2012—2021) in Tmin, Tmean, and Tmax for the impacted periods relative to the reference showed increase in both decades, with the recent decade (D IV) being the warmest (Table 3.5). Compared to mean and maximum temperatures, minimum temperature is observed to have a higher increasing rate (2.49° C/decade), and is indicative of a rapidly warming climate in the basin. Along with the increasing temperatures, actual ET is also observed to increase in both decades (2.58% and 3.98% for D III and D IV resp.). However, precipitation is observed to increase in D III but decreased in D IV. This decrease in precipitation, though marginal, suggests that the recent decade (D IV) experienced meteorological stressed conditions with respect to the baseline and as compared to D III. Typically, evapotranspiration is limited in such water stress conditions, and is therefore expected to decline in D IV. However, a decreased precipitation not resulting in a decreased ET for D IV suggests that the rapid warming observed in the area somewhat played a key role in the increased actual evapotranspiration. This partly explains why streamflow declined disproportionately in the recent decade.

At a glance, the observed increase in precipitation in D III by 9.29% resulting in an increase in flow by 1.46%, and a decrease in precipitation in D IV by 1.83% leading to a decrease in streamflow by 13.22% may lead one to conclude that precipitation is the main climatic factor for streamflow changes in the basin. However, recourse to the elasticity of climate variables to streamflow in the basin will lead to a different conclusion. In Table 3.6, we find that elasticities of precipitation and actual ET are 0.96 and -2.88 respectively. This suggests that, 10% increase in precipitation results in 9.6% increase in streamflow, while 10% increase in actual ET leads to 28.8% decrease in streamflow. Thus generally, streamflow is less sensitive to precipitation for the reference period. These elasticities also explain the relatively modest (1.46%) increase in streamflow for the 9.29% increase in precipitation in D III, and likewise the 13.22% decrease in flow for an only 1.83% decrease in precipitation in D IV with respect to the 1982—1991 baseline period. Thus it can be concluded from the above results that actual evapotranspiration is the main climatic factor responsible for streamflow dynamics in the Rockaway sub-basin for this reference period. Although this conclusion holds true, in respect of the actual contribution to the observed streamflow changes for D III, precipitation was entirely responsible with 100% contribution. This means that the amount of precipitation was more than sufficient to satisfy evaporative demands, with the left over going into streamflow generation. For D IV, the impact of actual ET sensitivity to streamflow was largely felt. Such that, while actual ET contributed to approximately 87% of streamflow, precipitation contributed only 13%.

Table 3.6: Annual streamflow elasticities and contribution of precipitation and actual ET to streamflow changes for respective baseline periods

Period	Contribution to Q change	Elasticity (ε) Precip	Evapo	Equation
I: 2002~2011				
		0.96	**-2.88**	
	relative to BLP I	100%	~	$9.29\varepsilon_P + 2.58\varepsilon_E = 1.46$
		1.35	**-0.74**	
	relative to BLP II	100%	~	$18.13\varepsilon_P + 6.25\varepsilon_E = 19.94$
		1.19	**-1.44**	~
	relative to BLP III	55%	-30%	$13.54\varepsilon_P + 4.38\varepsilon_E = 9.93$
II: 2012~2021				
		0.96	**-2.88**	
	relative to BLP I	13.28%	86.62%	$1.83\varepsilon_P - 3.98\varepsilon_E = 13.22$
		1.35	**-0.74**	
	relative to BLP II	100	~	$6.11\varepsilon_P + 7.71\varepsilon_E = 2.59$
		1.19	**-1.44**	
	relative to BLP III	~	100%	$1.99\varepsilon_P + 5.81\varepsilon_E = -5.97$

3.6.2.2. Hydro-climatic response to changes relative to 1992—2001 baseline, BLP II. Relative to 1992—2001 reference period, all temperature variables in the basin saw increases consistent with global trends (Hansen et al., 2006; NCA, 2018), with minimum temperature showing the largest increase in D IV (2.25^{o} C/decade). Unsurprisingly, actual ET followed along with temperature, with increases of 6.25% and 7.71% for D III and IV respectively. However, these increases were overwhelmed by the respective 18.13% and 6.11% increase in precipitation, leading to a rise in streamflow by 19.94% and 2.59% for D III and IV respectively. Here D III, having precipitation increase by 18.13% can be considered as a meteorologically wet decade compared to D IV and relative to the baseline period. While water limits ET values in dry conditions, energy limits ET values in wet conditions (Donohue, et al., 2012; Ajjur and Al-

Ghamdi, 2021). Similarly, actual evapotranspiration in D III was largely energy-limited, leading to a considerable streamflow generation by 19.94%.

In terms of sensitivity to streamflow, Table 3.6 shows that streamflow elasticity to precipitation is 1.35, indicating that a 10% rise in mean annual precipitation results in a 13.5% increase in streamflow. On the other hand, streamflow elasticity to actual ET is -0.74, which suggests a 7.4% decline in streamflow for a 10% increase in actual ET. This indicates that streamflow is more sensitive to precipitation than actual ET for this reference period and that evaporative demand was overcome by the relative increases in precipitation for D III and IV. As such, the observed increases in streamflow for both decades can be entirely attributed to precipitation as revealed in Table 3.6.

3.6.2.3. Hydro-climatic response to changes relative to 1982—2001 baseline, BLP III. Minimum, mean, and maximum temperatures showed increases in both decades (D III and D IV) relative to the baseline. With the recent decade being the warmest in the basin, minimum temperature is observed to have the highest increasing rate (2.37^{o}C/decade), followed by mean temperature (1.23^{o}C/decade), and then maximum temperature (0.09^{o}C/decade). Similarly, precipitation was observed to increase in both decades, with the largest increase in D III, having 170mm (13.54%) more than in the baseline period. Consistent with temperature, actual evapotranspiration was observed to increase in both decades compared to the baseline. Although the results in Table 3.5 show that both precipitation and evapotranspiration are increasing for all decades relative to the baseline, they induced varied signal and strength in streamflow. Whereas precipitation was the dominant contributor to streamflow in D III (55%) leading to an increased flow, actual ET entirely overwhelmed precipitation in D IV causing a decrease in flow. The reason for this is that in D III, water was sufficient, and energy becomes the more important control of evapotranspiration whereas in D IV, water was limited, and evapotranspiration, largely driven by energy, went into further decreasing streamflow (-5.97%).

This is confirmed by sensitivity results in Table 3.6. It reveals that, elasticity of streamflow in relation to precipitation (ε_p) and actual ET (ε_{ET}) for the Rockaway sub-basin are 1.19 and -1.44 respectively. This indicates that 10% increase in precipitation results in 11.9% increase in streamflow while 10% increase in actual ET would lead to 14.4% decrease in streamflow. Thus annual streamflow was generally more sensitive to the change in actual ET than the change in precipitation, although in D III, precipitation contributed 55% to streamflow changes whereas evapotranspiration contributed 30%.

3.7. Summary and Conclusions

At a time when the climate change problem has evolved into a crisis, the piece-meal approach to carrying out hydrological impact analysis at a single study location may no longer suffice. At best, a comprehensive study that combines the detection and analysis of trends along with hydrological modelling study will provide important foundations for understanding the hydro-climatic patterns in an area and the driving mechanisms behind these trends in the wake of a changing climate. In this study, we used long-term meteorological and hydrologic observations to identify trends in hydro-climatic indicator variables in the PRB. We also modelled streamflow and groundwater elevation using the Rockaway sub-basin as a case study to understand the impacts of recent climate changes to streamflow in the study basin. Recognizing that hydro-climatic variables, by their nature, are non-monotonic, we employed the wavelet transform— an advanced trend analysis tool— as against the frequently used MK trend test, to detect and identify patterns in hydro-climatic variables in the PRB. Rather than using the MK trend test directly on the raw data whose results are almost always ambiguous in respect of precipitation data for instance, the wavelet transform approach was applied to identify the hidden monotonic trends in the characteristically noisy hydro-climatic time series. For the hydrological impact assessments, the physically-based distributed MIKE SHE hydrologic model provided the platform to successfully simulate the hydrologic conditions of the Rockaway catchment. Based on the model's water balance outputs, the impacts of recent climate were assessed from changes in naturalized or baseline periods against impacted periods. Further analysis was carried out using climate elasticities to determine the sensitivities and contributions of climatic variables to streamflow changes in the sub-basin to three different baseline conditions. By this, we demonstrated that the time perspective or baseline condition used to assess climate change impacts can also substantially influence results.

Major sources of uncertainty in this study may be that which pertains to hydrological modelling such as input, output, structural, and parametric uncertainties (Renard et al., 2010; Ma et al., 2016). Because streamflow observations used in calibrating and validating the MIKE SHE hydrological model was based on reconstructed data, it is likely that errors emanating from the methods and data used in estimating daily reconstructed streamflow for the Rockaway catchment (refer to Hickman and McHugh, 2018) may be propagated in this study. Howbeit, conscious effort was made in minimizing uncertainties in our analyses first by the use of multiple objective function (i.e. observed streamflow and groundwater level data) that allowed for simultaneous optimization of model parameters. The model's ability to reasonably simulate both surface and subsurface flows as evidenced in the satisfactory performance criterion give credence to the findings in the study. In addition, one uncertainty that has almost been universally overlooked in climate impact studies is the choice of baseline condition. In our study, we assessed the hydrologic response to changes in climate using three different baseline climates against two recent future periods (i.e. 2002—2011, 2012—2021). We found that the choice of baseline condition constitutes an important source of uncertainty in the sensitivities of streamflow to precipitation and evapotranspiration changes and should routinely be considered in any climate impact assessment. Against this background, we present the key findings from our results below:

1) Over the period 1979—2021, minimum, mean, and maximum temperatures showed significantly upward trend in all studied sub-catchments of the PRB with minimum temperature having the highest rate of change at 0.059 $^{o}Cyr^{-1}$ in the Rockaway sub-basin. In contrast, maximum temperatures experienced the slowest rate of change at 0.0034 $^{o}Cyr^{-1}$. The rate of change of mean temperatures range from 0.025—0.035 $^{o}Cyr^{-1}$.
2) Overall, precipitation showed a significant increasing signal in all analyzed sub-basins with the fastest rate of 0.72mm/yr in the Ringwood catchment and the slowest rate at 0.13mm/yr in the Rockaway catchment. This observed long term increasing trend in precipitation and temperature in the PRB is indicative of a changing climate, consistent with the dominant trends in the broader Northeastern region. Spatially, trends in both precipitation intensity (R10) and consecutive dry days (CDD) were observed to decrease in the uppermost portion of the PRB at the Ringwood catchment but increases towards the south in the Rockaway and Upper Passaic sub-basins. This pattern is also dominant in the wider Northeast, and provide further evidence of the connection between extreme weather events and climate change.
3) In two out of the three analyzed sub-basins, streamflow displayed significantly downward trends with an increasing trend in the Upper Passaic sub-catchment. This is in spite of the increasing trends in both precipitation and temperature in all the three sub-catchments. Although it is well established that precipitation amounts and intensity directly affect streamflow (Lan et al. 2010), the present results rather show that an increase in

precipitation does not always lead to an increase in streamflow. From a hydrological modeling standpoint, attempt was therefore made to examine the causes of streamflow in the PRB using the Rockaway sub-catchment as a case study.

4) Decadal changes in climate revealed that the recent decade (2012—2021) was the warmest relative to the 1982—1991 baseline period. The wettest decade was 2002—2011 relative to all baseline periods with precipitation increase ranging from 9.29% in the 1982—1991 baseline to 18.13% in the 1992—2001 baseline. In contrast, the recent decade (2012—2021) was the driest period with precipitation changing from -1.83% to 6.11% relative to the 1982—1991 and 1992—2001 baselines respectively.

5) Across the three baseline periods, we found that precipitation elasticity to streamflow ranged from 0.96 to 1.35 suggesting that, a 10% rise in precipitation will result in between 9.6% to 13.5% increase in streamflow in the study basin. Similarly, evapotranspiration elasticity to streamflow ranged from -2.88 to -0.74 indicating that, a 10% increase in actual ET will lead to between 28.8% to 7.4% decrease in streamflow. The largely negative ET elasticity value also reflects the effect of warming climate in the basin. Generally, as temperature increases, ET increases and streamflow decreases. With streamflow showing high sensitivity to actual ET increases more than precipitation, it is safe to conclude that, to a large extent, actual evapotranspiration is more important in the flow dynamics of the PRB in the wake of a warming climate.

6) The general observation therefore is that in decades where water is available, energy limits actual evapotranspiration which makes streamflow more sensitive to precipitation increase. However, in meteorologically stressed or dry decades, water limits actual ET thereby making streamflow more sensitive to increases in actual evapotranspiration.

The application of discrete wavelet transform analysis and process-based hydrological modeling in this study adequately captured the hydro-climatic signatures as well as hydrologic response to climate change in the PRB. A broader study in the future that incorporates how hydrologic sensitivities vary spatially across the PRB will help in further minimizing the uncertainties in climate impact assessments for the basin.

3.8. References

Adamowski, J. F. (2008). Development of a short-term river flood forecasting method for snowmelt driven floods based on wavelet and cross-wavelet analysis. Journal of Hydrology, 353(3-4), 247-266.

Adamowski, J., & Chan, H. F. (2011). A wavelet neural network conjunction model for groundwater level forecasting. Journal of Hydrology, 407(1-4), 28-40.

Adamowski, J., & Chan, H. F. (2011). A wavelet neural network conjunction model for groundwater level forecasting. Journal of Hydrology, 407(1-4), 28-40.

Adamowski, J., Adamowski, K., & Bougadis, J. (2010). Influence of trend on short duration design storms. Water resources management, 24(3), 401-413.

Adamowski, K., Prokoph, A., & Adamowski, J. (2009). Development of a new method of wavelet aided trend detection and estimation. Hydrological Processes: An International Journal, 23(18), 2686-2696.

Adarsh, S., & Janga Reddy, M. (2015). Trend analysis of rainfall in four meteorological subdivisions of southern India using nonparametric methods and discrete wavelet transforms. International journal of Climatology, 35(6), 1107-1124.

Adarsh, S., & Janga Reddy, M. (2015). Trend analysis of rainfall in four meteorological subdivisions of southern India using nonparametric methods and discrete wavelet transforms. International journal of Climatology, 35(6), 1107-1124.

Ahmad, I., Tang, D., Wang, T., Wang, M., & Wagan, B. (2015). Precipitation trends over time using Mann-Kendall and spearman's rho tests in swat river basin, Pakistan. Advances in Meteorology, 2015.

Ajjur, S. B., & Al-Ghamdi, S. G. (2021). Evapotranspiration and water availability response to climate change in the Middle East and North Africa. Climatic Change, 166(3-4), 28.

Araghi, A., Baygi, M. M., Adamowski, J., Malard, J., Nalley, D., & Hasheminia, S. M. (2015). Using wavelet transforms to estimate surface temperature trends and dominant periodicities in Iran based on gridded reanalysis data. Atmospheric Research, 155, 52-72.

Araghi, A., Baygi, M. M., Adamowski, J., Malard, J., Nalley, D., & Hasheminia, S. M. (2015). Using wavelet transforms to estimate surface temperature trends and dominant periodicities in Iran based on gridded reanalysis data. Atmospheric Research, 155, 52-72.

Baguis, P., Roulin, E., Willems, P., & Ntegeka, V. (2010). Climate change scenarios for precipitation and potential evapotranspiration over central Belgium. Theoretical and applied climatology, 99(3), 273-286.

Campbell, J. L., Driscoll, C. T., Pourmokhtarian, A., & Hayhoe, K. (2011). Streamflow responses to past and projected future changes in climate at the Hubbard Brook Experimental Forest, New Hampshire, United States. Water Resources Research, 47(2).

Campbell, J. L., Ollinger, S. V., Flerchinger, G. N., Wicklein, H., Hayhoe, K., & Bailey, A. S. (2010). Past and projected future changes in snowpack and soil frost at the Hubbard Brook Experimental Forest, New Hampshire, USA. Hydrological Processes, 24(17), 2465-2480.

Chattopadhyay, S., & Edwards, D. R. (2016). Long-term trend analysis of precipitation and air temperature for Kentucky, United States. Climate, 4(1), 10.

Chattopadhyay, S., Edwards, D. R., Yu, Y., & Hamidisepehr, A. (2017). An assessment of climate change impacts on future water availability and droughts in the Kentucky River Basin. Environmental Processes, 4(3), 477-507.

Chellali, F., Khellaf, A., & Belouchrani, A. (2010). Wavelet spectral analysis of the temperature and wind speed data at Adrar, Algeria. Renewable Energy, 35(6), 1214-1219.

Csörgö, M., Csörgö, M., & Horváth, L. (1997). Limit theorems in change-point analysis.

Daubechies, I. (1990). The wavelet transform, time-frequency localization and signal analysis. IEEE transactions on information theory, 36(5), 961-1005.

de Artigas, M. Z., Elias, A. G., & de Campra, P. F. (2006). Discrete wavelet analysis to assess long-term trends in geomagnetic activity. Physics and Chemistry of the Earth, Parts A/B/C, 31(1-3), 77-80.

DHI: MIKE SHE Technical Reference, Version 2017 (2017), DHI Water and Environment, Danish Hydraulic Institute, Denmark, 2017.

Ding, Y. J., Li, C. Y., Xiaoming, W. A. N. G., Wang, Y., Wang, S. X., Chang, Y. P., ... & Wang, Z. R. (2021). An overview of climate change impacts on the society in China. Advances in Climate Change Research, 12(2), 210-223.

Dixon, H., Lawler, D. M., & Shamseldin, A. Y. (2006). Streamflow trends in western Britain. Geophysical Research Letters, 33(19).

Do, H. X., Westra, S., & Leonard, M. (2017). A global-scale investigation of trends in annual maximum streamflow. Journal of hydrology, 552, 28-43.

Domenico, P. A., & Mifflin, M. D. (1965). Water from low-permeability sediments and land subsidence. Water Resources Research, 1(4), 563-576.

Domenico, P. A., & Schwartz, F. W. (1998). Physical and chemical hydrogeology (Vol. 506). New York: Wiley.

Dong, X., Nyren, P., Patton, B., Nyren, A., Richardson, J., & Maresca, T. (2008). Wavelets for agriculture and biology: a tutorial with applications and outlook. BioScience, 58(5), 445-453.

Donohue, R. J., Roderick, M. L., & McVicar, T. R. (2012). Roots, storms and soil pores: Incorporating key ecohydrological processes into Budyko's hydrological model. Journal of Hydrology, 436, 35-50.

Drake, A.A., Volkert, R.A., Monteverde, D.H., Herman, G.C., Houghton, H.F., Parker, R.A. and Dalton, R.F. (1996) Bedrock geologic map of northern New Jersey. In: Miscellaneous Geological Investigation Map 1-2540-A. U.S. Geological Survey.

Fan, H., & He, D. (2015). Temperature and precipitation variability and its effects on streamflow in the upstream regions of the Lancang–Mekong and Nu–Salween Rivers. Journal of Hydrometeorology, 16(5), 2248-2263.

Ficklin, D. L., Robeson, S. M., & Knouft, J. H. (2016). Impacts of recent climate change on trends in baseflow and stormflow in United States watersheds. Geophysical Research Letters, 43(10), 5079-5088.

Freeze, R. A., & Cherry, J. A. (1979). Groundwater: Englewood Cliffs. New Jersey.

Gao, P., Zhang, X., Mu, X., Wang, F., Li, R., & Zhang, X. (2010). Trend and change-point analyses of streamflow and sediment discharge in the Yellow River during 1950–2005. Hydrological Sciences Journal–Journal des Sciences Hydrologiques, 55(2), 275-285.

Gardner, R. H., & Urban, D. L. (2003). Model validation and testing: past lessons, present concerns, future prospects. Models in ecosystem science, 184-203.

Gerstengarbe, F. W., & Werner, P. C. (1999). Estimation of the beginning and end of recurrent events within a climate regime. Climate Research, 11(2), 97-107.

Gong, S. L., Zhao, T. L., Sharma, S., Toom-Sauntry, D., Lavoué, D., Zhang, X. B., ... & Barrie, L. A. (2010). Identification of trends and interannual variability of sulfate and black carbon in the Canadian High Arctic: 1981–2007. Journal of Geophysical Research: Atmospheres, 115(D7).

Graham, D. N., & Butts, M. B. (2005). Flexible, integrated watershed modelling with MIKE SHE. Watershed models, 849336090, 245-272.

Guo, L. P., Yu, Q., Gao, P., Nie, X. F., Liao, K. T., Chen, X. L., ... & Mu, X. M. (2018). Trend and change-point analysis of streamflow and sediment discharge of the Gongshui River in China during the last 60 years. Water, 10(9), 1273.

Guo, L.P., Yu, Q., Gao, P., Nie, X.F., Liao, K.T., Chen, X.L., Hu, J.M. and Mu, X.M., 2018. Trend and change-point analysis of streamflow and sediment discharge of the Gongshui River in China during the last 60 years. Water, 10(9), p.1273.

Hamed, K. H., & Rao, A. R. (1998). A modified Mann-Kendall trend test for autocorrelated data. Journal of hydrology, 204(1-4), 182-196.

Hansen, J., Sato, M., Ruedy, R., Lo, K., Lea, D. W., & Medina-Elizade, M. (2006). Global temperature change. Proceedings of the National Academy of Sciences, 103(39), 14288-14293.

Hayhoe, K., Wake, C. P., Huntington, T. G., Luo, L., Schwartz, M. D., Sheffield, J., ... & Wolfe, D. (2007). Past and future changes in climate and hydrological indicators in the US Northeast. Climate Dynamics, 28, 381-407.

Hernández, E., & Weiss, G. (1996). A first course on wavelets. CRC press.

Hickman, R. E., & McHugh, A. R. (2018). Methods used to reconstruct historical daily streamflows in northern New Jersey and southeastern New York, water years 1922–2010 (No. 2018-5068). US Geological Survey.

Hoerling, M., J. Eischeid, J. Perlwitz, X.-W. Quan, K. Wolter, and L. Cheng, 2016: Characterizing recent trends in U.S. heavy precipitation. Journal of Climate, 29 (7), 2313–2332. doi:10.1175/jcli-d-15-0441.1.

Hoffman, J.L. (1989) Plan of Study for the Central Passaic River Basin Hydrogeologic Investigation, NJDEP New Jersey Geological Survey Open-File Report 88-4

Hu, Y., Maskey, S., Uhlenbrook, S., & Zhao, H. (2011). Streamflow trends and climate linkages in the source region of the Yellow River, China. Hydrological Processes, 25(22), 3399-3411.

Huntington, T. G. (2006). Evidence for intensification of the global water cycle: Review and synthesis. Journal of Hydrology, 319(1-4), 83-95.

Inclan, C., & Tiao, G. C. (1994). Use of cumulative sums of squares for retrospective detection of changes of variance. Journal of the American Statistical Association, 89(427), 913-923.

Kirchgässner, G.,Wolters, J., & Hassler, U. (2012). Introduction to modern time series analysis. Springer Science & Business Media.

Kucharik, C., Barford, C., El Maayar, M., Wofsy, S. C., Monson, R. K., & Baldocchi, D. D. (2006). Evaluation of a dynamic global vegetation model (DGVM) at the forest stand-level: Vegetation structure, phenology, and seasonal and inter-annual CO2 and H2O vapor exchange at three AmeriFlux study sites. Ecol. Modell, 196, 1-31.

Labat, D. (2005). Recent advances in wavelet analyses: Part 1. A review of concepts. Journal of Hydrology, 314(1-4), 275-288.

Lan, Y., Zhao, G., Zhang, Y., Wen, J., Liu, J., & Hu, X. (2010). Response of runoff in the source region of the Yellow River to climate warming. Quaternary International, 226(1-2), 60-65.

Lansbury Hall, N., & Crosby, L. (2022). Climate change impacts on health in remote indigenous communities in Australia. International Journal of Environmental Health Research, 32(3), 487-502.

Leng, G., Tang, Q., & Rayburg, S. (2015). Climate change impacts on meteorological, agricultural and hydrological droughts in China. Global and Planetary Change, 126, 23-34.

Li, M., Xia, J., Chen, Z., Meng, D., & Xu, C. (2013). Variation analysis of precipitation during past 286 years in Beijing area, China, using non-parametric test an d wavelet analysis. Hydrological Processes, 27(20), 2934-2943.

Lutgens, F. K., & Tarbuck, E. J. (2010). The atmosphere: An introduction to meteorology eleventh edition.

Lynch, C., A. Seth, and J. Thibeault, 2016: Recent and projected annual cycles of temperature and precipitation in the northeast United States from CMIP5. Journal of Climate, 29 (1), 347–365. doi:10.1175/jcli-d-14-00781.1

Ma, L., He, C., Bian, H., & Sheng, L. (2016). MIKE SHE modeling of ecohydrological processes: Merits, applications, and challenges. Ecological Engineering, 96, 137-149.

Mahmood, R., & Jia, S. (2017). Spatial and temporal hydro-climatic trends in the transboundary Jhelum River basin. Journal of Water and Climate Change, 8(3), 423-440.

Mahmood, R., Jia, S., & Zhu, W. (2019). Analysis of climate variability, trends, and prediction in the most active parts of the Lake Chad basin, Africa. Scientific Reports, 9(1), 1-18.

Marvel, K., Cook, B. I., Bonfils, C., Smerdon, J. E., Williams, A. P., & Liu, H. (2021). Projected changes to hydroclimate seasonality in the continental United States. Earth's Future, 9(9), e2021EF002019.

Matteson, D. S., & James, N. A. (2014). A nonparametric approach for multiple change point analysis of multivariate data. Journal of the American Statistical Association, 109(505), 334-345.

McBean, E., & Motiee, H. (2006). Assessment of impacts of climate change on water resources? a case study of the Great Lakes of North America. Hydrology and Earth System Sciences Discussions, 3(5), 3183-3209.

Monteith, J. L. (1965). Evaporation and environment. In Symposia of the society for experimental biology (Vol. 19, pp. 205-234). Cambridge University Press (CUP) Cambridge.

Nalley, D., Adamowski, J., & Khalil, B. (2012). Using discrete wavelet transforms to analyze trends in streamflow and precipitation in Quebec and Ontario (1954–2008). Journal of hydrology, 475, 204-228.

Nalley, D., Adamowski, J., Khalil, B., & Ozga-Zielinski, B. (2013). Trend detection in surface air temperature in Ontario and Quebec, Canada during 1967–2006 using the discrete wavelet transform. Atmospheric Research, 132, 375-398.

Nolan, P., O'Sullivan, J., & McGrath, R. (2017). Impacts of climate change on mid-twenty-first-century rainfall in Ireland: a high- resolution regional climate model ensemble approach. International Journal of Climatology, 37(12), 4347-4363.

NRCS, U. (2009). Soil Data Viewer.

Ojala, M., Cunsolo, A., Ogunbode, C. A., & Middleton, J. (2021). Anxiety, worry, and grief in a time of environmental and climate crisis: A narrative review. Annual review of environment and resources, 46, 35-58.

Olkkonen, H. (Ed.). (2011). Discrete Wavelet Transforms: Biomedical Applications. BoD–Books on Demand. InTech, Croatia (366 pp).

Oteng Mensah, F., & Alo, C. A. (2023). Modeling monthly actual evapotranspiration: an application of geographically weighted regression technique in the Passaic River Basin. Journal of Water and Climate Change, 14(1), 17-37.

Partal, T. (2010). Wavelet transform-based analysis of periodicities and trends of Sakarya basin (Turkey) streamflow data. River Research and Applications, 26(6), 695-711.

Partal, T., & Kahya, E. (2006). Trend analysis in Turkish precipitation data. Hydrological Processes: An International Journal, 20(9), 2011-2026.

Partal, T., & Küçük, M. (2006). Long-term trend analysis using discrete wavelet components of annual precipitations measurements in Marmara region (Turkey). Physics and Chemistry of the Earth, Parts A/B/C, 31(18), 1189-1200.

Pastén-Zapata, E., Jones, J. M., Moggridge, H., & Widmann, M. (2020). Evaluation of the performance of Euro-CORDEX Regional Climate Models for assessing hydrological climate change impacts in Great Britain: A comparison of different spatial resolutions and quantile mapping bias correction methods. Journal of Hydrology, 584, 124653.

Qian, S., Chen, J., Li, X., Xu, C. Y., Guo, S., Chen, H., & Wu, X. (2020). Seasonal rainfall forecasting for the Yangtze River basin using statistical and dynamical models. International Journal of Climatology, 40(1), 361-377.

R Core Team (2023). R: A language and environment for statistical computing. R Foundation for Statistical Computing, Vienna, Austria. URL https://www.R-project.org/

Renard, B., Kavetski, D., Kuczera, G., Thyer, M., & Franks, S. W. (2010). Understanding predictive uncertainty in hydrologic modeling: The challenge of identifying input and structural errors. Water Resources Research, 46(5).

Roudier, P., Ducharne, A., & Feyen, L. (2014). Climate change impacts on runoff in West Africa: a review. Hydrology and Earth System Sciences, 18(7), 2789-2801.

Saintilan, N., Rogers, K., Kelleway, J. J., Ens, E., & Sloane, D. R. (2019). Climate change impacts on the coastal wetlands of Australia. Wetlands, 39(6), 1145-1154.

Sang, Y. F., Sun, F., Singh, V. P., Xie, P., & Sun, J. (2018). A discrete wavelet spectrum approach for identifying non-monotonic trends in hydroclimate data. Hydrology and Earth System Sciences, 22(1), 757-766.

Sanson, A. V., Van Hoorn, J., & Burke, S. E. (2019). Responding to the impacts of the climate crisis on children and youth. Child Development Perspectives, 13(4), 201-207.

Schaake, J. C. (1990). From climate to flow. Climate change and US water resources., 177-206.

Schaap, M. G., & Leij, F. J. (1998). Using neural networks to predict soil water retention and soil hydraulic conductivity. Soil and Tillage Research, 47(1-2), 37-42.

Schaap, M. G., Leij, F. J., & Van Genuchten, M. T. (2001). Rosetta: A computer program for estimating soil hydraulic parameters with hierarchical pedotransfer functions. Journal of hydrology, 251(3-4), 163-176.

Schnorbus, M., Werner, A., & Bennett, K. (2014). Impacts of climate change in three hydrologic regimes in British Columbia, Canada. Hydrological Processes, 28(3), 1170-1189.

Sharma, A., Wasko, C., & Lettenmaier, D. P. (2018). If precipitation extremes are increasing, why aren't floods?. Water resources research, 54(11), 8545-8551.

Shiri, J., & Kisi, O. (2010). Short-term and long-term streamflow forecasting using a wavelet and neuro-fuzzy conjunction model. Journal of Hydrology, 394(3-4), 486-493.

Shrestha, N. K., Du, X., & Wang, J. (2017). Assessing climate change impacts on fresh water resources of the Athabasca River Basin, Canada. Science of the total environment, 601, 425-440.

Singh, V. P. (1995). Computer models of watershed hydrology. Water Resources Publications.

Sneyers R. 1990. On the statistical analysis of series of observations. WMO Technical Note 143, WMO No. 415, TP-103, World Meteorological Organization, Geneva, Switzerland, 192 pp.

Stanford, S. (2007b) Surficial Geology of the Pompton Plains Quadrangle Morris, Passaic, Essex,and Bergen Counties,, New Jersey. In: Open-File Map 68 edn. NJDEP, Land use management, NJGS.

Tang, Y., Tang, Q., Tian, F., Zhang, Z., & Liu, G. (2013). Responses of natural runoff to recent climatic variations in the Yellow River basin, China. Hydrology and Earth System Sciences, 17(11), 4471-4480.

Tekleab, S., Mohamed, Y., & Uhlenbrook, S. (2013). Hydro-climatic trends in the Abay/upper Blue Nile basin, Ethiopia. Physics and Chemistry of the Earth, Parts A/B/C, 61, 32-42.

Thibeault, J. M., and A. Seth, 2014: Changing climate extremes in the Northeast United States: Observations and projections from CMIP5. Climatic Change, 127 (2), 273–287. doi:10.1007/s10584-014-1257-2

Thompson, J. R., Sørenson, H. R., Gavin, H., & Refsgaard, A. (2004). Application of the coupled MIKE SHE/MIKE 11 modelling system to a lowland wet grassland in southeast England. Journal of Hydrology, 293(1-4), 151-179.

Venkata Ramana, R., Krishna, B., Kumar, S. R., & Pandey, N. G. (2013). Monthly rainfall prediction using wavelet neural network analysis. Water resources management, 27(10), 3697-3711.

Vonesch, C., Blu, T., & Unser, M. (2007). Generalized Daubechies wavelet families. IEEE Transactions on Signal Processing, 55(9), 4415-4429.

Wang, W., Hu, S., & Li, Y. (2011). Wavelet transform method for synthetic generation of daily streamflow. Water resources management, 25(1), 41-57.

Wei, S., Song, J., & Khan, N. I. (2012). Simulating and predicting river discharge time series using a wavelet-neural network hybrid modelling approach. Hydrological Processes, 26(2), 281-296.

Whitcher, B., Byers, S. D., Guttorp, P., & Percival, D. B. (2002). Testing for homogeneity of variance in time series: Long memory, wavelets, and the Nile River. Water Resources Research, 38(5), 12-1.

Wilks, D. S. 2011. Statistical Methods in the Atmospheric Science. 3rd ed. Academic Press, USA (704 pp)

Worsley, K. J. (1979). On the likelihood ratio test for a shift in location of normal populations. Journal of the American Statistical Association, 74(366a), 365-367.

Zhong, D., Dong, Z., Fu, G., Bian, J., Kong, F., Wang, W., & Zhao, Y. (2021). Trend and change points of streamflow in the Yellow River and their attributions. Journal of Water and Climate Change, 12(1), 136-151.

Ziervogel, G., New, M., Archer van Garderen, E., Midgley, G., Taylor, A., Hamann, R., ... & Warburton, M. (2014). Climate change impacts and adaptation in South Africa. Wiley Interdisciplinary Reviews: Climate Change, 5(5), 605-620.

CHAPTER 4 : ASSESSEMENT OF HYDROCLIMATIC CONDITIONS IN RESPONSE TO POTENTIAL CLIMATE CHANGE AT MID-21ST CENTURY IN THE PASSAIC RIVER BASIN.

4.1. Abstract

The quest to assess future water resource availability in the context of climate change largely hinges on reliable and representative hydroclimatic projections. In view of this, downscaled and bias-corrected climate data obtained from the Multivariate Adaptive Constructed Analog (MACA) datasets were used to drive the MIKE SHE hydrologic model developed for the Rockaway catchment of the Passaic River Basin. A priori analysis however involved the selection of subset models from the 20 MACA models that characterized the change in temperature and precipitation according to LEAST WARM, HOT, DRY, and WET at mid-21st century (2041—2070) as well as a mild future that typifies the MIDDLE of the temperature and precipitation range. In all, nine (9) different models, relative to two baseline periods, and under two different climate scenarios were selected. Results showed that against the 2041—2070 period, the margin of error owing to the use of different baseline conditions were +/- 0.3 — +/- 0.23 ^{o}C for temperature and +/-8.15— +/-6.9% for precipitation, indicating the extent to which the time perspective used in climate change impacts assessment significantly affect outcomes. Across all five (5) climate projections, and the two scenarios, a consistent warming from +1.21 to + 4.70 ^{o}C is projected in the Rockaway catchment at mid-21st century relative to the 1981—2010 baseline period. While precipitation is generally projected to increase, streamflow prediction shows an overall decreasing signal, a trend likely induced by the projected increase in actual evapotranspiration. In terms of climate extremes, an increase in the number heavy rainy days of approximately 2 days is projected in the coldest future whiles an increase of about 4 days is expected in the wettest future. In similar vein, the number days with consecutive dry spells is expected to decrease by approximately 2 days in the driest future whereas an increase of about 3

days is projected in the wettest future. Overall, climate change is expected to fuel flooding and drought conditions in the study catchment, and to cause alterations in river flows which will in turn affect reservoir operations. With this advance knowledge at hand, swift mitigation and adaptation plans are therefore needed.

4.2. Introduction

Three major phenomena of environmental significance are changing globally— *population, land-use/land-cover*, and *climate*. Of these three, climate change has continuously received sustained attention in recent decades, largely because it is occurring at a rate faster than plants and animal species can adapt. These major changes working in composite have contributed to the many varied and complex climatic impacts such as warmer temperatures, variable precipitation, dwindling snowpack, sea level rise, and increased evaporation (Huang et al., 2012; Schmucki et al., 2015; Clark et al., 2016; Yin and Tsai, 2018) over the last several decades. Extreme temperatures and precipitation have also been reported (e.g. Diaz et al., 2011; Wang et al., 2017a) and are projected to increase in both frequency and severity.

This rapidly changing climate has been linked to the heating effect created by anthropogenic greenhouse gas emissions into the atmosphere (IPCC, 2013; Masson-Delmotte, 2021). In particular, carbon dioxide has been observed to increase substantially beyond pre-industrial concentrations and is expected to continue in the course of the 21st century (IPCC, 2013; Masson-Delmotte, 2021). The direct impact from greenhouse gas addition to the atmosphere is an overall warming planet. Indirect impacts such as precipitation change, and sea level rise only emerge as a response to temperature change (Dessler, 2015). As such, climate change is in principle, temperature change.

Global temperatures have risen by an average of 0.08^{o} C per decade since 1880, with a rate of warming more than twice as fast since 1981 (0.18^{o} C per decade) (Lindsey and Dahlman, 2020). Since 1901, precipitation has increased at an average rate of approx. 1 mm per decade (NOAA, 2022). Various aspects of precipitation such as intensity, frequency, duration, extent, and timing have also been changing throughout many regions around the world (Tan et al., 2020). The ultimate effect of these shifts in climate are the changes in quantity and seasonal distribution of streamflow, mediated by changes in evapotranspiration. Although climate change is a global phenomenon, the underlying impacts are very local and varied. Such that, while some regions around the world are experiencing increases in streamflow, others are seeing decreases (Milly et al., 2005). It therefore behooves on societies to consider the options and responses to climate change by identifying the extent to which various sectors of the economy may be affected.

Currently, the general approach to climate change impacts studies require starting with one or more global climate models (GCMs), downscaling to the region of interest, and then used as inputs to a hydrological model to simulate hydrologic responses to changes in climate. The problem faced with such studies, however, is the choice of climate models used and what effect selecting any models have on the study results (Dettinger, 2005; Brekke et al., 2008). For most studies, the leeway is to compute the average over all models with available data (e.g., Seager et al., 2007), to establish a mean climate over the region of interest. While the superiority of an “average model” to any individual model has been largely upheld (e.g., Gleckler et al., 2008; Pincus et al., 2008; Reichler and Kim, 2008), questions have been raised as to whether such strategy is valid for model variability as well (Pierce et al., 2009). Recently, the United State Department of Agriculture Forest Services (USDA-FS) carried out an extensive evaluation to select a range of climate models from 20 downscaled GCMs (Joyce and Coulson, 2020). The process involved identifying a set of projections that characterize the range of temperature and precipitation changes as well as a mild projection that represent the middle of this range at conterminous scale. While the resulting GCMs have been adopted and used by a number of researchers (e.g., Heidari et al., 2020; Aliyari et al., 2021; Lawrence et al., 2021), the scale of their analysis precludes its usage at a basin scale. As such, this study employs similar approach to subset climate models over the Passaic River Basin and subsequently use in an impact assessment.

Through previous studies, it has become clear that the Northeast United States (which embodies the Passaic River Basin) has witnessed the strongest increase in extreme precipitation and temperatures among all US regions in the past five decades (Trenberth 1999; Groisman et al.2005; Allan & Soden 2008; Hoerling 2016; Easterling 2017). Whereas most regions have seen relative increases in precipitation extremes ranging from 5% to 37% (e.g., Groisman et al.2005), the U.S. Northeast has experienced a whopping 71 percent increase (e.g., Melillo et al., 2014; Horton et al., 2014; USGCRP, 2017). In the recent Fourth National Climate Assessment report (NCA 2018), it is projected that Northeast will continue to experience further increases in rainfall intensity, with total precipitation increase expected during the winter and spring seasons (Thibeault and Seth, 2014). On the other hand, temperatures are projected to increase beyond preindustrial average by 2ºC (3.6ºF) by 2035 under RCP4.5 and RCP8.5 scenarios. This is said to be the largest increase in the contiguous U.S. and is expected to occur as much as two decades before global average temperatures reach similar record (Karmalkar and Bradley 2017). Under such climate conditions and given the largely varied physiographic character of the Northeast, it is expected that the scope of climate vulnerabilities, impacts, and adaptation responses will be quite distinct (Rosenzweig et al. 2011, Leichenko and Solecki, 2013), and spatially diverse. A more locally relevant climate impact assessment study is therefore needed. This will help build the needed resilience and adaptation to possible climate impacts through incorporation of climate related risks in future water resource decision and planning process. In this context, the Passaic River Basin, located in the Northeast US, noted for its dense population, diverse land uses and many reservoirs, is a suitable candidate for such a study.

The Passaic River Basin is a bi-state watershed (New Jersey and New York) with a drainage area of about 2422km^2, and its tributaries supporting several large drinking water reservoirs that serve millions of inhabitants in northern New Jersey. The Passaic River is one of the major flood areas in the region, with its major tributaries already experiencing a 1% annual chance flood over a 60 square miles (155.4sqkm) area. Despite historic losses due to urbanization, wetlands in the central Passaic Basin provide essential ecosystem service deliveries which includes buffering natural flood. Amidst predicted 21st century changes in climate in the region, the environmental, hydrological, and economic impacts are expected to be far reaching. Thus, an evaluation of the impacts of climate change and variability on the basin's hydrology would greatly benefit both water resource managers and policymakers.

To this end, the study seeks first to select and identify climate models and projections that would characterize the temperature and precipitation changes for the basin according to least warm, hot, dry, and wet at the middle of the 21st century as well as a future that could characterize the middle of the temperature and precipitation ranges (e.g., Joyce and Coulson, 2020). Based on the selected models, further assessment will be carried out in the Rockaway catchment of the PRB to predict future flows and hydro-climatic conditions. This study will provide an important template of an envelope of future hydro-climatic conditions for the PRB, that can assist water managers and decision-makers in the planning of basin-specific adaptation and mitigation strategies.

4.3. Materials and Methods

To carry out the future climate impacts assessment in the PRB, it was important to first determine which future emission scenarios and climate models would be needed, based on which plausible future climate change scenarios would be projected and used in driving catchment hydrological model. More so, the choice of baseline period in climate impacts studies has been found to constitute an important source of uncertainty, often at par with, or more significant than uncertainties propagated through the choice of global climate models (GCMs) (Koczot et al., 2011; Baker et al., 2016; Peñaloza et al., 2019). For this reason, two reference periods (i.e., 1951—1980 and 1981—2010) were explored in the climate models sub-setting over the PRB. The impacts assessment in the Rockaway sub-basin was however restricted to the recent baseline period to ensure presentation clarity.

4.3.1 Description of the Study Area

The location map of the Passaic River Basin is delineated in Figure 4.1. For details regarding climate, land use/land cover, and the physiographic characteristics of the PRB, the reader is referred to Oteng Mensah and Alo (2023).

The Rockaway River, bolstered by the upstream Whippany River, forms a tributary watershed of about 300 square kilometers that flows into the Passaic River. This confluence occurs within the extensive wetland area encompassing Hatfield Swamp and Troy Meadows. The catchment is well suited for this hydrologic impact study because it is typical of the larger Passaic River Basin, having its extent intersecting two of the three physiographic provinces (Highlands and Central basin), clouded with numerous reservoirs, and featuring two groundwater wells that provide water supply for the local residents. With a greater portion falling within the Highlands to the south, the main land cover types in the Rockaway watershed include forest (50%), developed, open space (30%), wetlands (13%), open water (4.3%), and others (2.7%). Reconstructed streamflow data record (by Hickman and McHugh, 2018) of the gauge above the Boonton reservoir (USGS # 01380500), spanning the period 1981—2010 water years was used in the hydrological simulation and assessment.

4.3.2 Data Source

Two types of datasets were used in the model selection exercise: observed and the downscaled Multivariate Adaptive Constructed Analogs (MACA) datasets. The observed datasets were daily data obtained from Parameter-elevation Regressions on Independent Slopes Model (PRISM) (PRISM, Oregon State University, http://prism.oregonstate.edu), complemented with the Daymet (Thornton et al., 1997) datasets and aggregated into annual mean temperature, total annual precipitation, number of days with precipitation greater than 10mm (R10), and consecutive dry days (CDD). These variables were averaged from three stations: Ringwood, Rockaway, and Upper Passaic catchments within the PRB boundaries to evaluate the MACA climate models for the historical period, 1981—2005. Because the resolution of GCMs are two coarse, ranging from about 48—322 km (Naz et al., 2016; Hayhoe et al., 2017), they cannot be used directly for local scale hydroclimatic studies, and will require downscaling. Thus, the downscaled MACA climate datasets were acquired to provide the plausible future climate projections in this study

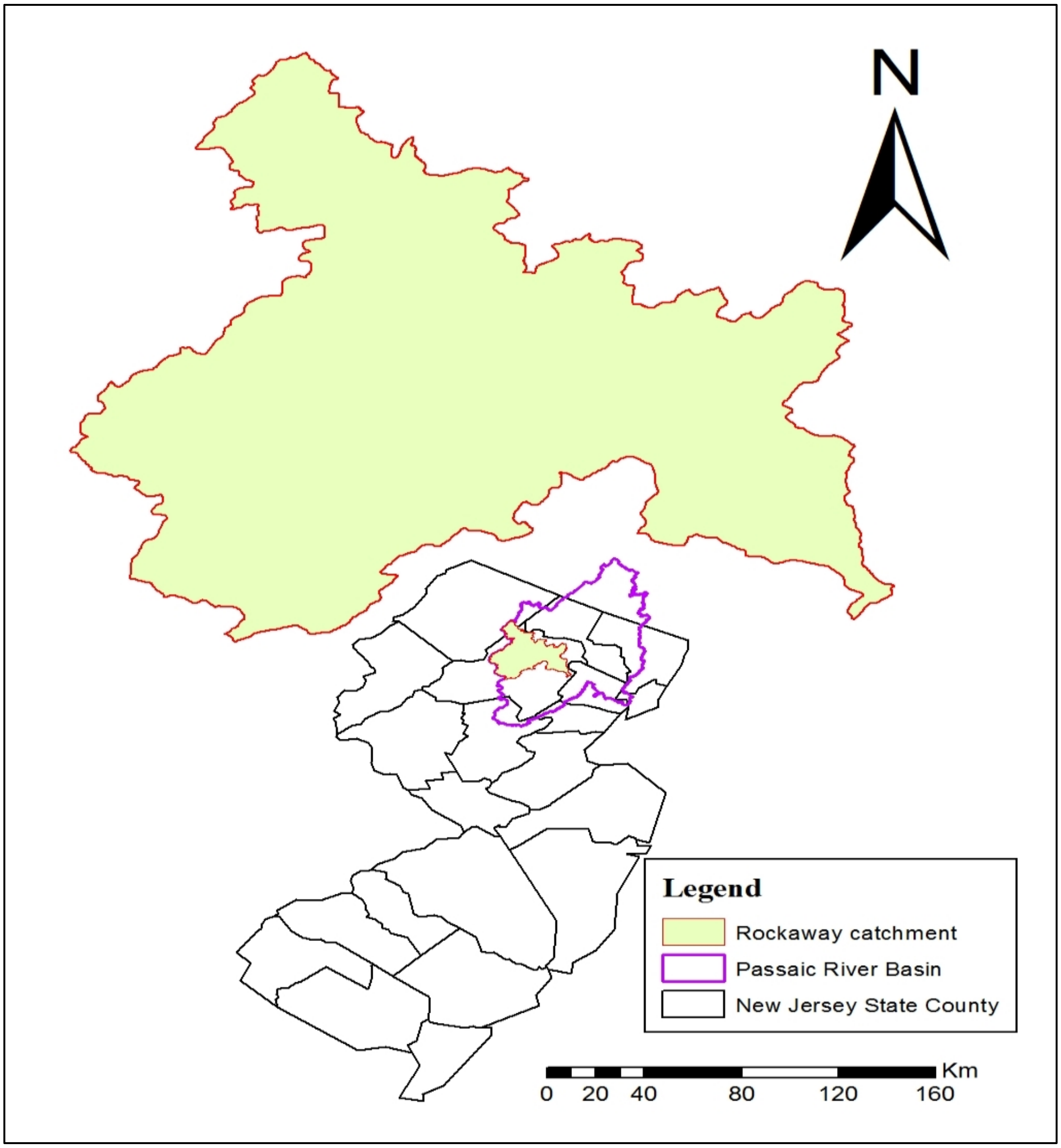

Figure 4.1: Location map of the Rockaway catchment in the Passaic River Basin

(Abatzoglou et al., 2018). Table 4.1 shows a summary of the MACA models, comprised of 20 models that were statistically downscaled and bias-corrected for the entire Conterminous United States (CONUS) at ~4 km (1/24 degree) cell size under two future Representative Concentration Pathways (RCPs) (i.e., RCP4.5 and RCP8.5).

Table 4.1: Summary of downscaled MACA models

No.	Model Name	Native Resolution	Model Institution	Model Country
1	BCC-CSM1-1	2.8 x 2.8	Beijing Climate Center, China Meteorological Administration	China
2	BCC-CSM1-1-m	1.12 x 1.12	Beijing Climate Center, China Meteorological Administration	China
3	BNU-ESM	2.8 x 2.8	College of Global Change and Earth System Science, Beijing Normal University, China	China
4	CanESM2	2.8 x 2.8	Canadian Centre for Climate Modeling and Analysis	Canada
5	CCSM4	1.25 x 0.94	National Center of Atmospheric Research, USA	USA
6	CNRM-CM5	1.4 x 1.4	National Centre of Meteorological Research, France	France
7	CSIRO-Mk3-6-0	1.8 x 1.8	Commonwealth Scientific and Industrial Research Organization/Queensland Climate Change Centre of Excellence, Australia	Australia
8	GFDL-ESM2G	2.5 x 2.0	NOAA Geophysical Fluid Dynamics Laboratory, USA	USA
9	GFDL-ESM2M	2.5 x 2.0	NOAA Geophysical Fluid Dynamics Laboratory, USA	USA
10	HadGEM2-CC365	1.88 x 1.25	Met Office Hadley Center, UK	United Kingdom
11	HadGEM2-ES365	1.88 x 1.25	Met Office Hadley Center, UK	United Kingdom
12	INMCM4	2.0 x 1.5	Institute for Numerical Mathematics, Russia	Russia
13	IPSL-CM5A-LR	3.75 x 1.8	Institut Pierre Simon Laplace, France	France
14	IPSL-CM5A-MR	2.5 x 1.5	Institut Pierre Simon Laplace, France	France
15	IPSL-CM5B-LR	2.75 x 1.8	Institut Pierre Simon Laplace, France	France
16	MIROC5	1.4 x 1.4	Atmosphere and Ocean Research Institute (The University of Tokyo), National Institute for Environmental Studies,and Japan Agency for Marine-Earth Science and Technology	Japan

17	MIROC-ESM	2.8 x 2.8	Japan Agency for Marine-Earth Science and Technology, Atmosphere and Ocean Research Institute (The University of Tokyo), and National Institute for Environmental Studies	Japan
18	MIROC-ESM-CHEM	2.8 x 2.8	Japan Agency for Marine-Earth Science and Technology, Atmosphere and Ocean Research Institute (The University of Tokyo), and National Institute for Environmental Studies	Japan
19	MRI-CGCM3	1.1 x 1.1	Meteorological Research Institute, Japan	Japan
20	NorESM1-M	2.5 x 1.9	Norwegian Climate Center, Norway	Norway

The climatic variables in the MACA dataset includes minimum temperature (tasmin), maximum temperature (tasmax), precipitation (pr), maximum relative humidity (rhsmax), minimum (rhsmin), eastward component of wind (uas), and northward component of wind (vas). In this study, the resultant wind speed was calculated as a combination of the eastward and northward winds ($\sqrt{uas^2 + vas^2}$). Reference evapotranspiration was further computed from these climatic variables to run the MIKE SHE hydrological model.

4.3.3 Selection criteria

In this study, the selection of climate models and projections were based on the downscaled MACA models for RCP4.5 (lower scenario) and RCP8.5 (higher or business-as-usual scenario) and modified according to the approach by Joyce and Coulson (2020), at a basin scale. The process is schematically illustrated in Figure 4.2. Evaluation of climate models was based on each model's ability to mimic historical climate. Thus, models that consistently underperformed in capturing observed historical climate conditions were removed from further consideration. For individual projections, selection was made on the basis of a set of climate projections that would characterize the changes in temperature and precipitation for the MACA models according to

LEAST WARM, HOT, DRY, and WET at mid-21st century as well as a mild future that typifies the MIDDLE of the temperature and precipitation range. Over the PRB, these changes were calculated as difference in temperature and percent change in precipitation, based on which models were ranked. Across the 20 models in the MACA dataset for each scenario, LEAST WARM and HOT defines the extreme ends of projected changes in temperature at mid-century relative to the baseline period. After arranging these projected changes from the smallest temperature change to the greatest, LEAST WARM will be the smallest change with HOT being the greatest change in temperature. Similarly, DRY and WET represent the extremes of projected precipitation change across all 20 MACA models for each scenario. Grouping these changes from the smallest precipitation change to the highest reveal the driest model as well as the wettest model which defines the DRY and WET projections at mid-century relative to the considered baselines. The MIDDLE of the range of projected temperature and precipitation changes represents the mild future climate which involve the computation of basin-average change in temperature and precipitation for the two baseline periods (1951—1980 and 1981—2010) relative to the mid-21st century (1941—1970) period under RCP 4.5 and RCP 8.5. To find the middle projection, the mean change in temperature and precipitation for all selected MACA models was first calculated under both scenarios. The model with projected temperature and precipitation change closest to the mean change of all the selected model was chosen as the middle projection. The closest model was determined by calculating the distance between each model and the mean of all models on a temperature—precipitation change Cartesian plane.

Thus relative to one baseline period (e.g. 1951—1980) from the middle of the century (2041—2070), and the two RCPs, a total of 40 climate models or projections (20 for each scenario) from the MACA dataset is considered: the first step in the process. The second step is the evaluation process where some models are dropped for poorly reproducing historical climate, and the last step will identify the five (5) projections (LEAST WARM, HOT, MIDDLE, DRY, WET) out of the now less-than-20 climate models for each scenario as described earlier. By this criteria, a total of ten (10) projections will be identified, five (5) for each RCP as illustrated in Figure 4.2.

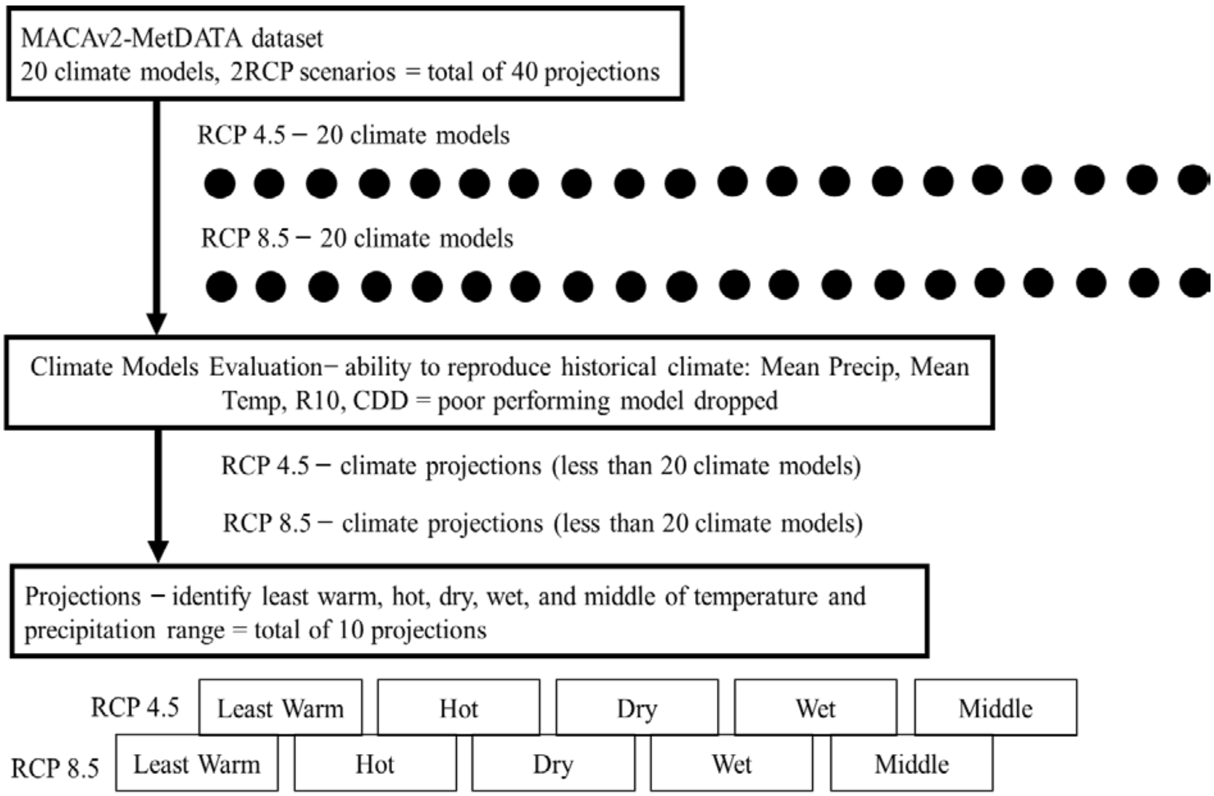

Figure 4.2: Schematic of the process used to identify five climate projections from the MACAv2-MetDATA climate datasets for use under RCP4.5 and RCP8.5 over the Passaic River Basin. Solid black circles denote the MACA climate models (modified after Joyce and Coulson (2020))

4.3.4. Performance Evaluation of MACA Models

The performance evaluation of the MACA climate datasets was guided by the model performance metrics developed by Rupp et al. (2013), selected on the basis of their theoretical merits and relevance for impact modelling. According to Rupp et al. (2013), mean annual temperature and precipitation rank highest among all performance metrics. For this study, because the Northeast region has over the past decades witnessed the strongest extreme climates

(Hoerling 2016; Easterling 2017), metrics that captured the extreme climate conditions of the PRB were also considered. As a result, four metrics—mean annual temperature, mean annual precipitation, number of days with precipitation greater than 10mm, and consecutive dry days—were used in the historical performance rankings in this study. For each of the 20 MACA models evaluated, the relative error (RE), root mean square error (RMSE), and correlation coefficient (r) for each metric was summed or averaged. Corresponding formulas for each statistic are shown in equations 4.1, 4.2, and 4.3.

$$RE = \frac{|M-O|}{O} \quad \text{Equation 4.1}$$

$$RMSE = \sqrt{\frac{1}{n}\sum(M-O)^2} \quad \text{Equation 4.2}$$

$$r = \frac{C_{MO}}{SD_M \times SD_O} \quad \text{Equation 4.3}$$

where, $M =$ baseline period (MACA models) time series

$O =$ corresponding observed time series for same variable

$C_{MO} =$ Covariance between baseline period (MACA models) and observation

$SD_M =$ Standard deviation of baseline period (MACA models)

$SD_O =$ Standard deviation of observation

On the basis of these statistics, models that consistently performed poor with any two of these statistics (i.e., the largest total mean relative error, largest mean RMSE, and/or the smallest mean (r)) were then dropped.

4.3.5. Hydroclimatic impacts assessment

The climate impacts assessment examines the future hydroclimatic conditions of the Rockaway sub-basin resulting from climate change/variability. Here, assessment was based on the selected

MACA models representing the plausible future trajectory of temperature and precipitation changes according to LEAST WARM, HOT, DRY, WET, and the MIDDLE of the range under the two emission scenarios (RCP4.5 and RCP8.5). Under each scenario, these five climate projections for the Rockaway sub-basin was used to force the MIKE SHE hydrological model to study: 1) monthly hydroclimatic ratios, 2) seasonal hydro-climatological changes, and 3) annual trends in precipitation, R10, CDD, actual evapotranspiration, streamflow, and groundwater recharge at mid-21st century relative to 1981—2010 baseline. These hydroclimatic variables were obtained from water balance outputs of the MIKE SHE hydrological model developed for the Rockaway sub-basin.

4.4. Results and Discussion

4.4.1. Temperature and precipitation change at mid-21st century in the PRB

Rankings for projected mean temperature and annual precipitation change across all MACA models at mid-21st century are shown in Figures 4.3 and 4.4 for the baseline periods 1951—1980 and 1981—2010 respectively. Over the PRB, mean temperature was projected to increase across all models and in both scenarios. For the 1951—1980 reference period relative to 2041—2070, increases range from 1.24 ^{o}C to 3.79 ^{o}C under RCP 4.5 and 1.92 ^{o}C to 4.63 ^{o}C under RCP 8.5. Relative to the 1981—2010 period, the least temperature change was 0.87 ^{o}C in INMCM4 and the highest change was 3.20 ^{o}C in MIROC-ESM-CHEM under RCP 4.5 and a 1.62 ^{o}C to 4.03 ^{o}C range under RCP 8.5 for same two models respectively. Although by individual model, projected changes in temperature was greater under RCP 8.5 than under RCP 4.5, more models under RCP 4.5 projected temperature changes greater than models under RCP 8.5. For example, considering the 1951—1980 baseline, only 6 models under RCP 8.5 projected changes greater than all the models under RCP 4.5. However, against the 1981—2010 reference period, only 3 models under RCP 8.5 projected temperature changes greater than all the models under RCP 4.5. Generally, projected changes in temperature for most models under RCP 4.5 are greater than projected changes in other models under RCP 8.5. Such overlap in projected changes in temperature between these scenarios have also been reported in other studies (e.g. Hayhoe et al., 2017; Joyce and Coulson, 2020).

Relative to the 1951—1980 reference, annual precipitation ranged from 1.04% increase in MRI-CGCM3 to 12.99% increase in NorESM1-M under RCP 4.5 and from 2.23% increase in INMCM4 to 23.29% increase in BCC-CSM1-1-m under RCP 8.5. Note that all models projected precipitation increase in the 1951—1980 baseline period under both scenarios. Measured against 1981—2010 reference however, some models projected decreases in annual precipitation. MRI-CGCM3 and IPSL-CM5A-MR for example, decreased by 2.02% and 2.49% respectively under RCP 4.5 whereas INMCM4 decreased by 5.91% under RCP 8.5. Thus projected changes in annual precipitation range from 2.02% decrease to 11.10% increase in HadGEM2-CC365 under RCP 4.5 and from 5.91% decrease to 16.39% increase in NorESM1-M under RCP 8.5. In general, the range of change in projected precipitation was wider in the 1981—2010 baseline than in 1951—1980 baseline and in RCP 8.5 than it is in RCP 4.5. This results were also corroborated by Joyce and Coulson, 2020) in their evaluation across the CONUS, though with a different reference period. In particular, they also found that IPSL-CM5A-MR projected a decrease in annual precipitation by

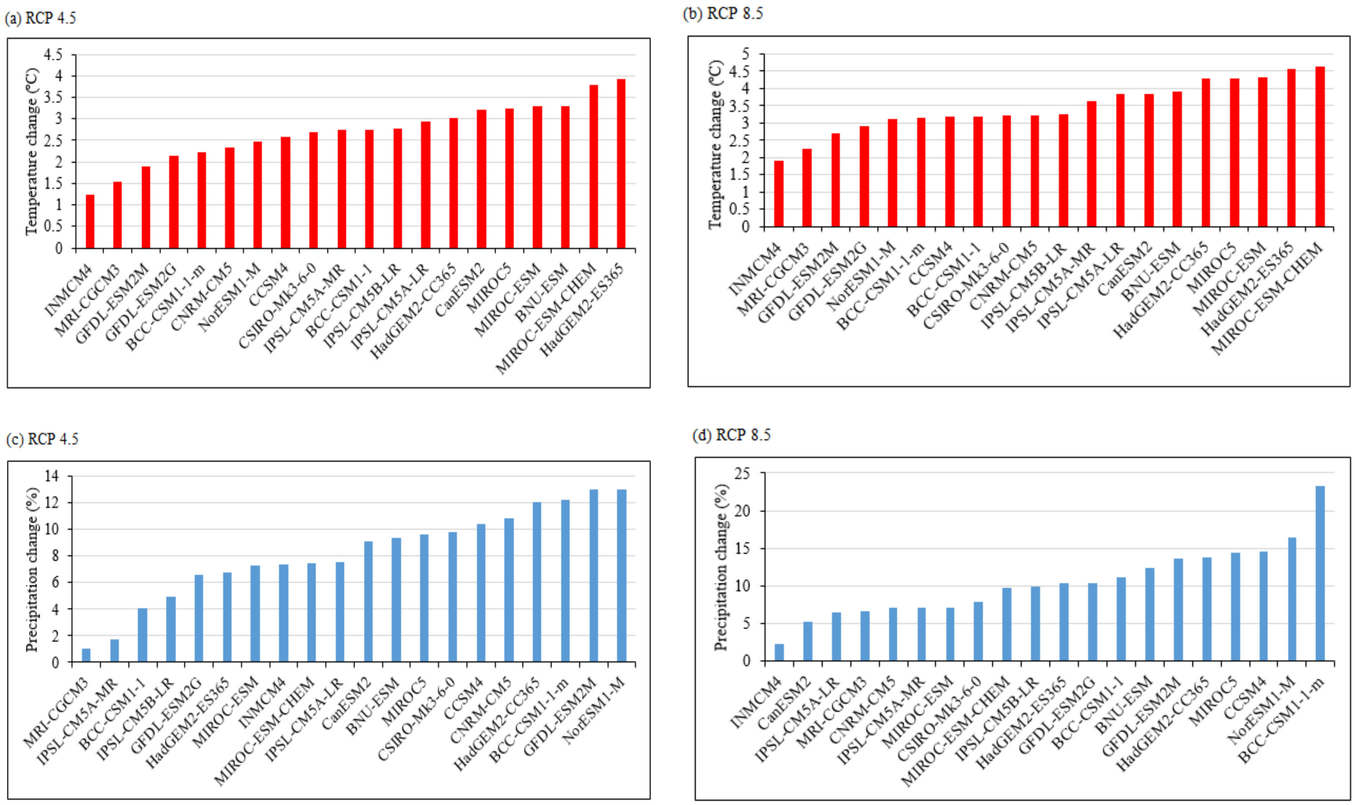

Figure 4.3: Change in mean temperature (oC) and annual precipitation (percent) at mid-century (2041–2070) relative to the historical period (1951–1980) under RCP 4.5 (a, b) and RCP 8.5 (c, d) for all 20 models over the Passaic River Basin

2041—2070 against 1971—2000 baseline period. In the selection process in this study, individual model projections either appeared under both scenarios or varied by scenario. For example, the same model, INMCM4, projected an increase in precipitation in the 1951—1980 baseline period and a decrease in the 1981—2010 baseline under RCP 8.5. However, under RCP 4.5 MRI-CGCM3 projected an increase in precipitation in the 1951—1980 reference period whereas IPSL-CM5A-MR projected a decrease in the 1981—2010 baseline period.

Thus on the basis of this initial ranking, the model with the smallest change in temperature (Least Warm), INMCM4, was the same by scenario and by baseline. The hottest model, having the largest change in temperature varied by scenario and by baseline. As shown in Figure 4.3a, b, the hottest projection by the 2041—2070 period was HadGEM2-ES365 and MIROC-ESM-CHEM models under RCP 4.5 and RCP 8.5 respectively relative to the 1951—1980 baseline. By baseline, the HadGEM2-ES365 model was the same, project the hottest under RCP 4.5 (Figures 4.3a and 4.4a), but differed with MIROC-ESM-CHEM being the hottest model for the 1951—1980 baseline period (Figure 4.3b) and likewise, the HadGEM2-CC365 model for the 1981—2010 baseline under RCP 8.5 (Figure 4.4b).

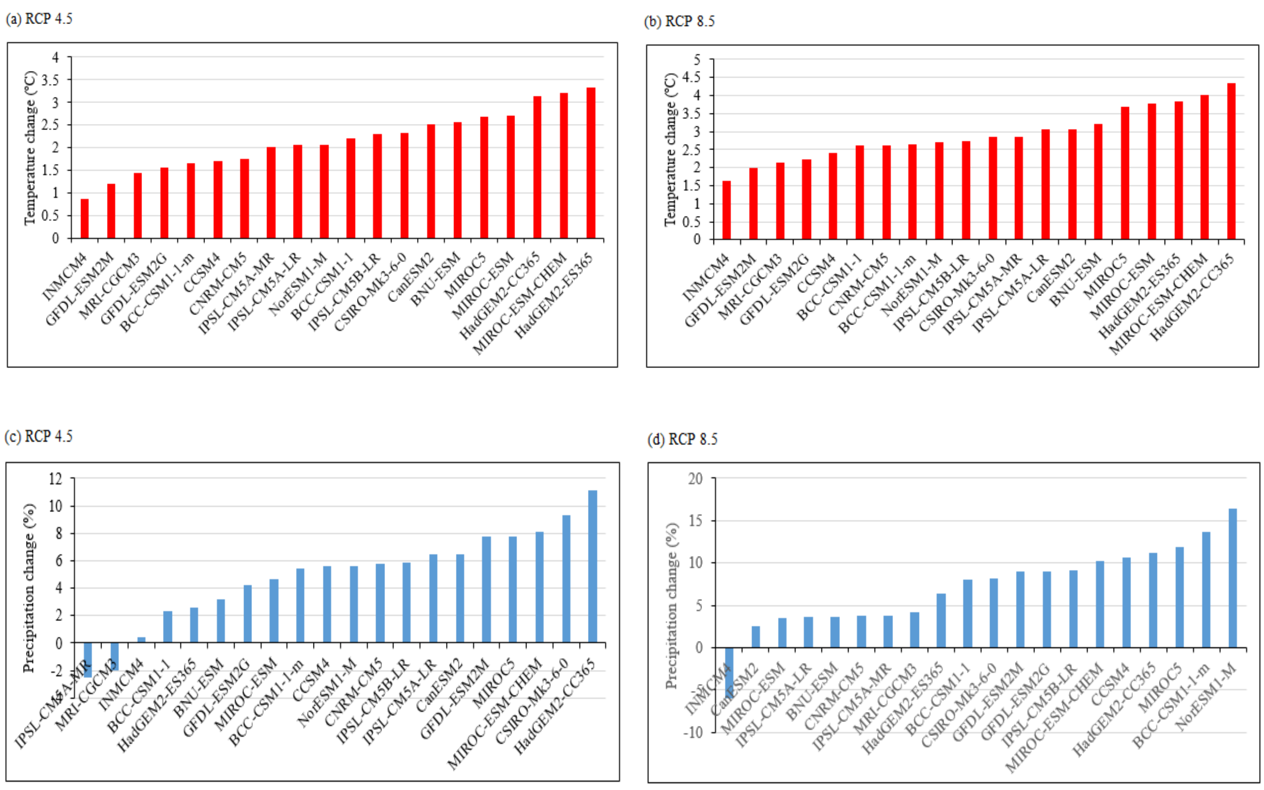

Figure 4.4: Change in mean temperature (oC) and annual precipitation (percent) at mid-century (2041–2070) relative to the historical period (1981–2010) under RCP 4.5 (a, b) and RCP 8.5 (c, d) for all 20 models over the Passaic River Basin

The driest and wettest projections largely differed by scenario and also by baseline. At mid-21st century relative to the 1951—1980 baseline, the driest model was projected by MRI-CGCM3 under RCP 4.5 and INMCM4 projected the smallest increase under RCP 8.5. In contrast, the NorESM1-M model, being the wettest, projected the largest increase in precipitation under RCP 4.5 and BCC-CSM1-1-m projected the greatest increase under RCP 8.5. Against the 1981—2010 baseline, the driest models were projected by IPSL-CM5A-MR and INMCM4 under RCP 4.5 and RCP 8.5 respectively. The wettest model was projected by HadGEM2-CC365 under RCP 4.5 and by NorESM1-M under RCP 8.5.

4.4.2. Model performance evaluation

The historical performance of each of the 20 models based on the four variable metrics typical of the climatic conditions over the Passaic River Basin have been ranked according to their mean total relative error (RE), mean root mean square error (RMSE), and mean correlation coefficient (r) and shown in Figure 4.5. A lower rank in RE and RMSE, and a higher rank in r indicated a

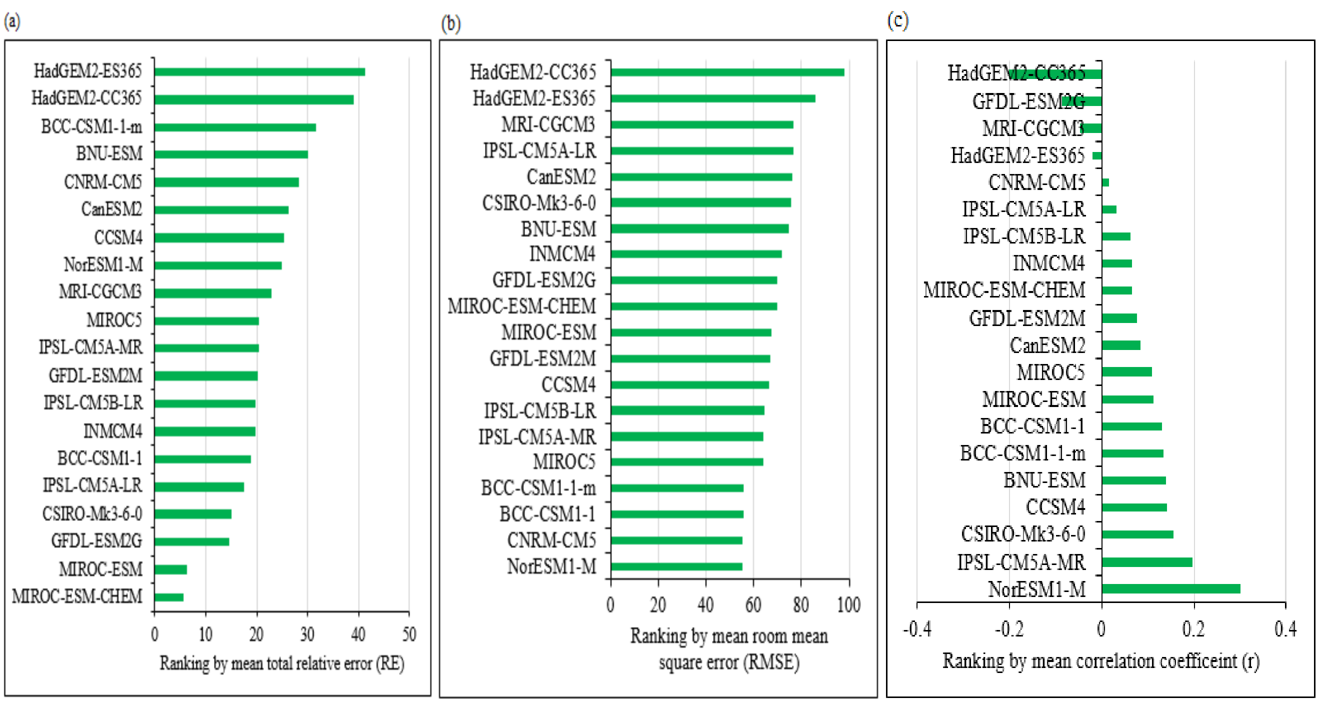

Figure 4.5: Model performance results for 20 models for the 3-region mean results over the Passaic River Basin for (a) RE, (b) RMSE, and (c)r. For RE and RMSE, the lower the performance metric, the better the projection reproduced the observed historical climate 1981-2005). The order of the performance results in each graph was based on the rankings of the mean of Tmean, Precip, R10, and CDD

better model performance in matching historical climate. Based on the RMSE and r statistics, the same model (NorESM1-M) ranked the lowest, being the best model to fairly capture the historical mean temperature, precipitation, rainy days greater than 10mm, and consecutive dry days in the PRB.

In respect of the worst models, the criteria were to drop models that consistently appeared to rank poorly in any two of the three statistics in capturing the historical observed climate. Accordingly, and as depicted in Figure 4.5, two models (HadGEM2-ES365 and HadGEM2-CC365) performed worst. They were consistently in the worst performing ranks in both mean RE and mean RMSE, with the order shifting between the last two poorly performing ranks. Consequently, they were removed from further consideration, affecting the range of mid-21st century changes in temperature and precipitation. For instance, HadGEM2-ES365 model will no longer be the hottest projection among the models for both baseline periods under RCP 4.5. Similarly, HadGEM2-CC365 ceases to be the wettest model under RCP 4.5 and the hottest projection under RCP 8.5 for the 1981—2010 baseline period.

4.4.3. Middle of the projected changes in temperature and precipitation range

The model that could represent the middle of the temperature and precipitation change was based on projections by the remaining 18 models after dropping HadGEM2-ES365 and HadGEM2-CC365. These models must show a projection with a change in temperature and precipitation proximal to the 18-model mean change in temperature and precipitation. By computing the distance from the 18-model mean change in temperature and precipitation on a Cartesian plane, the middle projection that reflected the mean change over the PRB was identified. This is illustrated in Figures 4.6 and 4.7 and tabulated in Tables 4.2 and 4.3. Based on the computations, the projections closest to the 18-model mean temperature and precipitation change were IPSL-

CM5A-LR and IPSL-CM5B-LR under RCP 4.5 and RCP 8.5 respectively, against the 1951—1980 baseline period (Figure 4.7, Table 4.2). Similarly, the projected temperature and precipitation change in close proximity to the overall mean change for the 18 models was found in GFDL-ESM2G under RCP 4.5 and BCC-CSM1-1 under RCP 8.5 relative to the 1981—2010 reference period (Figure 4.7, Table 4.3). Note that though the precipitation or temperature change projected by another model may be closer to the mean projected change than the selected model, the other corresponding variable may be drier, hotter, wetter, or cooler than the overall mean change. For example, in Figure 4.7 (a), although temperature projection under RCP 4.5 for NorESM1-M was closer to the 18-model mean change temperature, the precipitation change was wetter at 5.74% increase as against 4.70% for the overall model mean change. Thus, the model chosen to represent the middle of the temperature and precipitation range rather produces the right combination of temperature and precipitation change with the minimum distance from the 18-model mean change.

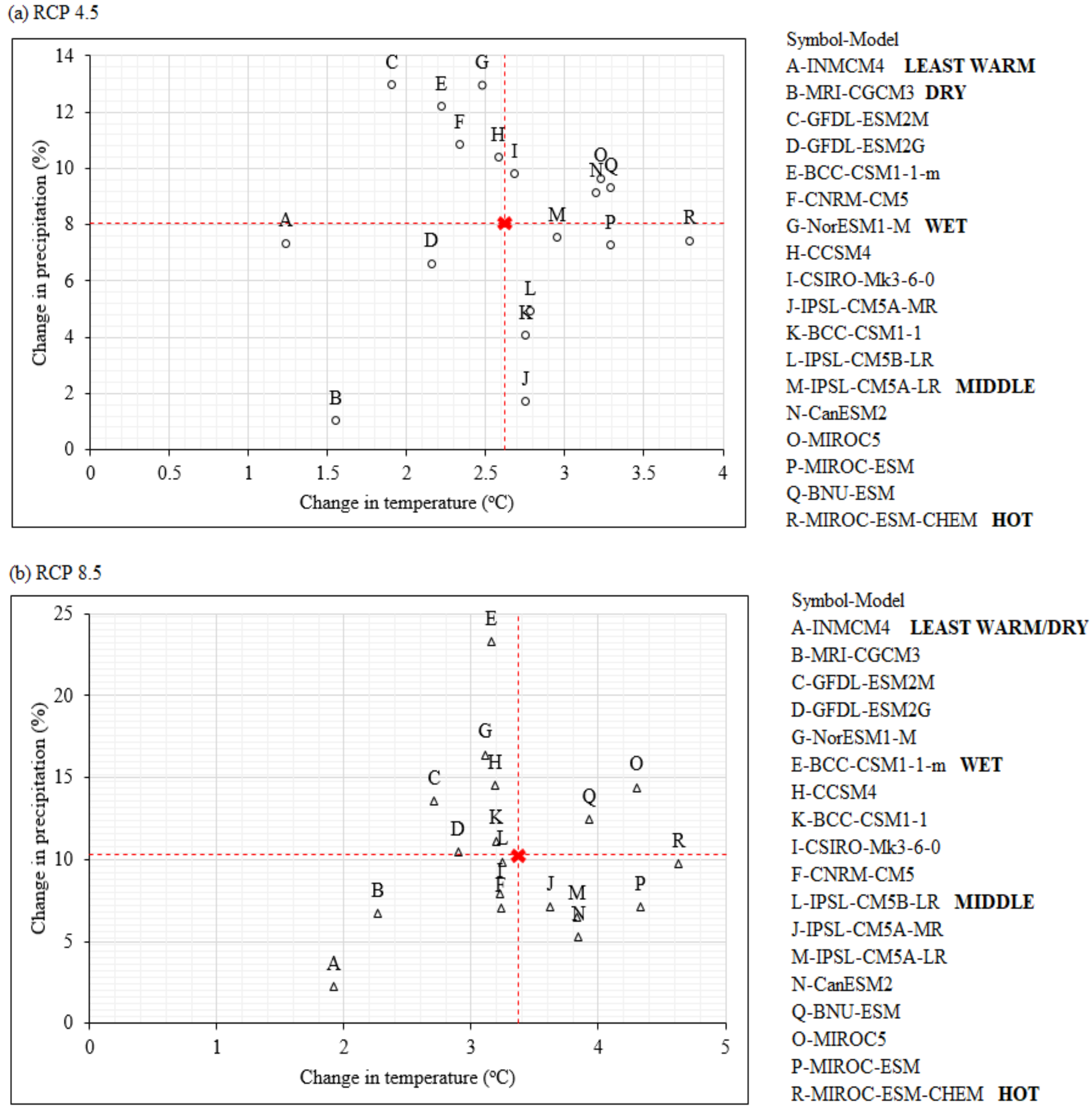

Figure 4.6: Annual precipitation change (percent) plotted against mean temperature change (°C) at mid-century (2041–2070) from the historical period (1951–1980) under RCP 4.5 (a) and RCP 8.5 (b) for all 18 selected MACA models over the PRB. Individual models are denoted by open circles in the RCP 4.5 scenario and open triangles in the RCP 8.5 scenario. The red “X” represents the mean temperature and precipitation change for the 18 selected models in each scenario. The five model projections are noted LEAST WARM, HOT, DRY, WET, and MIDDLE in the legend.

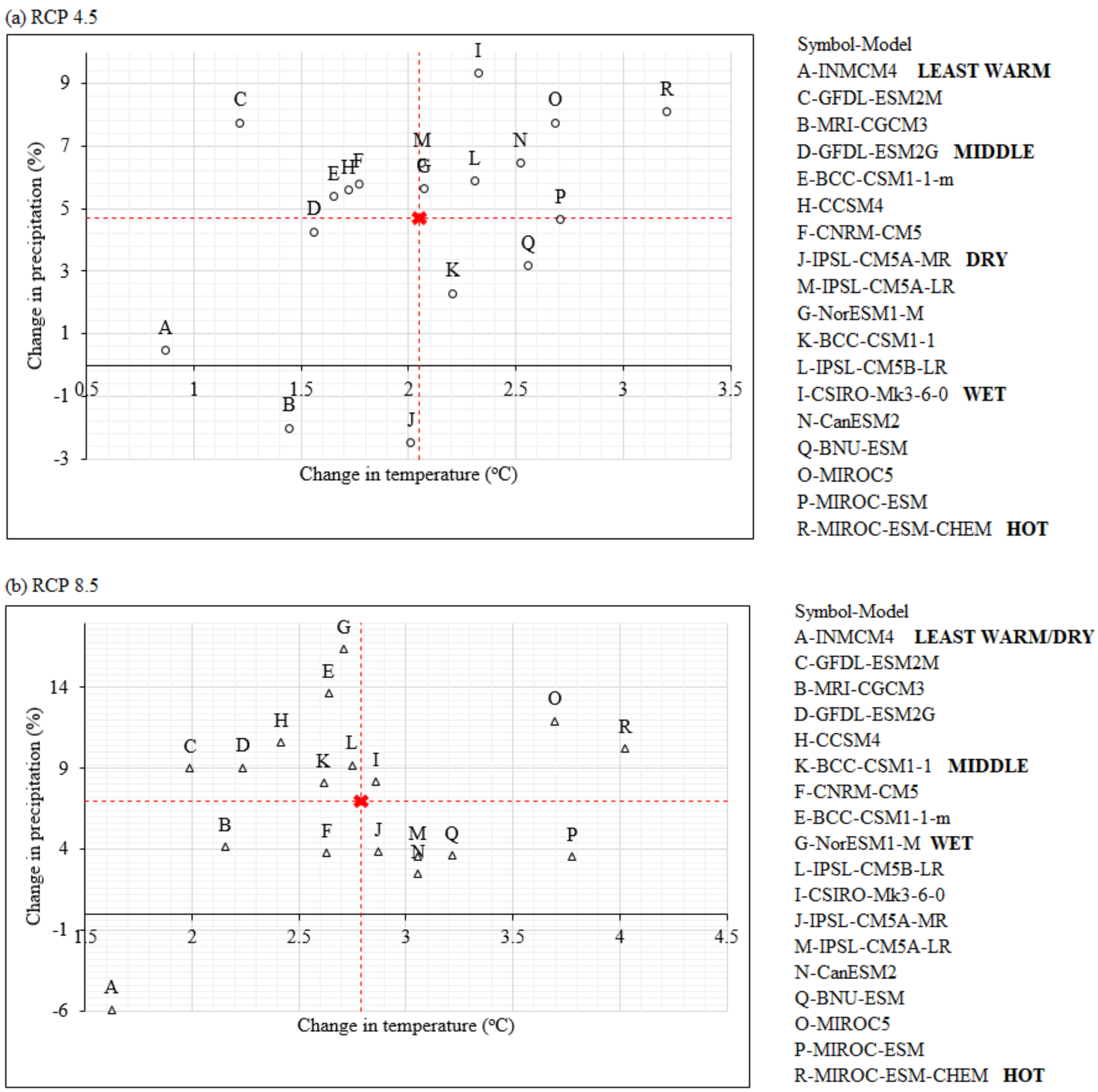

Figure 4.7: Annual precipitation change (percent) plotted against mean temperature change (°C) at mid-century (2041–2070) from the historical period (1981–2010) under RCP 4.5 (a) and RCP 8.5 (b) for all 18 selected MACA models over the PRB. Individual models are d denoted by open circles in the RCP 4.5 scenario and open triangles in the RCP 8.5 scenario. The red "X" represents the mean temperature and precipitation change for the 18 selected models in each scenario. The five model projections are noted Least Warm, Hot, Dry, Wet, and Middle in the legend.

4.4.4. Mid-21st century selected models over the Passaic River Basin

Thus far, the set of projections that characterize climate change at mid-century over the PRB have been determined. Using the change in temperature and precipitation between 2041—2070 period and two different baseline periods (1951—1980 and 1981—2010), three projections that form the lower and upper range of the changes under RCP 4.5 and RCP 8.5 were selected, as shown in Table 4.4. Quite interestingly, under the Least Warm category, the same models under both scenarios and having the same rank order appeared in the top three ranks for the two baseline periods. The same pattern was also seen for the Hot category except under RCP 4.5 for the 1951—1980 baseline. For the dry category, only one model appeared under both scenarios for both baseline periods, the IPSL-CM5A-MR model for the 1951—1980 baseline, and the INMCM4 model for the 1981—2010 baseline. In the Wet category two models (NorESM1-M and BCC-CSM1-1-m) appeared under both scenarios for the 1951—1980 baseline period, and one model (INMCM4) under both scenarios for the 1981—2010 baseline. By and large, the middle category was the only projection that showed variations in the models selected under the two scenarios and baseline periods. Note that, unlike Joyce and Coulson (2020), this study placed no restriction on the selection of the number of models from a modeling institution. The selection process in this study considered all 20 MACA models as distinct on the basis of their unique physical characteristic including their native resolution and the role they play in their representation of aspects of the climate system based on their numerical formulations. For example, while HadGEM2-ES365 and HadGEM2-CC365 may come from the same modeling institution, one incorporates an earth system component with the added capability of explicitly representing biogeochemical processes that interact with the physical climate, while the later has the carbon cycle inclusion. Table 4.5 shows the rankings of various selected models under each category, by scenarios for the two baseline periods considered. By this, models or projections that encapsulate the plausible range of temperature and precipitation change as well as a mild projection at the middle of the range for the Passaic River Basin is projected at mid-century.

Under the two different baseline period, this evaluation captures the uncertainty that may arise as a result of different baseline condition, which has been noted to be comparable to or more important than the uncertainty arising from the choice of GCMs (Peñaloza et al., 2019).

Table 4.2: Change in mean temperature and annual precipitation from historical to mid-21st century over the Passaic River Basin for the 18-model ensemble and the distance of each model from the ensemble mean under the RCP 4.5 and RCP 8.5 scenarios. The minimum po possible distance colored in red representing the model for middle of the temperature and precipitation range relative to the 1951—1980 baseline.

2041-2070 minus 1951-1980							
		RCP 4.5			RCP 8.5		
Model	Symbol	Temp	Precip	Dist. from mean	Temp	Precip	Dist. from mean
BCC-CSM1-1	K	2.75	4.05	4.02	3.20	11.14	0.83
BCC-CSM1-1-m	E	2.22	12.20	4.15	3.16	23.29	12.97
BNU-ESM	Q	3.29	9.33	1.43	3.93	12.47	2.22
CanESM2	N	3.20	9.13	1.20	3.85	5.30	5.04
CCSM4	H	2.58	10.40	2.33	3.19	14.54	4.23
CNRM-CM5	F	2.34	10.85	2.79	3.23	7.06	3.27
CSIRO-Mk3-6-0	I	2.68	9.82	1.75	3.23	7.90	2.42
GFDL-ESM2G	D	2.15	6.62	1.52	2.89	10.45	0.49
GFDL-ESM2M	C	1.91	12.98	4.96	2.71	13.59	3.33
INMCM4	A	1.24	7.34	1.56	1.92	2.23	8.22
IPSL-CM5A-LR	M	2.95	7.54	**0.62**	3.83	6.50	3.85
IPSL-CM5A-MR	J	2.75	1.70	6.37	3.62	7.11	3.22
IPSL-CM5B-LR	L	2.78	4.91	3.16	3.25	9.85	**0.48**
MIROC5	O	3.23	9.66	1.70	4.30	14.41	4.19
MIROC-ESM	P	3.29	7.27	1.05	4.33	7.11	3.35
MIROC-ESM-CHEM	R	3.79	7.44	1.33	4.63	9.77	1.38
MRI-CGCM3	B	1.55	1.04	7.12	2.27	6.68	3.80
NorESM1-M	G	2.48	12.99	4.92	3.11	16.39	6.08
Mean of 18 Models	x	2.62	8.07		3.37	10.32	

Table 4.3: Change in mean temperature and annual precipitation from historical to mid-21st century over the Passaic River Basin for the 18-model ensemble and the distance of each model from the ensemble mean under the RCP 4.5 and RCP 8.5 scenarios. The minimum possible distance colored in red representing the model for middle of the temperature and precipitation range relative to the 1981—2010 baseline

2041-2070 minus 1981-2010

		RCP 4.5			RCP 8.5		
Model	Symbol	Temp	Precip	Dist. from mean	Temp	Precip	Dist. from mean
BCC-CSM1-1	K	2.21	2.30	2.40	2.61	8.11	**1.15**
BCC-CSM1-1-m	E	1.65	5.40	0.81	2.64	13.62	6.65
BNU-ESM	Q	2.56	3.19	1.58	3.21	3.65	3.35
CanESM2	N	2.52	6.46	1.84	3.06	2.51	4.47
CCSM4	H	1.72	5.61	0.98	2.42	10.61	3.66
CNRM-CM5	F	1.77	5.81	1.15	2.63	3.80	3.18
CSIRO-Mk3-6-0	I	2.32	9.34	4.66	2.86	8.15	1.19
GFDL-ESM2G	D	1.56	4.27	**0.65**	2.24	9.05	2.16
GFDL-ESM2M	C	1.22	7.75	3.17	1.99	9.04	2.22
INMCM4	A	0.87	0.45	4.40	1.62	-5.91	12.94
IPSL-CM5A-LR	M	2.06	6.46	1.77	3.05	3.58	3.40
IPSL-CM5A-MR	J	2.01	-2.49	7.18	2.87	3.84	3.13
IPSL-CM5B-LR	L	2.31	5.88	1.22	2.75	9.20	2.23
MIROC5	O	2.68	7.75	3.13	3.70	11.94	5.05
MIROC-ESM	P	2.71	4.64	0.66	3.78	3.53	3.58
MIROC-ESM-CHEM	R	3.20	8.10	3.60	4.03	10.22	3.48
MRI-CGCM3	B	1.44	-2.02	6.73	2.15	4.17	2.87
NorESM1-M	G	2.07	5.64	0.95	2.71	16.39	9.42
Mean of 18 Models	x	2.05	4.70		2.80	6.97	

Table 4.4: Top three ranked projections in terms of temperature (Least Warm, Hot) and precipitation (Dry, Wet) change and the Middle projection representing the temperature and precipitation range at mid-21st century (2041—2070) relative to the baseline periods 1951—1980 and 1981—2010 under scenarios (RCP 4.5, RCP 8.5) over the Passaic River Basin.

Scenario	Rank	Least Warm	Hot	Dry	Wet	Middle
1951-1980 baseline						
RCP 4.5	1	INMCM4	MIROC-ESM-CHEM	MRI-CGCM3	NorESM1-M	IPSL-CM5A-LR
	2	MRI-CGCM3	BNU-ESM	IPSL-CM5A-MR	GFDL-ESM2M	MIROC-ESM
	3	GFDL-ESM2M	MIROC-ESM	BCC-CSM1-1	BCC-CSM1-1-m	CanESM2
RCP 8.5	1	INMCM4	MIROC-ESM-CHEM	INMCM4	BCC-CSM1-1-m	IPSL-CM5B-LR
	2	MRI-CGCM3	MIROC-ESM	CanESM2	NorESM1-M	GFDL-ESM2G
	3	GFDL-ESM2M	MIROC5	IPSL-CM5A-LR	CCSM4	BCC-CSM1-1
1981-2010 baseline						
RCP 4.5	1	INMCM4	MIROC-ESM-CHEM	IPSL-CM5A-MR	CSIRO-Mk3-6-0	GFDL-ESM2G
	2	GFDL-ESM2M	MIROC-ESM	MRI-CGCM3	MIROC-ESM-CHEM	MIROC-ESM
	3	MRI-CGCM3	MIROC5	INMCM4	MIROC5	BCC-CSM1-1-m
RCP 8.5	1	INMCM4	MIROC-ESM-CHEM	INMCM4	NorESM1-M	BCC-CSM1-1
	2	GFDL-ESM2M	MIROC-ESM	CanESM2	BCC-CSM1-1-m	CSIRO-Mk3-6-0
	3	MRI-CGCM3	MIROC5	MIROC-ESM	MIROC5	GFDL-ESM2G

4.4.5. Hydro-climatic impacts of climate change in the Rockaway watershed

In examining hydroclimatic response to future climate, the top ranked model of each category in Table 4.4 for the 1981—2010 baseline under both scenarios was used to drive the MIKE SHE hydrologic model developed for the Rockaway catchment. In all, 9 models (5 under RCP 4.5 and 4 under RCP 8.5) representing the range of temperature and precipitation change over the basin at mid-21st century produced future hydrological outputs (e.g., streamflow, actual evapotranspiration, recharge) needed for the impacts assessment. This future hydroclimatic response was assessed by evaluating, 1) monthly evapotranspiration—precipitation (ET/P) and recharge—streamflow ratios (R/Q); 2) seasonal changes in precipitation (P), temperature (T), actual evapotranspiration (ET), and streamflow (Q); and 3) annual trends in water balance outputs, as presented in the subsections below. In respect of the R/Q ratio, note that values change from positive to negative in months where ET exceeds precipitation, leading to a net negative recharge. This means that ET borrows water from the groundwater system due to the deficit of precipitation in a given month and rendering recharge negative for that month.

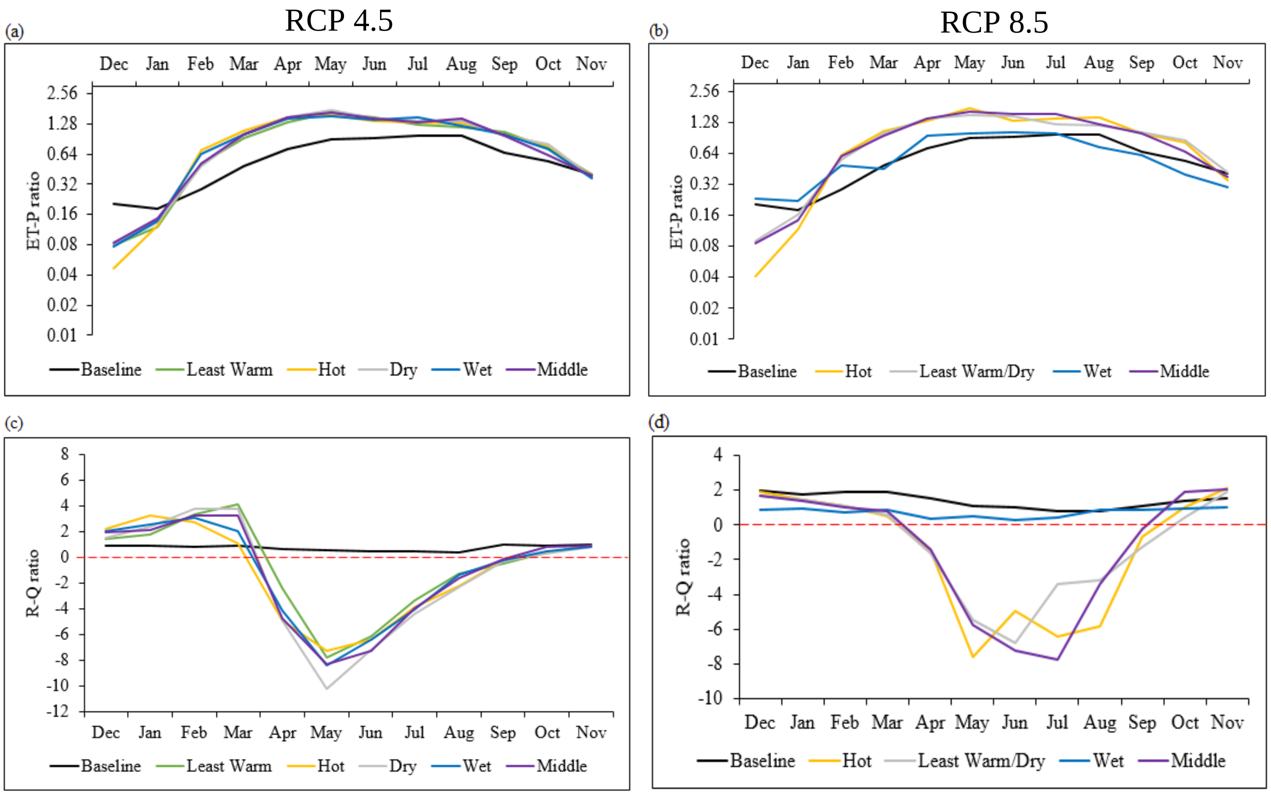

Figure 4.8: Monthly hydroclimatic ratios for the period 2041—2070 relative to the 1981—2010 baseline. (a) and (b) are evapotranspiration—precipitation ratios (E/P) and (c) and (d) are recharge—streamflow ratios (R/Q) for RCP 4.5 and RCP 8.5 respectively

4.4.6. Monthly hydroclimatic ratios

In Figure 4.8, the mid-21st century (2041—2070) outlook of ET-P and R-Q ratios are compared with the 1981—2010 baseline on a monthly basis in the Rockaway catchment. The magnitude of ET-P index is of interest to a number of hydrometeorological considerations, including but not limited to hydrologic systems monitoring (e.g., storage changes), basin-wide water budget accounting, water footprint, and climate change indexing (Blatchford et al., 2020; Senay et al., 2016; Oteng Mensah and Alo, 2023). In Figure 4.8a, b, the projected E/P ratio for all five projections is higher than that of the baseline for most months in the year, with values ranging from 0.04 in December and 1.76 in May. Excepting the WET model that projects near unity values under the highest scenarios, all other models project above-one values, suggesting significant water deficit in more than half of the year at mid-century.

The largely high ET index value foreseen is also reflected in the exceptionally high R-Q ratios less than 0.5 in corresponding months as shown in Figure 4.8c, d. Because of possible evapotranspiration losses, more than half of the entire year's total precipitation is consumed, and none emerging as water available to streams, and seepage into the groundwater system. Between March and August, all models under RCP 4.5 foresee huge deficit in water availability relative to the baseline, with R-Q ratio ranging from -10.24 under the DRY projection to 4.16 in the LEAST WARM model. It appears that projected deficits occur in the April—September window while surpluses are foreseen in the October—March time period for all five climate model projections under both scenarios. Flint and Flint (2007) noted that, estimates of R-Q ratio are indicative of the mechanisms that largely control groundwater recharge in a basin. Such that, a ratio of 0.5 or less suggests that more than twice as much water has the tendency to become surface runoff than to recharge the saturated zone whereas ratios of 2.0 or greater indicates that water has more than twice the potential to favor recharge than overland flow. Thus, given the results in this study the future outlook on water resource in the study basin appear dire, and calls for swifter action by decision-makers.

4.4.7. Changes in temperature and precipitation

Table 4.5 shows the projected seasonal change in temperature, precipitation, streamflow, actual ET and recharge for the range of climate projection under both RCPs at 2041—2070 period relative to 1981—2010 period. Evident as one of the key impacts of global temperature change is the shift in the seasonal cycle of hydroclimate variables, in particular precipitation and streamflow. Modulated by changes in actual evapotranspiration, the magnitude and direction of change in precipitation and flow point to the character of hydroclimatic sensitivity to climate forcing as well as the varying nature from one location to another. In the case of the Rockaway catchment, a consistent warming from +1.21 to + 4.70 ^{o}C is projected by the five models in all seasons under both emission scenarios. The greatest temperature rise is projected by the HOT model in the winter under RCP 4.5 and in the spring under RCP 8.5. This projected seasonal changes are generally consistent with other studies in the northeastern US (Melillo et al., 2014; Naz et al., 2016).

Along with temperature, all models project increases in precipitation with the exception of the LEAST WARM model that projects decrease in the fall and winter seasons under both scenarios. Projected changes in precipitation ranges from 3.43% decrease in the fall season by the LEAST WARM model to 16.32% increase in the summer by the WET model under RCP 4.5. Under RCP 8.5 (the business as usual (BAU) scenario), changes are relatively large, ranging from 12.09% decrease in the winter by the LEAST WARM/DRY model to 20.63% increase in the spring by the WET model (Table 4.5). Consistent with the general trends in the region, this increases in the winter and spring precipitation are also reported in the Forth National Climate Assessment report (NCA, 2018) and others for the Northeastern US (e.g., Thibeault and Seth, 2014).

Table 4.5: Projected seasonal change in precipitation, temperature, actual evapotranspiration, recharge, and streamflow in the mid-21st century (2041–2070) relative to the baseline period (1981–2010) summarized over the Rockaway catchment in the PRB

		RCP 4.5					RCP 8.5			
	Baseline	Least Warm	Hot	Dry	Wet	Middle	Least Warm/Dry	Hot	Wet	Middle
Temperature (ºC change)										
DJF	-1.83	1.25	4.14	2.04	2.91	2.35	2.02	4.67	3.00	3.08
MAM	8.75	1.43	4.06	2.61	2.56	2.10	2.25	4.70	2.87	3.12
JJA	20.47	1.28	3.33	3.04	2.75	1.68	1.96	4.46	3.56	3.49
SON	10.57	1.21	3.36	2.81	2.66	2.39	1.67	4.41	3.12	3.11
Precipitation (% change)										
DJF	3.06	-2.51	5.17	6.80	10.13	5.90	-12.09	15.39	12.91	5.21
MAM	3.59	11.04	9.69	0.19	13.78	5.02	5.88	17.32	20.63	18.11
JJA	3.72	13.96	14.12	4.20	16.32	4.68	15.35	8.87	18.05	6.37
SON	3.66	-3.43	11.69	2.78	11.01	15.23	-10.84	10.76	7.44	20.26
Evapotranspiration (% change)										
DJF	0.67	-8.00	10.04	3.12	17.14	3.72	-2.70	14.37	51.72	10.35
MAM	2.54	106.25	120.13	103.71	117.61	109.45	98.58	132.48	32.26	123.92
JJA	3.55	55.71	59.01	52.13	65.22	53.77	54.76	57.41	12.19	56.42
SON	1.98	28.25	44.78	33.28	39.18	38.78	24.41	41.76	-14.06	46.97
Flow (% change)										
DJF	7.80	-52.73	-50.45	-51.70	-44.25	-49.22	-59.88	-46.91	10.79	-46.59
MAM	6.14	-75.50	-80.90	-77.51	-77.43	-76.82	-79.52	-79.31	-4.60	-74.45
JJA	3.59	-84.01	-86.06	-87.25	-85.62	-86.42	-86.01	-86.30	9.00	-85.98
SON	5.45	-78.81	-78.29	-79.40	-74.41	-74.28	-81.79	-77.75	32.39	-73.78
Recharge (% change)										
DJF	-1.67	-24.79	-18.44	-19.42	-12.50	-17.52	-35.87	-9.85	7.13	-16.49
MAM	-1.06	-156.66	-170.04	-171.17	-165.81	-166.63	-153.75	-172.99	-18.85	-164.18
JJA	-0.41	-238.12	-255.35	-269.28	-272.13	-274.25	-228.84	-273.04	-41.65	-282.15
SON	-1.31	-80.32	-73.03	-77.74	-68.91	-61.92	-89.15	-74.63	25.49	-60.40

4.4.8. Seasonal changes in streamflow

Table 4.5 also summarizes the range of plausible changes in streamflow in the Rockaway catchment from 1981—2010 baseline to the 2041—2070 future period. The results show that decreasing changes in seasonal flow are foreseen by all climate projections except the WET model in winter, summer, and fall under RCP 8.5 which show increasing changes. This general projected decrease in flow as opposed to the projected increase in precipitation can largely be attributed to increasing evapotranspiration, driven by rapidly increasing temperatures to a large extent. In the paragraphs that follow, focus is given to the DRY, WET, and MIDDLE climate models under the business as usual scenario (RCP 8.5) to capture the broad range of potential future climate changes over the study catchment.

In the DRY model, projected increases in seasonal temperature by 1.67 to 2.25 ^{o}C and that of precipitation by 12.09% decrease to 15.35% increase is expected to trigger a decrease in streamflow by 82.01 to 59.88%. With the projected seasonal changes in evapotranspiration by 2.70% decrease to 98.58% increase, this potential deficit in seasonal streamflow can be linked to the relatively high evaporative demand on precipitation due to projected warmer temperatures.

Unlike the DRY climate model, the WET model projects relatively high changes in temperature. An increasing change in projected temperature by 2.87 to 3.56 ^{o}C corresponds to projected seasonal precipitation increase by 7.44% to 20.63% resulting in changes in projected seasonal flows by a 4.60% decrease, 9% increase, 10.79% increase, and a 32.39% increase in the spring, summer, winter and fall seasons respectively. This overall increase in streamflow can be attributed to the combined effect of projected precipitation increase and the relatively modest increase (excepting the 14.01% decreasing change for fall) in projected seasonal evapotranspiration. The findings by Hodgkins and Dudley (2005) that indicated a general increase in March streamflow and a decline in May was also captured by the present study. In the WET model under RCP 8.5, streamflow increased by 20.14% in March, decreased by 16.39% in April, and decreased again by 17.56% in May (not shown).

Under the MIDDLE climate projection, seasonal actual evapotranspiration, associated with projected warming, is expected to increase, ranging from 10.35% increase in the winter to 123.92% increase in the spring. Because projected precipitation increase (+5.21 to +20.26%) is relatively marginal and unable to satisfy the high demand of evapotranspiration, a reduction in seasonal streamflow by 85.98% decrease in the summer to 46.59% decrease in the winter is projected.

This overall projected decrease in streamflow in the study catchment is well in line with trends in the northeastern US, where there is a strong consensus among models in some basins (e.g. Naz et al., 2016). Note here that, projected trends in recharge are associated with that of streamflow, and that all the models—except winter, summer, and the fall seasons under the WET model—also projected reduction in recharge. As corroborated by findings in earlier study, the results indicate that the causes of streamflow in the study catchment is largely dictated by the availability of energy and water, which controls the amount of evapotranspiration rates. It was noted in earlier study that in meteorological stressed period, streamflow is more sensitive to actual ET than it is to precipitation in the study catchment.

4.4.9. Annual trends in hydroclimatic metrics

To better assess on-going effects of climate change, it is important to track the trajectory of hydroclimate indicator variables over the long term (at least 30 years). Analyzing hydrologic variables in relation to their climate drivers over the long term is fundamental for improved water resource predictions under a constantly changing climate. Within the context of the LEAST WARM, HOT, DRY, WET, MIDDLE climate projections, trends in baseline (1981—2010) hydroclimatic metrics are compared with that at mid-21st century (2041—2070). It is worth pointing out that trends shown in the figures below are statistically significant at 95%

confidence level. These trends were derived from the decomposition of the original time series into their low and high frequencies via discrete wavelet transform in earlier studies.
Figures 4.9, 4.10, 4.11, and 4.12 show a comparison of the temporal evolution of hydroclimatic variables and metrics for the historical period as against the future period under RCP 4.5 and RCP 8.5 emission scenarios. In terms of precipitation, projected models largely demonstrate increasing trends over the baseline period through the mid-21st century except in the DRY projection under RCP 4.5 and both LEAST WARM/DRY and MIDDLE under RCP 8.5 that deviate from the baseline. The projected rate of change lies between -4.64mm/year in the MIDDLE projection under the worst scenario and 8.27mm/year in the MIDDLE projection under RCP 4.5. This is relative to the baseline period which increased at a rate of 0.13mm/year over the 30 years. On average, total projected precipitation would be approximately 50mm more at mid-21st century.

Conversely, mid-21st century projection of streamflow reflects a decrease (relative to the baseline) under both emission scenarios for all projections except the WET model that remarkably exhibit an isolated increasing trend relative to the baseline under the high emission scenario. Projected rate of streamflow reduction ranges from -14.6m^3/year (or -438m^3 in total for 2041—2070) in the WET model to -0.21m3/year (or -6.3m^3 in total for 2041—2070) in the DRY model under RCP 4.5. This potentially incongruous signal between precipitation and flow further highlight the important influence of actual evapotranspiration on water available in the study basin. This finding also corroborate the study by Huntington (2003), who noted that streamflow under a warmer climate will be significantly lower because of an increase in evapotranspiration.

Projected temperature follows the same increasing trajectory as the baseline for all projections though in varying degrees under both scenarios. For the range of projections considered in this study, the rate of annual warming trend is in the range of -0.0051^{o}C/year in the LEAST WARM model under RCP 4.5 to 0.081 ^{o}C/year in the WET model under RCP 8.5 or a total of -0.15^{o}C — 2.43^{o}C for the 30 years from 2041—2070. This is relative to the historical period at 0.035 ^{o}C/year or a total of 1.04 ^{o}C for the 30 years from 1981—2010. Although baseline conditions differ, the projected temperature change reported in this study falls in the range of change reported by Hayhoe and others (2007) in the Northeastern region. They examined past and future changes in climate indicators and indicated a regional warming of 2.1 ^{o}C to 5.3 ^{o}C. Similar range was also reported by Karmalkar and Bradley (2017) in the Northeastern region.

Along with temperature increase is the projected increase in actual evapotranspiration that also continues into the future under both scenarios. Relative to the baseline that showed increases at a rate of 0.91mm/year, evapotranspiration rate is in the range of -6.97mm/year in the DRY model under RCP 4.5 to 2.75mm/year in the LEAST WARM/DRY model under RCP 8.5. Although the decreasing trend in recharge and streamflow largely correspond to actual evapotranspiration in the historical period, it appears that projected recharge is rather increasing, responding instead to the projected precipitation increases under both scenarios. The range of projected recharge is decreasing from -0.16mm/year in the DRY model towards an increase at 0.2mm/year under RCP 4.5. Note that recharge, while appearing to increase at mid-21st century is largely in the deficit, likely due to projected high evaporative demand.

Temperature increases are expected to induce climatic extremes as a result of increase in atmospheric moisture. Across scenarios, Figure 4.12a, c, indicates generally increasing trends in R10 across all projections, except the DRY model under RCP 4.5 and both DRY and MIDDLE projections under RCP 8.5 that deviate from the increasing baseline trends with higher magnitudes. Projected rate of change in R10 ranges between -0.16days/year (or 4.8days reduction in total for 2041—2070) in the DRY model to 0.2days/year (or 6days increase in total for 2041—2070) in the WET model. Findings regarding CDD generally complements that of R10 in that, decreases in CDD were accompanied by increases in R10. Under RCP 4.5, projected decrease in CDD are generally consistent with trends observed in the baseline period for all models, with the exception of the DRY model that is projected to continue an increasing trajectory from the baseline period. However, under the high emission scenario, all four models foresee an increasing trend, as reflected in the historical period. Rate of projected changes in CDD ranges from -0.083days/year (or 2.49days reduction in total for 2041—2070) in the WET model under RCP 4.5 to 0.094days/year (or 2.82days increase in total for 2041—2070) in the LEAST WARM model under RCP 8.5. Taken together, the R10 and CDD results largely suggest increases in runs of wet days along with decrease in runs of dry days under RCP 4.5 but the opposite is the case under RCP 8.5, especially for CDD. For both R10 and CDD, Schoof, (2015) in investigating changes in extreme precipitation in the CONUS, reported similar trends in the northeastern US, highlighting longer extreme wet and dry spells.

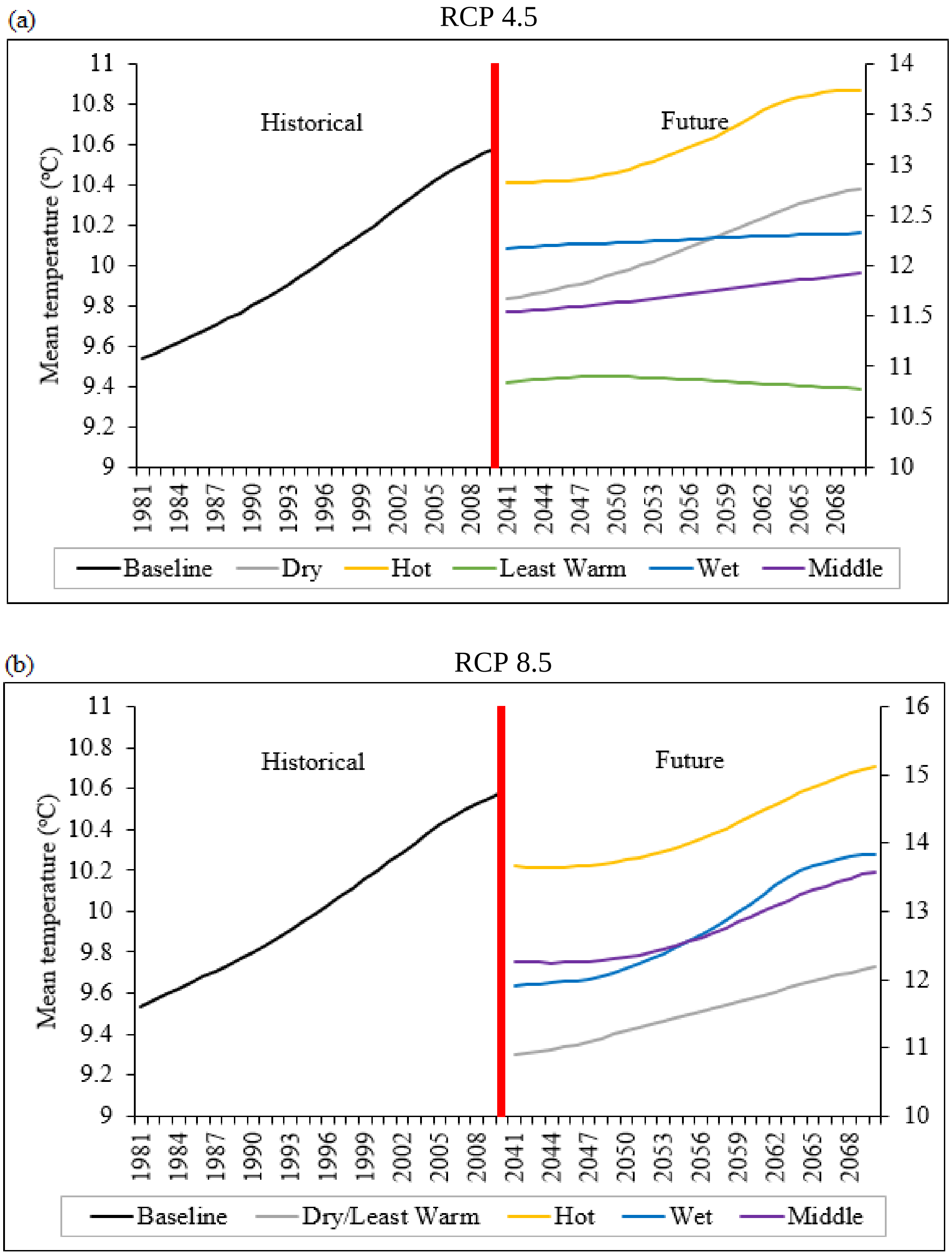

Figure 4.9: Annual trends temperature under RCPs 4.5 and 8.5 emission scenarios derived from discrete wavelet analysis

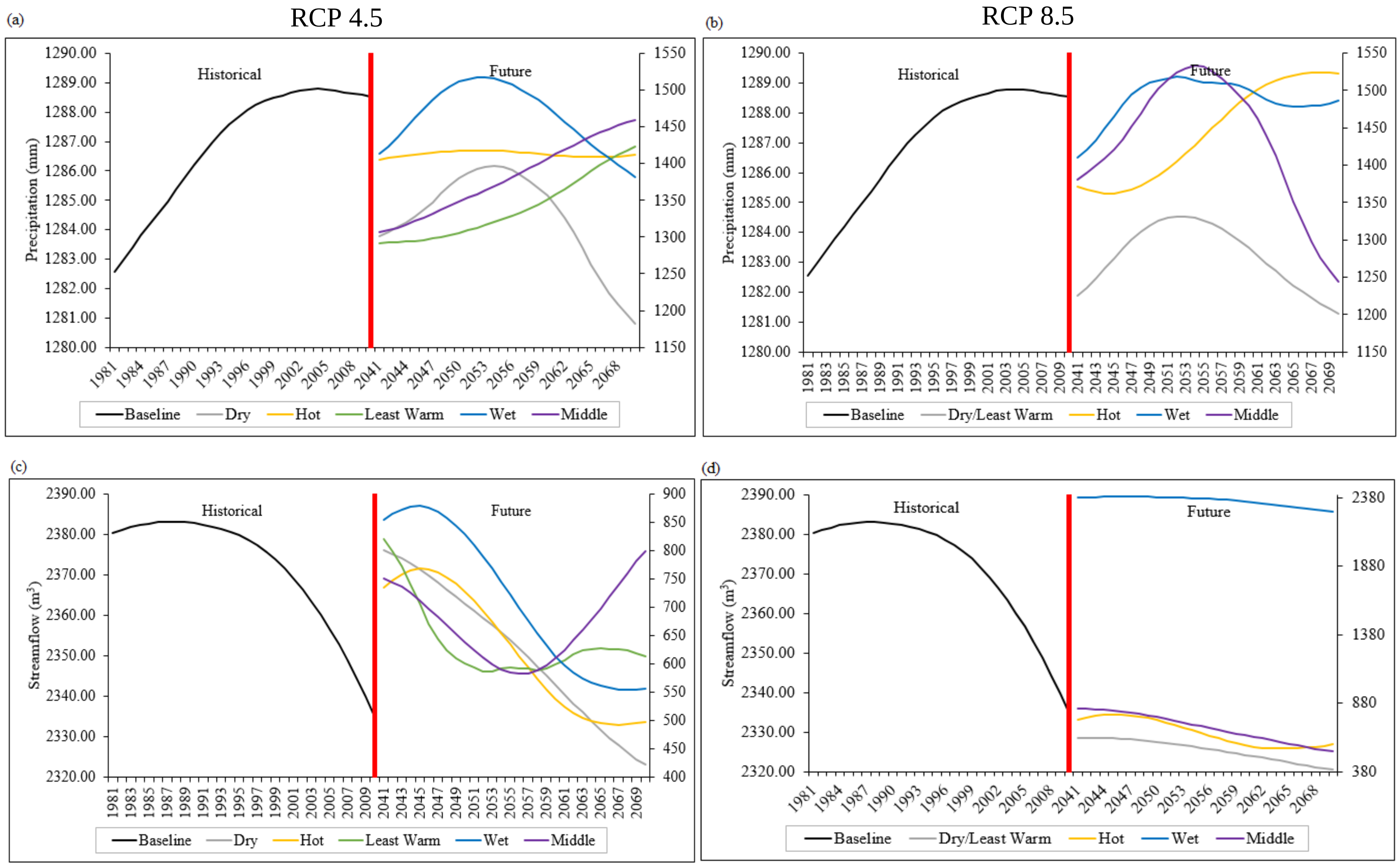

Figure 4.10: Annual trends in precipitation (a, b) and streamflow (c, d) under RCPs 4.5 and 8.5 emission scenarios derived from discrete wavelet analysis

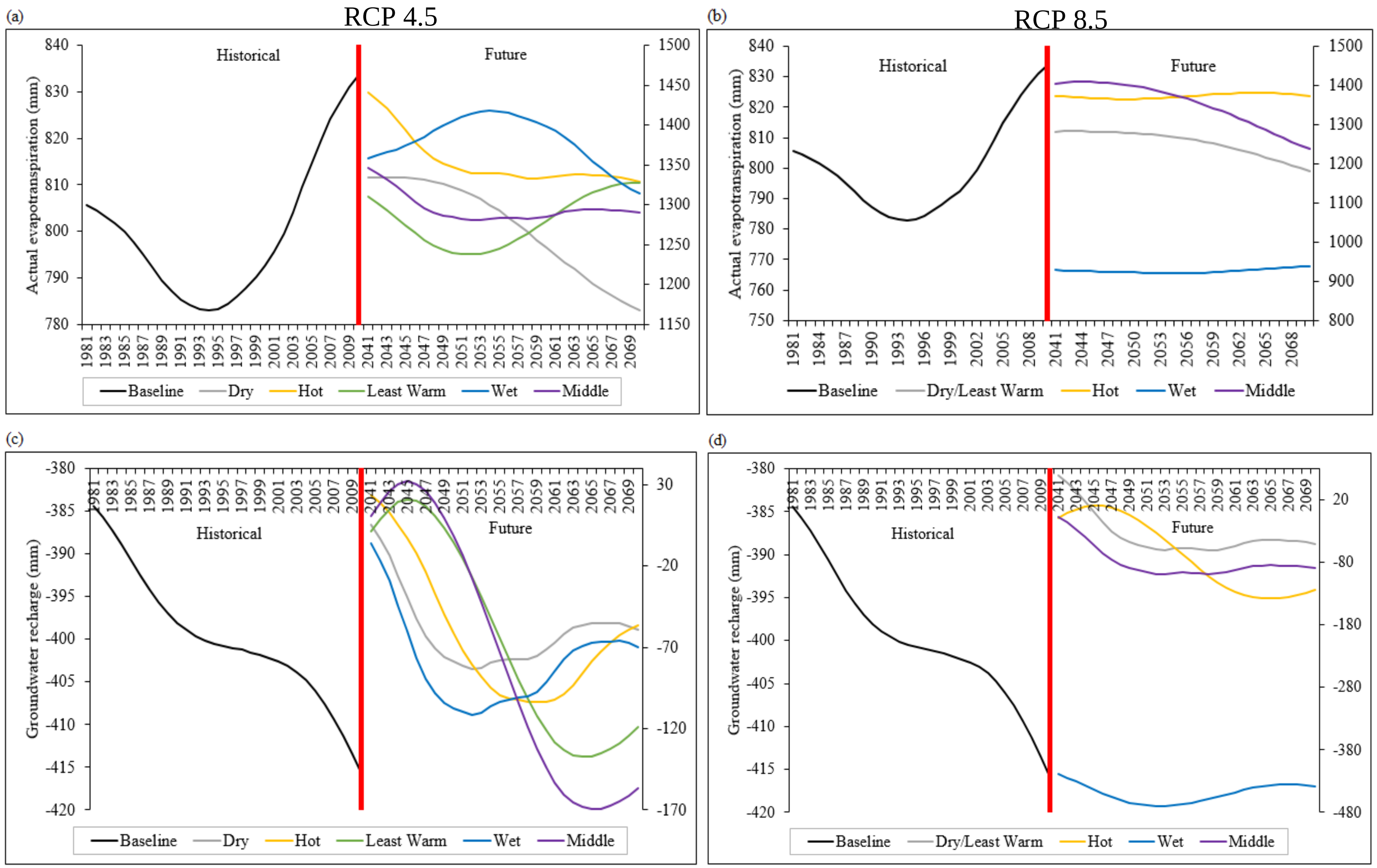

Figure 4.11: Annual trends in actual evapotranspiration (a, b) and groundwater recharge (c, d) under RCPs 4.5 and 8.5 emission scenarios derived from discrete wavelet analysis

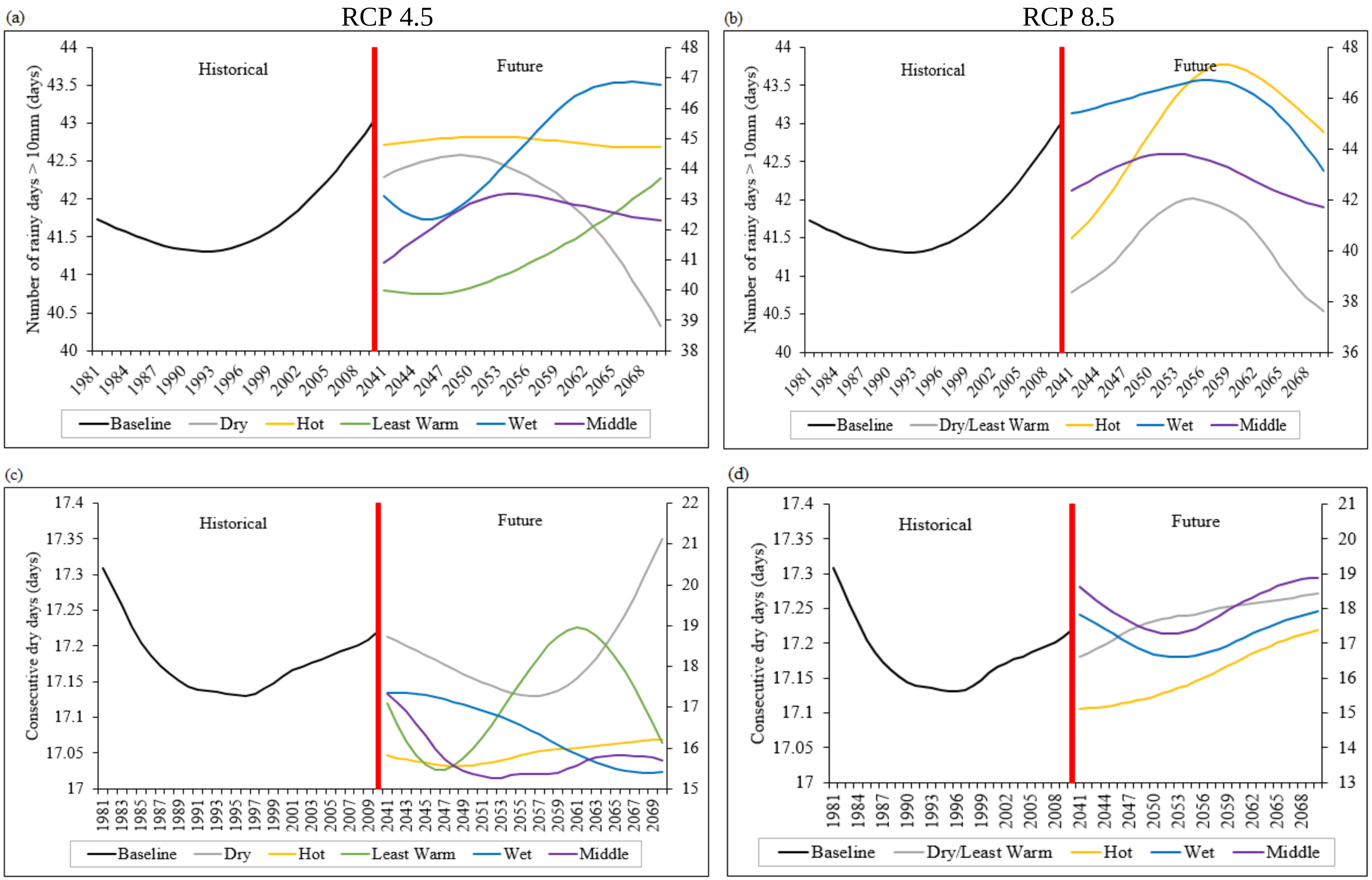

Figure 4.12: Annual trends in number of rainy days greater than 10mm (R10) (a, b) and consecutive dry days (CDD) (c, d) under RCPs 4.5 and 8.5 emission scenarios derived from discrete wavelet analysis

4.5. Implications of Mid-21st Climate Change on Reservoirs in the PRB

With the frequency of heavy precipitation (R10) depicted by the LEAST WARM and WET projections under RCP 4.5 projected to increase, accompanied with the projected increase in dry spells (CDD) by all projections under RCP 8.5 and the driest future under RCP 4.5, the optimal operations of reservoirs across the Passaic River Basin may be significantly challenged, given their various competing uses in the basin. For example, in a drier future, prolonged dry spells may lead to difficulty in sustaining minimum water release levels from reservoirs. Conversely, while reservoirs may store more waters under increased duration of rainfall, it could trigger unregulated water releases, causing damages downstream. Variations in annual precipitation and the resulting alterations in runoff could disrupt downstream reservoirs operations, impacting recreational activities, water quality, and the overall health of streams and ecosystem services.

Regarding water quality, an expected increase in extreme precipitation is projected to hasten soil erosion, leading to significant economic and environmental consequences (Lal, 2017). Under such intense rainfall, eroded sediments carry harmful substances like nutrients, pesticides, and contaminants into streams, rivers, groundwater, and reservoirs (Kumar and Singh, 2021), resulting in decline in water quality. Moreover, a strong correlation appear to exist between evapotranspiration and water quality. In analyzing evapotranspiration effect on seasonal water quality index, Ruzvidzo, (2021) found that, high evapotranspiration rates resulted in poor water quality in the summer season due to the presence of high chemical concentrations in water. Thus, along with the sweeping of pollutants into water bodies, evapotranspiration increases as projected in the study basin will not only affect available water resources but also compromise the quality of drinking water supply. Additionally, sediment accumulation in surface reservoirs tend to reduce their active storage capacity, posing a substantial challenge to sustainable reservoir planning and management. Thus the envelope of future precipitation and streamflow events as shown in this study over the Rockaway catchment, particularly regarding the Boonton reservoir, will offer insights crucial for enhancing future reservoir operations in the area. According to the US Federal Emergency Management Agency (FEMA) on dam safety (Normand, 2019), it was discovered that numerous dams built in the last century are deficient in proper risk assessments, posing a danger to the safety of communities residing downstream. The Boonton reservoir which was completed in 1902, may fall under this category of dams, lying at the mercy of the projected wider variability in future extreme conditions. Thus, the region's aging water-related infrastructure, nearing the end of its expected lifespan (NCA, 2018), coupled with projected climate variability, suggests that climate-related disruptions could exacerbate existing issues, disproportionately affecting vulnerable communities. Also, traditional assumptions of stability in designing water-related structures may not hold under future climate conditions. Thus, apart from helping to build the needed resilience and adaptation to possible climate impacts through incorporation of climate related risks in future water resource decision and planning process, this study will provide advanced knowledge and sufficient lead time for water managers to take precautionary measures against projected extreme events that would induce environmental pollution in the study basin.

4.6. Conclusion

Evaluation of future water availability under a changing climate is contingent upon reliable hydroclimatic projections, often generated by forcing a calibrated hydrological model with outputs of global climate models. In this study, the MIKE SHE hydrological model developed for the Rockaway catchment was driven by the downscaled MACA datasets. First, a selection process was conducted and nine (9) different models out of the 20 MACA models under RCP 4.5 and 8.5 emission scenarios was chosen on the basis of their ability to capture the average historical climatic condition over the PRB. Relative to two baseline periods (1951—1980 and

1981—2010), the subset models characterized the change in temperature and precipitation for the MACA models according to LEAST WARM, HOT, DRY, and WET at mid-21st century (2041—2070) as well as a future that typifies the MIDDLE of the temperature and precipitation range. To assess the hydrologic response to future climate change in the PRB, these selected future projections were compared with the 1981—2010 baseline simulation, and the simulated hydrologic outputs analyzed. Set in the Rockaway sub-catchment, and used as a case study, this analysis will inform understanding of how future temperature and precipitation changes impact streamflow dynamics, which directly control available water resource at a basin scale. Below are the key conclusions that can be drawn from the analyses.

1) The largely different outcome obtained by the use of different baseline period in the model selection process demonstrates the influence of baseline conditions on model results. From the results, the top ranked models under DRY, WET, and MIDDLE category were different for the 1951—1980 as well as the 1981—2010 baseline periods. Similarly, the range of projected temperature and precipitation at the mid-21st century over the PRB were different for both baseline periods. For example, under the business-as-usual scenario, projected mean temperature and precipitation change over the PRB ranged from 1.92—4.63 ^{o}C and 2.23—23.29% respectively for the 1951—1980 baseline. However, for the 1981—2010 baseline period, projected mean temperature and precipitation change ranged from 1.62—4.35 ^{o}C and -5.92—16.39% respectively. The margin of error in these projected changes owing to the different baseline conditions will be +/- 0.3 — +/-0.23 ^{o}C for temperature and +/-8.15— +/-6.9% for precipitation, and this indicates the extent to which the time perspective used in climate change impacts assessment significantly affect outcomes. In investigating the effects of baseline

conditions on simulated hydrologic response to projected climate change, Koczot et al, (2011) noted substantial amplification in some hydrologic variables under specific time periods. They also recognized the uncertainties related to baseline period selection and suggested that results from climate impact studies should be evaluated by considering a range of different baseline conditions. Baker et al. (2016) also indicated that such uncertainties are comparable or more important than that arising from the choice of GCMs, and must be routinely considered.

2) In the Rockaway catchment, results from evaporation and recharge ratios indicate very dire situation in terms of future water availability. With the exception of the WET model that projects near unity values under the highest scenarios, all other models project above-one values for E-P ratio. An above-one value means that projected evapotranspiration in the basin exceeds precipitation in the future, indicative of significant water deficit in more than half of the year at mid-century. This is also reflected in the R-Q results with exceptionally high R-Q ratios less than 0.5 projected. Ratios less than one-half suggest that more than twice as much water is likely to run off the surface than to recharge the groundwater system. The largely negative ratios in the results is an indication that water would not even be available for surface runoff as projected evapotranspiration far exceeds projected precipitation.

3) Across all five (5) climate projections (i.e. LEAST WARM, HOT, DRY, WET, and MIDDLE) and scenarios (RCP 4.5 and RCP 8.5), a consistent warming from +1.21 to + 4.70 ^{o}C is projected in the Rockaway catchment at mid-21st century relative to the 1981—2010 baseline period. The greatest temperature rise is projected by the HOT model in the winter under RCP 4.5 and in the spring under RCP 8.5, generally consistent

with other results in the northeastern US. For the range of projections considered in the study, the rate of annual warming trend is in the range of -0.0051^{o}C/year in the LEAST WARM model and 0.042/year in the DRY model under RCP 4.5 or a total of -0.15^{o}C—1.26^{o}C for the 30 years from 2041—2070. Under RCP 8.5, projected rate of warming is between 0.04 ^{o}C/year in the HOT model to 0.081 ^{o}C/year in the WET model or a total of 1.2 ^{o}C—2.43 ^{o}C for the 30 years from 2041—2070. This is relative to the historical at 0.035 ^{o}C/year or total of 1.04 ^{o}C for the 30 years from 1981—2010.

4) All but the LEAST WARM climate projection foresee increases in precipitation in the Rockaway catchment at mid-21st century. Projected changes in precipitation ranges from 3.43% decrease in the fall season by the LEAST WARM model to 16.32% increase in the summer by the WET model under RCP 4.5. Under the business as usual (BAU) scenario, changes are relatively large, ranging from 12.09% decrease in the winter by the LEAST WARM/DRY model to 20.63% increase in the spring by the WET model. Annual trends in precipitation show overall increasing trend by all models over the baseline period except in the DRY projection under RCP 4.5 and both LEAST WARM/DRY and MIDDLE under RCP 8.5 that deviate from the baseline.

5) While precipitation is generally projected to increase, streamflow shows an overall decreasing signal. Decreases in seasonal flow are foreseen by all climate projections except the WET model in winter, summer, and fall under RCP 8.5 which shows increasing changes. In the DRY model, a change in precipitation by 12.09% decrease to 15.35% increase corresponds to a projected decrease in streamflow by 82.01 to 59.88%. It appears that increases in streamflow were mainly projected by the WET model. For a projected seasonal precipitation increase by 7.44% to 20.63% in the WET model,

associated changes in seasonal flows by only 4.60% decrease, 9% increase, 10.79% increase, and a 32.39% increase in the spring, summer, winter and fall seasons respectively was projected. This translates into projected annual decreasing trend across all models and scenarios, excepting the WET model.

6) It appears that actual evapotranspiration, driven by rapidly increasing temperature, to a large extent, influences flow dynamics in the Rockaway catchment. Apart from the winter and fall seasons that projected decreases under the LEAST WARM and WET models, all other seasons across model and scenarios projected increases in actual ET. This projected increase is largely reflected in the projected reductions in streamflow and groundwater recharge in the study basin.

7) Accompanying higher temperatures are climatic extremes (i.e. R10 and CDD in this study) that result from increased atmospheric moisture. Findings regarding CDD generally complements that of R10 in that, projected decreases in CDD were accompanied by projected increases in R10. Projected rate of change in R10 ranges between -0.16days/year (or 4.8days reduction in total for 2041—2070) in the DRY model to 0.2days/year (or 6days increase in total for 2041—2070) in the WET model. With the rate of 2.49 days total for the baseline period, an increase in the number of days with heavy rain of approx. 2 days is projected in the coldest future whiles an increase of about 4 days is expected in the wettest future. In similar vein, projected rate of change in CDD ranges from -0.083days/year (or 2.49days reduction in total for 2041—2070) in the WET model under RCP 4.5 to 0.094days/year (or 2.82days increase in total for 2041—2070) in the LEAST WARM model under RCP 8.5. Relative to the baseline, having a total of 0.13days, suggests that, in the driest future, the number days with consecutive dry spells is expected to decrease by approximately 2 days whereas an increase of about 3 days have been projected in the wettest future.

In an area that has long suffered the devastating impacts of climate change and variability, a targeted but more comprehensive study such as this will as least provide sufficient advance knowledge and a broad view to water managers and decision makers on the potential impacts of climate change on water availability. It is however important to point out that, while the study sought to minimize uncertainty in terms of considering the full range of climate model projections as well as that emanating from the different choice of baseline conditions, other uncertainties pertaining to the choice of GCMs, downscaling and bias correction of GCMs, hydrological modeling procedures, and the likely changes in future land use pattern persist. Nevertheless, the projected hydrologic response to climate change as revealed in this study can be far reaching, affecting water supply that will in turn affect reservoir operations, and fuel flooding and drought conditions among others. These findings thus, necessitate swift mitigation and adaptation plans.

4.7. References

Abatzoglou, J. T., Dobrowski, S. Z., Parks, S. A., & Hegewisch, K. C. (2018). TerraClimate, a high-resolution global dataset of monthly climate and climatic water balance from 1958–2015. Scientific data, 5(1), 1-12.

Aliyari, F., Bailey, R. T., & Arabi, M. (2021). Appraising climate change impacts on future water resources and agricultural productivity in agro-urban river basins. Science of the Total Environment, 788, 147717.

Allan, R. P., & Soden, B. J. (2008). Atmospheric warming and the amplification of precipitation extremes. Science, 321(5895), 1481-1484.

Baker, D. J., Hartley, A. J., Butchart, S. H., & Willis, S. G. (2016). Choice of baseline climate data impacts projected species' responses to climate change. Global change biology, 22(7), 2392-2404.

Baker, D. J., Hartley, A. J., Butchart, S. H., & Willis, S. G. (2016). Choice of baseline climate data impacts projected species' responses to climate change. Global change biology, 22(7), 2392-2404.

Blatchford, M. L., Mannaerts, C. M., Njuki, S. M., Nouri, H., Zeng, Y., Pelgrum, H., ... & Karimi, P. (2020). Evaluation of WaPOR V2 evapotranspiration products across Africa. Hydrological processes, 34(15), 3200-3221.

Clark, P. U., Shakun, J. D., Marcott, S. A., Mix, A. C., Eby, M., Kulp, S., ... & Plattner, G. K. (2016). Consequences of twenty-first-century policy for multi-millennial climate and sea-level change. Nature climate change, 6(4), 360-369.

Dessler, A. (2015). Introduction to modern climate change. Cambridge University Press.

Diaz, H. F., Giambelluca, T. W., & Eischeid, J. K. (2011). Changes in the vertical profiles of mean temperature and humidity in the Hawaiian Islands. Global and Planetary Change, 77(1-2), 21-25.

Easterling, D., Kunkel, K., Arnold, J., Knutson, T., LeGrande, A., Leung, L., ... & Wehner, M. (2017). Precipitation change in the United States. In climate science special report: fourth national climate assessment, volume I.[Wuebbles D, Fahey D, Hibbard K, Dokken D, Stewart B, Maycock T (eds.)]. US Global Change Research Program, Washington, DC, 207–230.

Flint, L. E., & Flint, A. L. (2007). Regional analysis of ground-water recharge. US Geological Survey Professional Paper, 1703, 29-60.

Groisman, P. Y., Knight, R. W., Easterling, D. R., Karl, T. R., Hegerl, G. C., & Razuvaev, V. N. (2005). Trends in intense precipitation in the climate record. Journal of climate, 18(9), 1326-1350.

Heidari, H., Arabi, M., Warziniack, T., & Kao, S. C. (2020). Assessing shifts in regional hydroclimatic conditions of US river basins in response to climate change over the 21st century. Earth's Future, 8(10), e2020EF001657.

Hoerling, M., Eischeid, J., Perlwitz, J., Quan, X. W., Wolter, K., & Cheng, L. (2016). Characterizing recent trends in US heavy precipitation. Journal of Climate, 29(7), 2313-2332.

Horton, R., Yohe, G., Easterling, W., Kates, R., Ruth, M., Sussman, E., Whelchel, A., Wolfe, D., Lipschultz, F. (2014). Chapter 16: Northeast, in: Climate Change Impacts in the United States: The Third National Climate Assessment. pp. 371–395. doi:10.7930/J0SF2T3P

Huang, G., Kadir, T., & Chung, F. (2012). Hydrological response to climate warming: the upper feather river watershed. Journal of hydrology, 426, 138-150.

IPCC, 2013a: Climate Change 2013: The Physical Science Basis. Contribution of Working Group I to the Fifth Assessment Report of the Intergovernmental Panel on Climate Change. Cambridge University Press, Cambridge, UK and New York, NY, 1535 pp. http://www.climatechange2013.org/report/

Joyce, L. A., & Coulson, D. P. (2020). Climate scenarios and projections: A technical document supporting the USDA Forest Service 2020 RPA Assessment.

Karmalkar, A. V., & Bradley, R. S. (2017). Consequences of global warming of 1.5 C and 2 C for regional temperature and precipitation changes in the contiguous United States. PloS one, 12(1), e0168697.

Koczot, K. M., Markstrom, S. L., & Hay, L. E. (2011). Effects of baseline conditions on the simulated hydrologic response to projected climate change. Earth Interactions, 15(27), 1-23.

Kumar, N., & Singh, S. K. (2021). Soil erosion assessment using earth observation data in a trans-boundary river basin. Natural Hazards, 107, 1-34.

Lal, R. (2017). Soil erosion by wind and water: problems and prospects. In Soil erosion research methods (pp. 1-10). Routledge.

Lawrence, D. J., Runyon, A. N., Gross, J. E., Schuurman, G. W., & Miller, B. W. (2021). Divergent, plausible, and relevant climate futures for near-and long-term resource planning. Climatic Change, 167(3-4), 38.

Leichenko, R. M., & Solecki, W. D. (2013). Climate change in suburbs: An exploration of key impacts and vulnerabilities. Urban Climate, 6, 82-97.

Lindsey, R., & Dahlman, L. (2020). Climate change: Global temperature. Climate. gov, 16.

Masson-Delmotte, V., Zhai, P., Pirani, A., Connors, S. L., Péan, C., Berger, S., ... & Zhou, B. (2021). Climate change 2021: the physical science basis. Contribution of working group I to the sixth assessment report of the intergovernmental panel on climate change, 2.

McDonald, J. E. (1961). On the ratio of evaporation to precipitation. Bulletin of the American Meteorological Society, 42(3), 185-189.

Melillo, J. M., Richmond, T. T., & Yohe, G. (2014). Climate change impacts in the United States. Third national climate assessment, 52, 150-174.

Milly, P. C., Dunne, K. A., & Vecchia, A. V. (2005). Global pattern of trends in streamflow and water availability in a changing climate. Nature, 438(7066), 347-350.

Naz, B. S., Kao, S. C., Ashfaq, M., Rastogi, D., Mei, R., & Bowling, L. C. (2016). Regional hydrologic response to climate change in the conterminous United States using high-resolution hydroclimate simulations. Global and Planetary Change, 143, 100-117.

NCA (2018). Highlights of Climate Change Impacts in the United States: The Forth National Climate Assessment 2018 Global Change Research Program. U.S. Government Printing Office, Washington, D.C U.S. 10.7930/J0Z31WJ2

NOAA (National Oceanic and Atmospheric Administration). 2022. Climate at a glance. Accessed March 2022. www.ncdc.noaa.gov/cag.

Normand, A. E. (2019). Dam Safety Overview and the Federal Role. Congressional Research Service.

Peñaloza, D., Røyne, F., Sandin, G., Svanström, M., & Erlandsson, M. (2019). The influence of system boundaries and baseline in climate impact assessment of forest products. The International Journal of Life Cycle Assessment, 24, 160-176.

Rosenzweig, C., Solecki, W., & DeGaetano, A. (2011). ClimAID: Integrated assessment for effective climate change adaptation strategies in New York State. RESPONDING TO

CLIMATE CHANGE IN NEW YORK STATE: THE CLIMAID INTEGRATED ASSESSMENT FOR EFFECTIVE CLIMATE CHANGE ADAPTATION IN NEW YORK STATE: FINAL REPORT, 1244, 1-14.

Ruzvidzo, S. (2021). Effects of evapotranspiration on water quantity and quality along the Modder River catchment using remote sensing.

Schmucki, E., Marty, C., Fierz, C., & Lehning, M. (2015). Simulations of 21st century snow response to climate change in Switzerland from a set of RCMs. International journal of climatology, 35(11), 3262-3273.

Senay, G. B., Friedrichs, M., Singh, R. K., & Velpuri, N. M. (2016). Evaluating Landsat 8 evapotranspiration for water use mapping in the Colorado River Basin. Remote Sensing of Environment, 185, 171-185.

Szilagyi, J. (2013). Recent updates of the calibration-free evapotranspiration mapping (CREMAP) method. Evapotranspiration—An Overview.

Tan, X., Wu, Y., Liu, B., & Chen, S. (2020). Inconsistent changes in global precipitation seasonality in seven precipitation datasets. Climate Dynamics, 54, 3091-3108.

Thibeault, J. M., and A. Seth, (2014). Changing climate extremes in the Northeast United States: Observations and projections from CMIP5. Climatic Change, 127 (2), 273–287. doi:10.1007/s10584-014-1257-2

Thornton, P. E., Running, S. W., White, M. A. (1997). Generating surfaces of daily meteorological variables over large regions of complex terrain. Journal of hydrology 190, 214–251. https://doi.org/10.1016/S0022-1694(96)03128-9

Trenberth, K. E. (1999). Conceptual framework for changes of extremes of the hydrological cycle with climate change. In Weather and Climate Extremes (pp. 327-339). Springer, Dordrecht.

USGCRP (2017). Climate Science Special Report: Fourth National Climate Assessment, Volume I [Wuebbles, D.J., D.W. Fahey, K.A. Hibbard, D.J. Dokken, B.C. Stewart, and T.K. Maycock (eds.)]. U.S. Global Change Research Program, Washington, DC, USA, 470 pp., doi: 10.7930/J0J964J6.

Wang, G., Wang, D., Trenberth, K. E., Erfanian, A., Yu, M., Bosilovich, M. G., & Parr, D. T. (2017). The peak structure and future changes of the relationships between extreme precipitation and temperature. Nature Climate Change, 7(4), 268-274.

Yin, J., & Tsai, F. T. C. (2018). Saltwater scavenging optimization under surrogate uncertainty for a multi-aquifer system. Journal of hydrology, 565, 698-710.

CHAPTER 5 : CONCLUSIONS

In a substantially heterogeneous terrain like the Passaic River Basin where the presence of highly complex river systems present multifaceted mix of competing interests and water related issues, coupled with projected temperature increases (Karmalkar and Bradley 2017, NCA 2018) expected to enhance evapotranspiration and snowpack loss (Campbell et al., 2010, 2011), the concomitant effect on streamflow can be far reaching. It is in this light that this dissertation attempts to the better understand the mechanism behind streamflow dynamics in the basin, noting that it is a major driver of available water resource. Furthermore, given the relative underrepresentation of climate impacts assessments studies in the vicinity of the Passaic River Basin, this dissertation will also become part of the literature responding to the call by the Intergovernmental Panel on Climate Change (IPCC) to embark on more research to document climate change and assess its impacts (Solomon et al., 2007).

In doing so, three questions introduced in Chapter 1 have been explored, specifically: (1) How has the physiographic characteristics of the area influenced the spatial and temporal dynamics of actual evapotranspiration in the PRB? (2) From a hydrological modeling perspective, what mechanism likely drives observed hydro-climatic patterns in the PRB? (3) Will recent trends in precipitation and temperature changes continue into the future, and if so, how will they alter water resource availability in the PRB? These questions form the basis of the three core chapters

(Chapters 2, 3, and 4) of this dissertation and feeds into the overall objective to assess climate change impacts on the hydrology and water resource availability in the PRB.

Thus in this Chapter, the main conclusions drawn from the results based on the three (3) research questions are presented. The implications of this study and summary of some key uncertainties and limitations in the study are also presented, with possible future research that can be pursued.

5.1. Spatio-temporal controls on actual evapotranspiration

Forgoing actual evapotranspiration (ET) in any comprehensive climate impacts studies on water resource could be likened to trying "to undo a knot without the thumb". This is because, apart from being an index to climate change, actual evapotranspiration is considered as the primary determinant of available water resources. It is the water that would otherwise become streamflow if not released into the atmosphere. Thus in Chapter 2, an attempt was made to examine the physiographic and biophysical influence on actual ET in space and time in the PRB. This was necessary in recognition of the fact that, the Passaic River Basin forms part of a complex and highly diverse physiographic terrain, and will thus present diverse hydrologic conditions in response to climate. In examining the environmental controls on actual evapotranspiration, the classical ordinary least square (OLS) technique was used to identify and determine major internal (i.e. leaf area index (LAI), elevation) and external (i.e. mean temperature, precipitation, dew point, mean vapor pressure deficit (VPD), solar radiation, wind speed) predictor variables known to influence ET at monthly time scale. Recognizing the spatial heterogeneity of the PRB, the geographically-weighted regression method, belonging to the family of local statistics comprised of multi-valued estimates as opposed to the global (OLS) statistics, was employed to explain the spatially varying relationships that exist between the predictor and response variables in the highly diverse PRB. Key conclusions drawn from the results are as follows:

1) Temporal and spatial variabilities in mean monthly ET over the PRB are significantly controlled by climatic (i.e. TEMP, WS, DEWPT, VPD, PPT) and biophysical (i.e. LAI, ELEV) drivers. The analysis revealed that key controlling factors may be different from month to month, with wind speed taking dominance throughout the year in the study basin. Precipitation, while appearing insignificant in the course of the year, appears to be a limiting factor in the summer months.
2) Modeled spatially varying monthly ET developed from this study offer convenient and cost effective means to empirically estimate monthly water loss in the basin and from other similar ecosystems.
3) The ET index map generated for the PRB illustrates areas where ET exceeds precipitation especially in the summer months, and hence useful for water resource planning and decision making by water managers in the basin. Moreover, reliable quantification of ET has been made possible in the study basin. As such, the amount of water loss due to evapotranspiration can be accounted for in future water supply plans for the basin.

5.2. Observed hydroclimatic trends and their drivers

In Chapter 3, two bodies of research—1) to detect and analyze hydro-climatic trends, and 2) model streamflow at a watershed outlet—were carried out in one study with the aim of revealing the basin's hydro-climate patterns as well as hydrologic response to recent climate change using the Rockaway sub-catchment as a case study. By this study, a solid foundation was laid in understanding the driving mechanism that underlie streamflow dynamics in the basin, and to pave way for potential future climate impacts studies. In detecting and analyzing the trend in hydro-climatic variable in the PRB, the commonly used Mann-Kendal (MK) trends test was sidestepped, recognizing that hydro-climatic variable are inherently noisy, and that using MK test directly on the raw the hydro-climatic series may lead to erroneous interpretation of results.

As such, the wavelet transform, a precise mathematical operation that looks at the data through the noise and quantifies the structure present in the signal was employed to determine trends in the hydro-climatic time series. By this approach, one commonly encountered challenge with respect to identifying reliable and significant trends in precipitation data was overcome. With hydro-climatic trends clearly identified in the PRB, it was important to be able to explain the driving mechanisms behind the observed trend, and this was achieved in the context of hydrological modeling framework. It involved the development, calibration, and validation of a hydrological model for the Rockaway sub-basin. The performance of this model was evaluated against observed streamflow and groundwater data based on standard statistical criterion. Subsequently, water balance was computed to obtain the components required to explain the hydrologic response to recent climate in the basin. Thus, in a novel application of advanced trend analysis tool (i.e. wavelet transform) with a physically-based hydrological model that simulates both surface and subsurface flows in the land phase of the hydrological cycle, important clues on the key underlying mechanism behind the observed hydro-climatic trends as well as insights into how these trends may change the future were obtained. Based on the results, the study showed that:

1) Whereas trends in temperature and precipitation are increasing in the PRB, streamflow trends are decreasing.
2) Streamflow is more sensitive to actual ET than it is to precipitation. The general observation was that in decades where water is available, energy limits actual evapotranspiration which makes streamflow more sensitive to precipitation increase. However, in meteorologically stress or dry decades, water limits actual ET thereby making streamflow more sensitive to increases in actual evapotranspiration.

3) The choice of baseline condition constitutes an important source of uncertainty in the sensitivities of streamflow to precipitation and evapotranspiration changes and should routinely be considered in any climate impact assessment

5.3. Future climate impacts on water resource availability

In the quest to assess future water resource availability in the context of climate change, a priori analysis was carried out to subset nine (9) different models out of 20 that characterized the change in temperature and precipitation according to LEAST WARM, HOT, DRY, and WET at mid-21st century (2041—2070) as well as a mild future that typifies the MIDDLE of the temperature and precipitation range. LEAST WARM and HOT defines the extreme ends of projected changes in temperature at mid-1st century relative to the baseline periods. After arranging these projected changes from the smallest temperature change to the greatest, LEAST WARM would be the smallest change with HOT being the greatest change in temperature. Similarly, DRY and WET represent the extremes of projected precipitation change across all models for each scenario. Grouping these changes from the smallest precipitation change to the highest reveal the driest model as well as the wettest model which defines the DRY and WET projections at mid-century relative to the considered baselines. The MIDDLE of the range of projected temperature and precipitation changes represents the mild future climate which involves the computation of basin-average change in temperature and precipitation for the two baseline periods (1951—1980 and 1981—2010) to the middle of the 21st century (1941—1970) period for the PRB under RCP 4.5 and RCP 8.5. The final outcome of the selection process revealed the models deemed to represent the historical climate conditions in the study basin, and were forced with the MIKE SHE hydrological model to simulate observed streamflow in the Rockaway catchment. Conclusions from the study in Chapter 4 are presented below:

1) Relative to the 2041—2070 period, the margin of error owing to the use of different baseline conditions were +/- 0.3 — +/-0.23 ^{o}C for temperature and +/-8.15— +/-6.9% for precipitation, indicating the extent to which the time perspective used in climate change impacts assessment significantly affect outcomes.
2) Across all five (5) climate projections, and the two scenarios, a consistent warming from +1.21 to + 4.70 ^{o}C is projected in the Rockaway catchment at mid-21st century relative to the 1981—2010 baseline period.
3) While precipitation is generally projected to increase, streamflow prediction shows an overall decreasing signal, a trend likely induced by the projected increase in actual evapotranspiration.
4) In terms of climate extremes, an increase in the number heavy rainy days of approximately 2 days is projected in the coldest future whiles an increase of about 4 days is expected in the wettest future. In similar vein, the number days with consecutive dry spells is expected to decrease by approximately 2 days in the driest future whereas an increase of about 3 days is projected in the wettest future

The implication of the result of this dissertation is that increased evapotranspiration, which is a primary indicator of climate change is expected to alter the streamflow dynamic. Because the availability of water resource is largely driven by river flows in channels, possible increase or decrease in flow as depicted in the study will fuel flooding and drought conditions. Given that streamflow is highly sensitive to precipitation increases decades where water is sufficiently available, even higher risk of extreme floods can be expected. On the other hand, longer dry spells will lead to water scarcity and higher risk of drought potentials. Either way, alterations in river flows will affect routine reservoir operations under a changing climate. Particularly, a crucial basis for examining possible environmental impacts on dam failure, including physical sedimentation, erosion from floodwaters, and chemical contamination has been established in this study. With this advance knowledge in hand, swift mitigation and adaptation plans are therefore needed.

5.4. Uncertainties

The results from this dissertation reveal that actual evapotranspiration plays an important role in the water resource availability in the Passaic River Basin and constitutes the main driving mechanism behind streamflow dynamics in the basin both at present and into the future under a changing climate. Employing advanced techniques and state of the art hydrological models, a more comprehensive and in-depth understanding of hydroclimatic patterns and projected response of hydrologic variables to climate change at basin scale have been harnessed. Although attempts were made to, at best, minimize uncertainty in the results, GCMs come with their own set of uncertainties arising from assumptions chosen in the process of global climate modeling as well as greenhouse gas emission scenarios. This can also be propagated into the hydrological modeling process in addition to uncertainties that are characteristic of hydrological modelling such as input, output, structural, and parametric uncertainties (Ma et al., 2016). More so, because in Chapter 3 the calibration and validation process was based on reconstructed streamflow data, it is possible that errors emanating from the methods and data used in estimating the daily reconstructed streamflow (refer to Hickman and McHugh, 2018) may be propagated into this study.

It is important to however add that, the aforementioned uncertainties do not at all cast any shred of doubt on the results presented in this dissertation as conscious effort were made to incur the least additional uncertainty apart from those obvious. These efforts include the use of multi-objective model calibration in Chapter 3, where both observed streamflow and groundwater data was used as reference datasets. Yin et al. (2020) noted that such an approach helps improve model performance and reduce parameter equifinality. In addition, the choice of baseline periods used in climate impacts assessment studies is known to constitute an important source of uncertainty, comparable to that introduce by global climate models. Again, Chapters 3 and 4 of this dissertation utilized multiple baseline periods to at least capture the range of uncertainty in the analyses.

5.5. Limitations and Future Research

An important limitation of this study and countless other studies on future climate impacts assessment is the assumption of stationarity pertaining to future land-use patterns. Non-stationarity of land-use will most certainly change catchment hydrologic behavior and can influence hydrologic response to climate change. In this study, future simulation of streamflow did not incorporate land use/land cover change, which will be a likely future reality in line with population and urban growth. Because land use/ land cover change interacts synergistically with climate change, their impacts on streamflow can be amplified. Therefore, studies that can integrate land use/ land cover change models in future hydrologic simulations in the Passaic River Basin will be greatly beneficial in effectively quantifying future risks associated with the ongoing environmental changes.

Another assumption pertains to the routing of water to channels in the development of the hydrodynamic model. The study also assumed that the shape of the channel will remain constant over time. However, it's important to recognize that channel form can be influenced by various factors like the characteristics of the flow, erosion rates upstream, and the supply of sediment, all of which can be affected by both human activities and fluctuations in hydrology. Therefore, if there are alterations in the flow characteristics, it's likely that the channel shapes will also change. This is significant because modifications in channel structure can lead to adjustments in hydraulic properties, ultimately affecting the accuracy of estimated river discharges. Consequently, it is recommended to incorporate information about potential changes in channel morphology to enhance the precision of streamflow predictions.

5.6. References

Campbell, J. L., Driscoll, C. T., Pourmokhtarian, A., & Hayhoe, K. (2011). Streamflow responses to past and projected future changes in climate at the Hubbard Brook Experimental Forest, New Hampshire, United States. Water Resources Research, 47(2).

Campbell, J. L., Ollinger, S. V., Flerchinger, G. N., Wicklein, H., Hayhoe, K., & Bailey, A. S. (2010). Past and projected future changes in snowpack and soil frost at the Hubbard Brook Experimental Forest, New Hampshire, USA. Hydrological Processes, 24(17), 2465-2480.

Hickman, R. E., & McHugh, A. R. (2018). Methods used to reconstruct historical daily streamflows in northern New Jersey and southeastern New York, water years 1922–2010 (No. 2018-5068). US Geological Survey.

Karmalkar, A. V., & Bradley, R. S. (2017). Consequences of global warming of 1.5 C and 2 C for regional temperature and precipitation changes in the contiguous United States. PloS one, 12(1), e0168697.

Ma, L., He, C., Bian, H., & Sheng, L. (2016). MIKE SHE modeling of ecohydrological processes: Merits, applications, and challenges. Ecological Engineering, 96, 137-149.

NCA (2018). Highlights of Climate Change Impacts in the United States: The Forth National Climate Assessment 2018 Global Change Research Program. U.S. Government Printing Office, Washington, D.C U.S. 10.7930/J0Z31WJ2

New Jersey Department of Environmental Protection (2017). New Jersey Water Supply Plan 2017-2022: 484p, access [May 7, 2020], at URL [http://www.nj.gov/dep/watersupply/wsp.html]

Solomon, S. (Ed.). (2007). Climate change 2007-the physical science basis: Working group I contribution to the fourth assessment report of the IPCC (Vol. 4). Cambridge university press.

Yin, J., Pham, H. V., & Tsai, F. T. C. (2020). Multiobjective spatial pumping optimization for groundwater management in a multiaquifer system. Journal of Water Resources Planning and Management, 146(4), 04020013.